1989

Auger effect on the output power of InGaAsP DH lasers

Mani Mina
Iowa State University

6

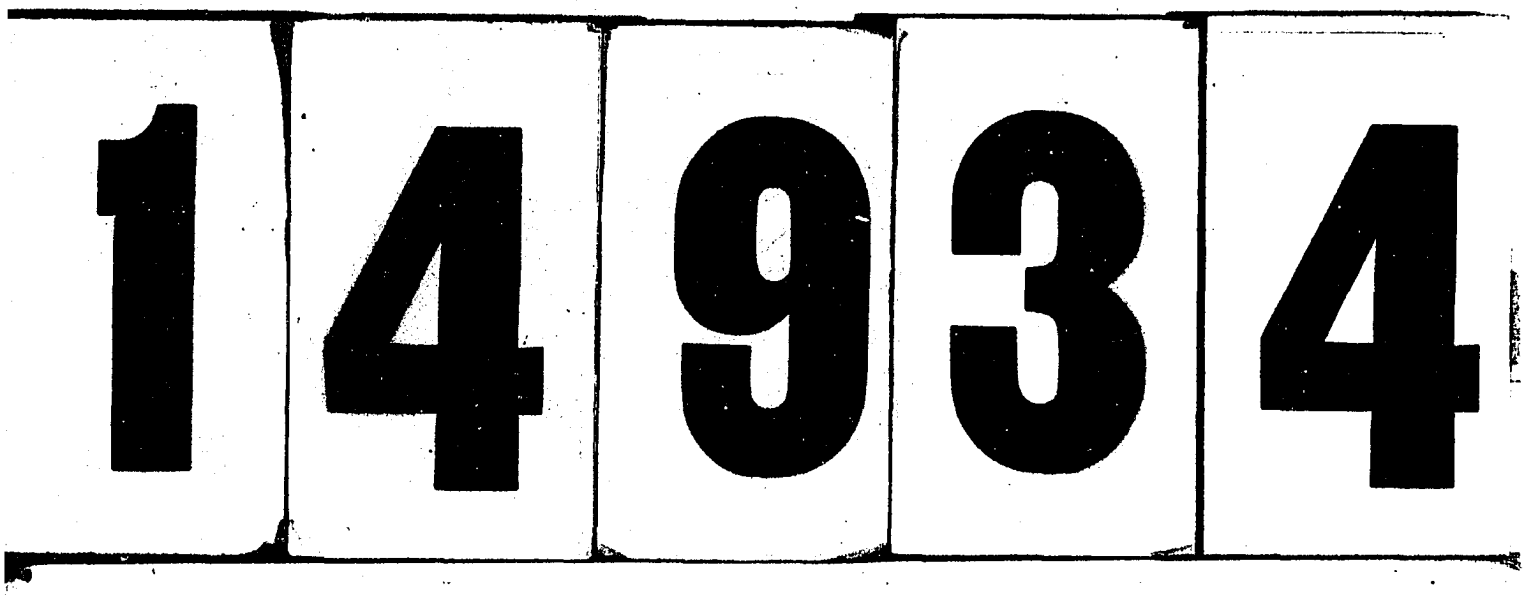

Order Number 9014934

Auger effect on the output power of InGaAsP DH lasers

Mina, Mani, Ph.D.

Iowa State University, 1989

U·M·I
300 N. Zeeb Rd.
Ann Arbor, MI 48106

Auger effect on the output power of InGaAsP DH lasers

by

Mani Mina

A Dissertation Submitted to the

Graduate Faculty in Partial Fulfillment of the

Requirements for the Degree of

DOCTOR OF PHILOSOPHY

Department: Electrical Engineering and Computer Engineering
Major: Electrical Engineering (Electromagnetics)

Approved;

Signature was redacted for privacy.

In Charge of Major Work

Signature was redacted for privacy.

For the Major Department

Signature was redacted for privacy.

For the Graduate College

Members of the Committee:

Signature was redacted for privacy.

Iowa State University
Ames, Iowa
1989

TABLE OF CONTENTS

LIST OF TABLES

LIST OF FIGURES

ACKNOWLEDGEMENTS

I would like to express my gratitude and indebtedness:

To Dr. Hsung-Cheng Hsieh for his support and supervision during my research and preparation of this manuscript. During the last five years, I have had the honor and pleasure of working with Professor Hsieh, learning from him, and appreciating his scientific scholarship. Professor Hsieh has been more than an academic advisor to me. I have enjoyed talking to him about the widest variety of subjects and learning from him about almost all aspects of life. He has been a true teacher in the most philosophical sense and a model gentleman in my life.

To Professor James Corones, one of the best scientists and intellectuals I have met in my life. I have always enjoyed and appreciated Dr. Corones questions and comments about my research and interests. I am honored that he could take time off his very busy schedule to be in this committee.

To Professor Glenn Fanslow for his support and encouragement during the course of my research as well as my years in the Electrical and Computer Engineering Department. I appreciate all the time that he supportively and patiently listened to me and gave me helpful and thoughtful suggestions. I am also very grateful to him for reading this manuscript and suggesting many helpful changes.

To Professor Alvin Read, who was the first person patient enough to show me

the true beauty of Maxwell's equations. I am very grateful to him for reading this work and making many helpful suggestion to improve it. I have been more than lucky to work for Dr. Read and learn many aspects of Electromagnetics since 1986. In my teaching, he has always been patient with me and supportive of my style, for which I am very thankful. I think, I will remember Dr. Read every time I work with Maxwell's equations for the rest of my life. However, my memories, thanks, and appreciation for Dr. Read far exceeds the 4 equations describing EM fields.

To Dr. Costas Soukoulis for taking time off his busy schedule and being on my committee. I have had the opportunity to work for him as a teaching assistant and again during my M.S. and PH.D. research. During all this time Dr. Soukoulis has been most supportive and I have learned much from him.

To Ms. Nazanin Imani, my dearest wife, for her support and patience during the last six years, and for helping me with many little details in my research as well as in the preparation of this dissertation.

To my parents Ms. Mahin Farjavan and Mr. Mohammad-Taghi Mina for their lifetime encouragement and care, and for teaching me the importance of education and the satisfaction of learning.

To my two best friends Mr. Bjorn Stevens and Mr. Paul Stucky, for their strong support and help. During the preparation of this work, Mr. Stevens has patiently read many chapters and suggested many constructive corrections. He also has been kind enough to help me with some of the graphics. Mr. Stucky has been kind enough to read parts of this work (sometimes until midnight) and to give me his opinion and suggestions for some important changes. During the last four years I have had the

pleasure of knowing and working with these gentlemen and enjoyed their enthusiasm and learned from them in many aspects of science and life.

To Dr. Nosrat Mokhtari, my friend and teacher for being one of the most important sources of my enthusiasm in Physics and Electrical Engineering.

Finally, to Dr. Housien Jadvar (M.D. to be) for his encouragement. For some reasons unknown to me, he has insisted on having a copy of this dissertation even before the actual writing was started.

1. INTRODUCTION

We are living in a new era of human technology. While the 1960s and 1970s were the glorious years of electronics and microelectronics, one can characterize the 1970s and the 1980s as the decades that gave birth to opto-electronics in particular and photonics in general. This is a technology in which information is transmitted using photons as opposed to electrons (which are used in electronics). The prospect of this era came about in early 1960 when the first laser was successfully operated by Maiman [1]. Since then, laser technology has come a very long way. It has advanced in many different and ever expanding areas. However, the true photonics building blocks, especially for small scale integrated circuits and fiber optics, are light emitting diodes and semiconductor injection lasers [2, pages 252–278].

Since its invention in 1962, semiconductor laser technology has experienced tremendous advancement. Technological advances in material purification and processing, and sophisticated epitaxial growth techniques have led to a large variety of semiconductor lasers operating over the wide wavelength range of 0.3 to 100μm [3, page vii]. Semiconductor lasers have revolutionized many industries, and its impact on many others remains to be seen. Today, the semiconductor laser is used for a variety of purposes in many branches of industry and research laboratories. However, the impact of lasers has been felt most significantly by the communication industry.

From the very beginning, lasers (specially semiconductor lasers) have proved to be promising for many possibilities in communication. This has led to extensive research in various branches of the communication industry [4, page xiii].

The early developments of optical cables with 20 dB/km of attenuation in the early 1970s, the realization that pure silica can give the lowest optical loss of any similar media, and eventually the achievement of low loss optical fiber with 0.12 dB/km of attenuation in the late 1970s were all contributing factors for the development of sources compatible with this medium of data transmission [5]. Semiconductor injection lasers and light emitting diodes (LEDs) were the most suitable sources for optical communication using optical fibers [6]. This is due to the fact that they have adequate power, easy modulation capability, relatively long lifetimes, relatively high power efficiencies, and high coupling coefficients [7, page 704].

With the development of GaAs in the 1970s, and ternary compounds (which are made of three elements) such as GaAlAs and InAsP, semiconductor lasers emitting at 0.8-0.9 μm were invented. These lasers together with the available optical cables led to the development of a whole new generation of optical systems. In the late 1970s, numerous light wave communication systems were installed utilizing short wavelength GaAlAs/GaAs lasers (λ = 0.82-0.88 μm) as their light sources [8].

As the improvements in optical fibers continued during the late 1970s and early 1980s, which led to even lower loss and dispersion, the possibility of using optical transmission for long distance communication became feasible. This opened a whole new field called long-haul optical communications [9]. Using a powerful and very coherent light source, one could send data through optical fibers without the frequent

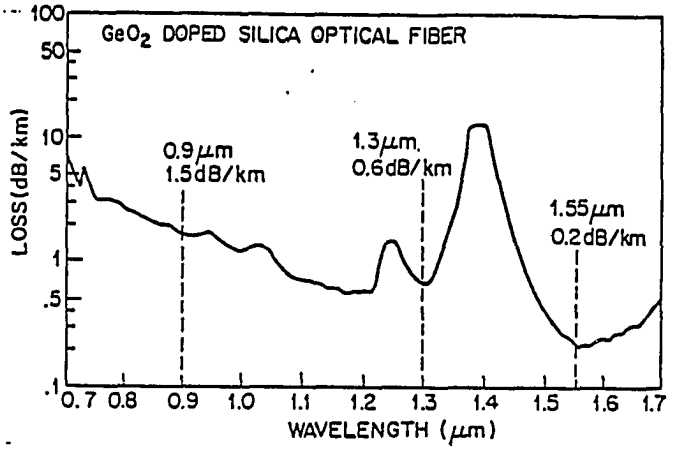

Figure 1.1: Loss characteristics of a silica fiber [5, page 704]

need for repeaters [8]. This trend has made semiconductor injection lasers prevail as the main source of optical communication over long distances.

In order to take advantage of the lower dispersion and lower attenuation in silica fibers at 1.3 and 1.55 μm as shown in Figure 1.1, there has been extensive efforts in the development of long wavelength semiconductor lasers [10]. Several semiconductor compounds exhibit efficient light emission in the infrared region (see Figure 1.2). Although several III-V materials are capable of emitting in wavelengths of 1.3 to 1.55 μm, the quaternary compound InGaAsP material system has been studied the most. Today, this is the most promising material for the purpose of long-haul optical communication.

The reason for the development of InGaAsP system is probably three fold: First, due to the mature material processing technology of GaAs and InP based ternary compounds (like GaAsP and InAsP), it was easier to develop quaternary compounds

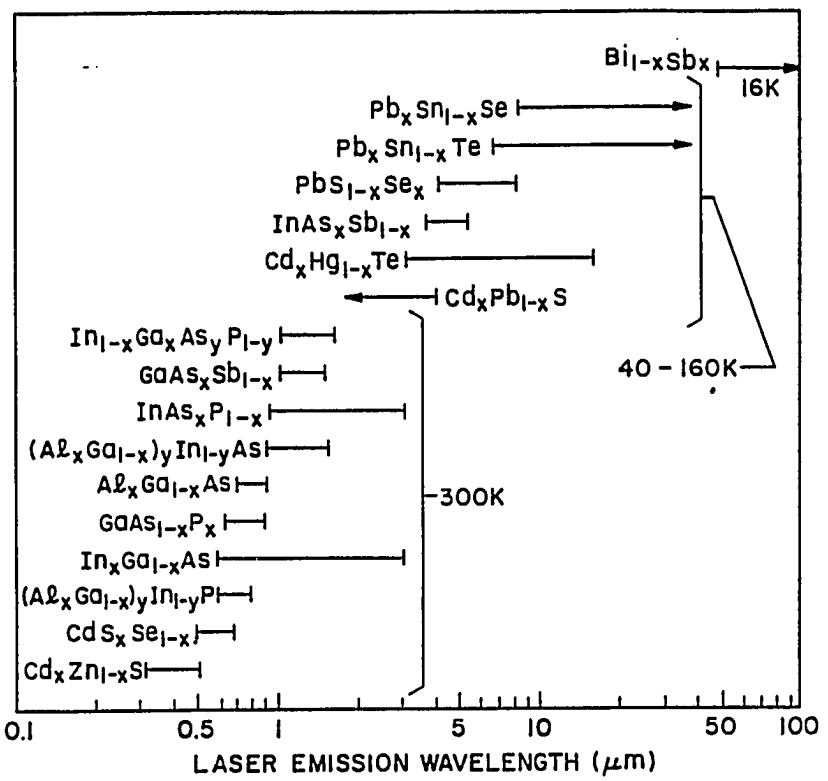

Figure 1.2: Wavelength range of semiconductor lasers covered by different materials [3, page 6]

with a similar base. Second, the lasers developed by InGaAsP could easily be made to cover the wavelength range of 1.1 to 1.7 μm with almost perfect lattice alignment with the substrate material (which is usually InP or GaAs). Third and most important, has been the fact that InGaAsP lasers exhibit a very stable output in the 1.3 and 1.55 μm range [8].

Today, with the prospect of multipurpose optical lines (which can carry telephone, cable, computer, and other data on the same cable) the need for sources such as semiconductor lasers is growing rapidly. These are devices with coherent output, compact size, narrow linewidth, and capability of high frequency modulation. Such sources, together with low loss fibers, have revolutionized (and continue to change) the communication industry [10]. During the latter part of the 1980s, the intense development efforts devoted to InGaAsP lasers have resulted in a very mature technology. At present, many lightwave transmission systems using InGaAsP lasers have been installed, and many others are being deployed within the U.S and throughout the world [6].

Important characteristic quantities for a semiconductor laser include: threshold current density J_{th}; threshold carrier density n_{th}; quantum efficiency η_d; and light output power P_L. It is an urgent practical problem to predict and control the temperature dependence of J_{th}, n_{th}, and η_d, and to relate these temperature dependences to the light output under continuous wave operation (CW operation) of semiconductor lasers [11]. Despite the fact that InGaAsP lasers are very promising sources and are being used in many communication systems, their temperature behavior is not very well understood. These lasers show very sensitive thermal be-

havior of J_{th} around room temperature. Such unfavorable behavior, which has been well documented [3, 4, 8], limits the laser's application specially for CW operation. Consequently there is a need to understand, formulate, and control the temperature characteristics of InGaAsP lasers.

The purpose of this study is to investigate the temperature characteristics of the important parameters of a special type of light source called the InGaAsP double heterojunction (DH) lasers. This is done using theoretical models for calculation of J_{th}, n_{th}, and η_d, and assuming that band-to-band Auger recombination is the most important carrier loss mechanism in the active region of such injection lasers.

In order to study and evaluate the performance of a laser, one needs to know and understand basic laser operation and its characteristics. Regardless of what kind of injection laser is considered, its basic operation is governed by the same physics. Thus, in order to enhance ones appreciation of the nature of our problem, a brief review and an introduction to the principles of semiconductor injection lasers is presented in this chapter. This is followed by a discussion of the problem and in the second chapter, threshold conditions and losses, together with important laser parameters such as: current density, carrier density, quantum efficiency, and output power. In Chapter 3, the Auger process and models for calculating J_{th}, n_{th}, and η_d as a function of temperature are reviewed. Then, in Chapter 4, a two dimensional model for calculating the temperature distribution in DH lasers, and the kinds and locations of the heat sources (and their importance) together with algorithms for laser parameter calculations will be discussed. Finally, results of theoretical calculation for laser parameters will be presented, discussed, and compared to some experimental

values in the last chapter.

1.1 Semiconductor Injection Laser

After the successful operation of the first solid state laser in May 1960, and of the He-Ne gaseous laser in December 1960 [12], many scientists began looking at the possibility of lasing in semiconductor materials. The feasibility of this kind of laser was suggested and studied during the years 1960 and 1961. In 1962 several groups reported lasing action in semiconductors [7, page 682]. Their devices consisted of a forward biased GaAs p-n junction. All published reports show the devices were cooled by liquid Helium (or liquid Nitrogen) and were operated in a pulsed mode with emissions at about 0.84 μm. Shortly thereafter, lasers made of GaAsP operating at 0.71 μm were developed. Ever since the first semiconductor lasers were invented, the development of different types of lasers using different structures and materials became an ongoing process.

Semiconductor lasers are similar to all other lasers in the fact that they emit radiation which is monochromatic and also is highly directional. However, there are two major characteristics which make this type of laser different from other types: First, it is typically very small (about 0.1 mm long). Second, it can be modulated at relatively high frequency simply by modulation of the applied current. Due to these special characteristics, semiconductor lasers became the most important light source in long-haul optical communication [13], video recording [14], optical recording [15], and high speed printing. The list of application of this type of laser has been expanding during the years. Today, its application has extended into atmospheric

pollution monitoring [16] and many basic research and technological areas [2, page 267].

As a result of all the various applications of semiconductor lasers in the course of the years, laser designs have diversified to give us a whole range of sophisticated opto-electronics devices. In some cases the changes are so immense that the resultant device is beyond recognition. Despite all the complications and sophistications involved, all devices utilizing injection lasers follow the same basic physical principles; the same principles which made the realization of the first laser possible. Hence, it becomes very important to look into the basic concepts and ideas involved in a semiconductor laser.

1.1.1 Laser action

In order to achieve laser action we need to achieve stimulated emission of light. There are three basic interactions between electrons and photons. These are shown in Figure 1.3. In a semiconductor there are two energy bands called the conduction and valence bands (see Figure 1.4). At room temperature in a semiconductor, there are some electrons in the conduction band and some holes in the valence band due to thermal agitation. The holes and electrons constantly recombine and give off radiation. However, at equilibrium this radiation gets absorbed by the material. Two conditions must be satisfied for lasing to take place: First, we need to make the rate of radiation high enough to overcome the losses in the material. Second, this rate must be enhanced to get stimulated emission in a particular direction. These two conditions are necessary ingredients for any laser.

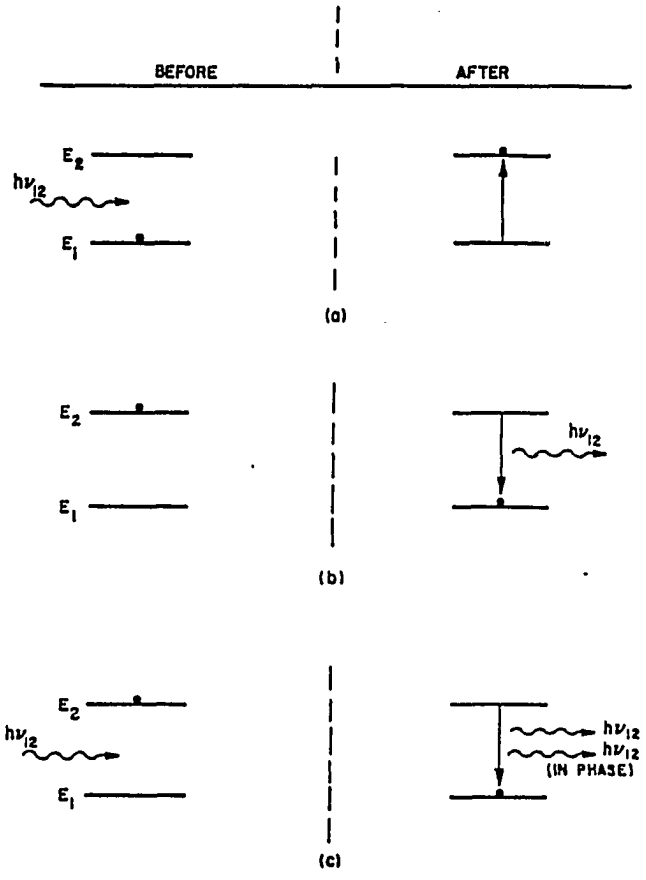

Figure 1.3: Three basic transitions between two energy levels (a) absorption (b) spontaneous emission (c) stimulated emission [7, page 707]

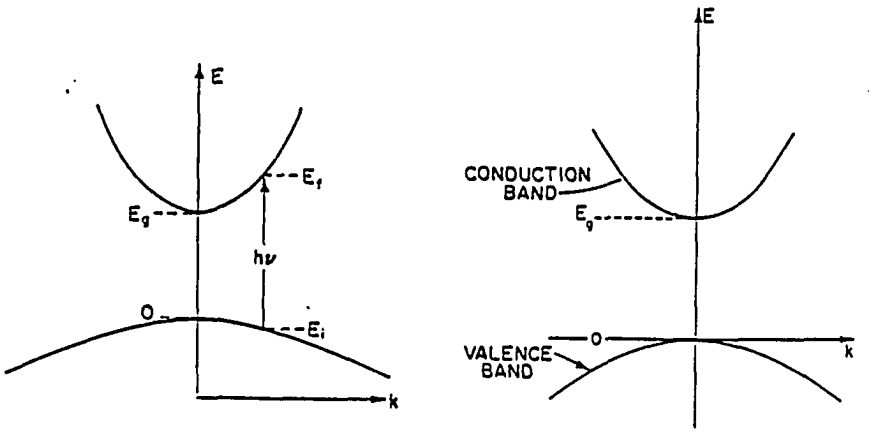

Figure 1.4: Parabolic band diagram for a two band semiconductor [11, pages 4, 35]

1.1.2 Semiconductor materials

The list of semiconductor materials suitable for laser action has always kept growing. At present, these materials cover the optical spectrum from near ultraviolet to far infrared [3, page 5]. It is important to note that virtually all lasing semiconductors have direct band gaps. This is due to the fact that the radiation transition in a direct band gap semiconductor is a first order process (i.e., the momentum is automatically conserved). Hence, it is possible to get a high radiation rate as well as a high rate of stimulated emission. In an indirect band gap semiconductor the radiative emission process involves phonons and other scattering agents to satisfy energy and momentum conservation requirement. Consequently it is not possible to get a high radiation rate in an indirect band gap material. Currently, gallium arsenide and other direct band

gap III-V compound alloys are the most extensively studied and developed materials. At the present time, one can say the two most important III-V compound alloy systems are the two alloys $Al_xGa_{1-x}As_ySb_{1-y}$ and $Ga_xIn_{1-x}As_yP_{1-y}$. These quaternary systems are the best suited materials for long wavelength lasers.

As explained later, to achieve high efficient lasers one needs to alternate different layers of semiconductor materials within the laser structure. When doing this, lattice matching between the adjacent layers is very important. The better lattice matching between adjacent layers, the better laser we have. The two quaternary alloys mentioned above have the capability of almost perfect lattice matching to InSb and InP respectively. Figure 1.5 shows the relationship between the band gap energy (or the wavelength), and the lattice constant of the quaternary compounds.

In the figure solid dots represent binary compounds and solid lines correspond to the ternary compounds (with three elements). The clear region bounded by the polygon, whose edges represent ternary compounds, denotes the possible values for band gap and the lattice constant for the quaternary solution of $In_xGa_{1-x}As_yP_{1-y}$. The dotted line shows the range of band gap values that can be achieved by varying the x and y mole fractions to obtain a quaternary material that is lattice matched to the binary InP.

The relation between the band gap energy and the wavelength of a material is given as

$$\lambda \cong 1.24/E_g \tag{1.1}$$

where E_g is in eV and λ is in μm. For InGaAsP lasers a wavelength range of 1.1-1.65 μm can be covered by choosing x and y as shown in Figure 1.6. For example to have a

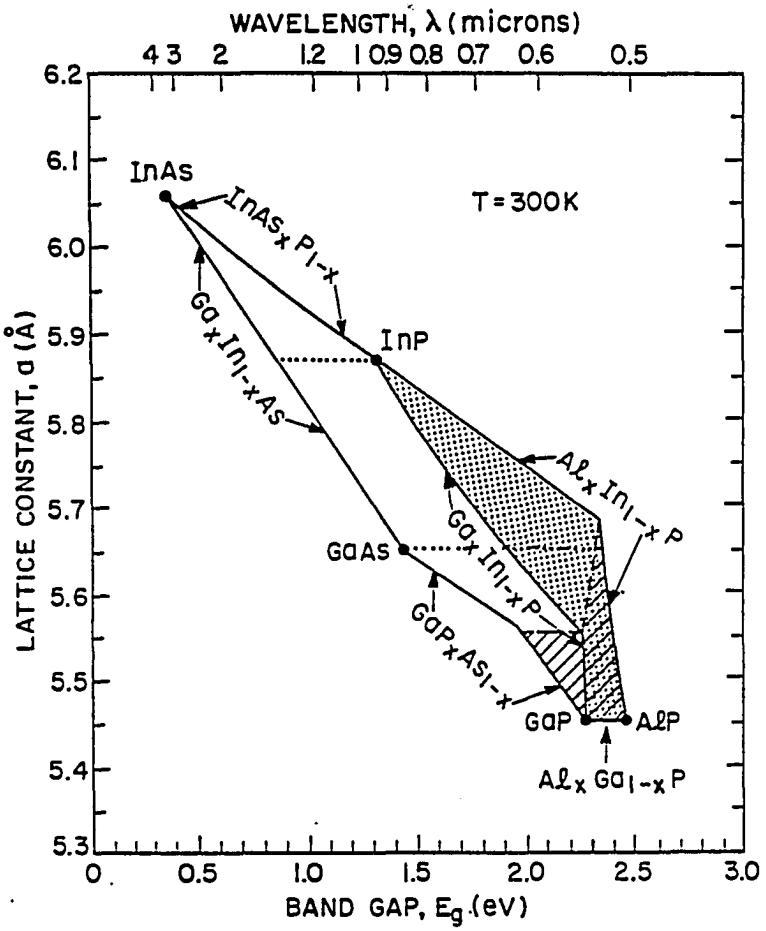

Figure 1.5: Band gap and lattice constant for InGaAsP(clear region) and AlGaInP (shaded region) [3. page 7]

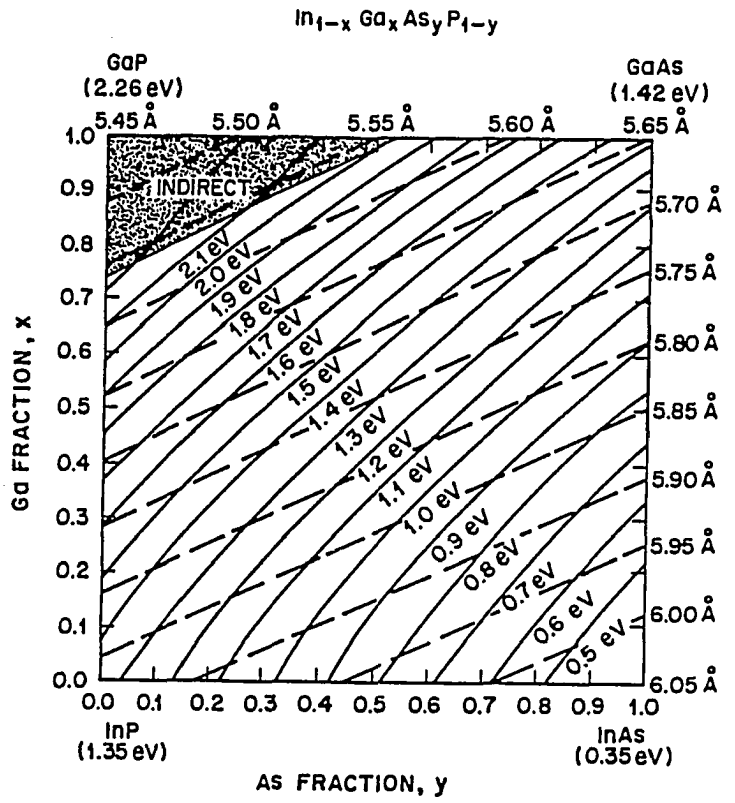

Figure 1.6: Contours of constant band gap and lattice spacing in x-y compositional plane of InGaAsP [3. page 8]

laser lattice matched to InP at 1.3 μm ($E_g \cong 0.95$ eV) one needs x=0.28 and y=0.6. This figure can also be helpful in choosing the adjacent layers in such lasers.

1.1.3 Laser structure

A semiconductor laser is a specially prepared p-n junction under forward bias. In order to get lasing, we need to enhance the rate of stimulated emission in a particular direction. One can enhance the light in a certain direction using a resonant cavity structure. The typical structure for such a cavity used in semiconductor lasers is

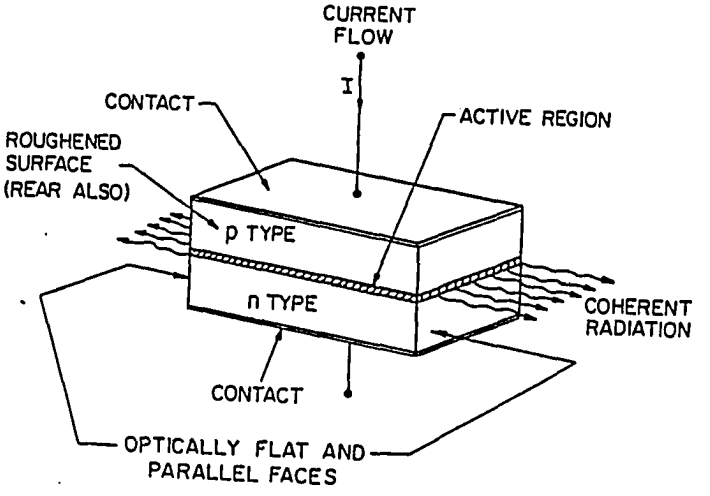

Figure 1.7: The basic Fabry-Parot-Cavity configuration [7, page 708]

called a Fabry-Parot-Cavity and is illustrated in Figure 1.7.

The development of the semiconductor lasers started with basic structures made of only one material. They were called homojunction lasers (see Figure 1.8). In 1963 it was proposed that the laser behavior would improve by making a layer of semiconductor sandwiched between two cladding layers [17]. The cladding layers should have lower band gap energies and lower indices of refraction. Such a device is commonly called a double hetrojunction (or DH) laser (see Figure 1.8b). The DH laser illustrated in Figure 1.8b, like the first fabricated lasers does not incorporate any mechanism for the lateral (parallel to the junction plane) confinement of the injection current or the optical mode. This type of structure is called broad area laser.

As early as 1967, there were proposals for stripe-geometry lasers [3, page 4] . However in the early 1970s, due to the possibility of optical fiber communication stripe-geometry DH lasers were adapted. This way one could get lower current levels

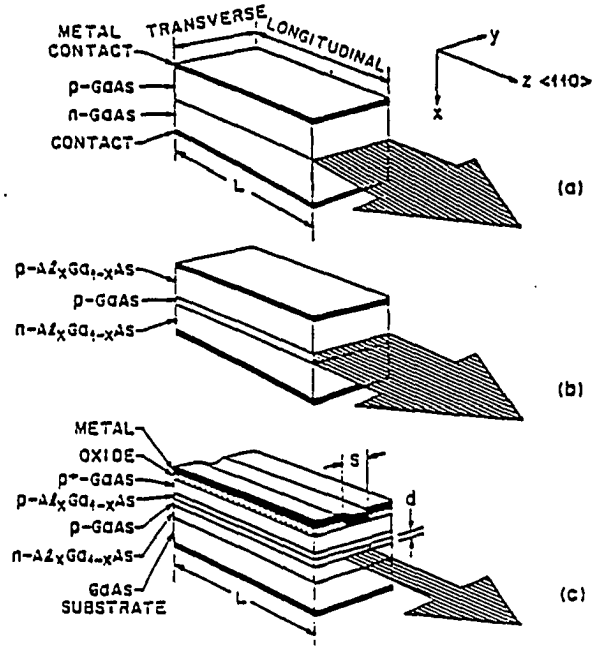

Figure 1.8: Semiconductor laser structure in Fabry-Parot-cavity configuration (a) Homojunction (b) Double hetrojunction (c) Stripe geometry [2. page 269]

which means less heating and a more stable output. The DH structure also provides the best coupling to the core of optical fiber due to the small stripe size of the lasing region (in a typical stripe geometry 5 to 30 μm widths are very common). In the early 1970s, researchers using InGaAsP stripe-geometry DH lasers achieved pulsed and continuous wave (CW) operations of lasers at 1.3 μm. This permitted the designers to take advantage of the the low loss 1.3 μm window of the silica fibers. In the late 1970s, InGaAsP lasers using similar structures were reported operating at 1.55 μm where ultra low loss in silica occurs. Today, many variations of stripe-geometry DH lasers are being used in long-haul optical communication systems [3, page 5].

1.2 Laser Operation

1.2.1 Population inversion

In order to get enhanced stimulated emission for laser operation we need to get to a particular condition. When this condition is achieved, the recombination rate between electrons in the conduction band and holes in the valence band is high enough to overcome the absorption and other losses inside the laser. This situation is called population inversion. Once population inversion is reached, radiation (which is spontaneous radiation at this point) can be enhanced in a particular direction by the help of a resonant cavity.

Population inversion is achieved in the following way: Consider a degenerate p-n junction, which has very high doping levels in both sides of the junction causing the Fermi levels to lie within the valence band on the p-side and within the conduction

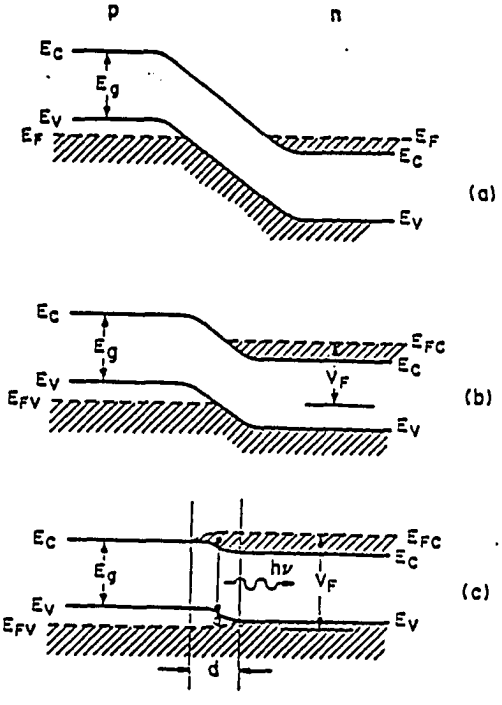

Figure 1.9: Energy band diagram of a degenerate p-n junction (a) at equilibrium, (b) under forward bias, (c) under high injection condition [2, page 270]

band on the n-side. Figure 1.9a shows a typical band diagram of such a device at the thermal equilibrium. Under the application of a forward bias (see Figure 1.9b), electrons will be injected from the n-side and holes from the p-side. This will give a high carrier concentration around the junction area. The high carrier concentration will result in a high recombination rate, which means a higher rate of spontaneous emission.

When a sufficiently large bias is applied, the high injection condition takes place. As a result, a region around the junction known as the active region (indicated by d in Figure 1.9c) will contain a large concentration of electrons and holes. Under

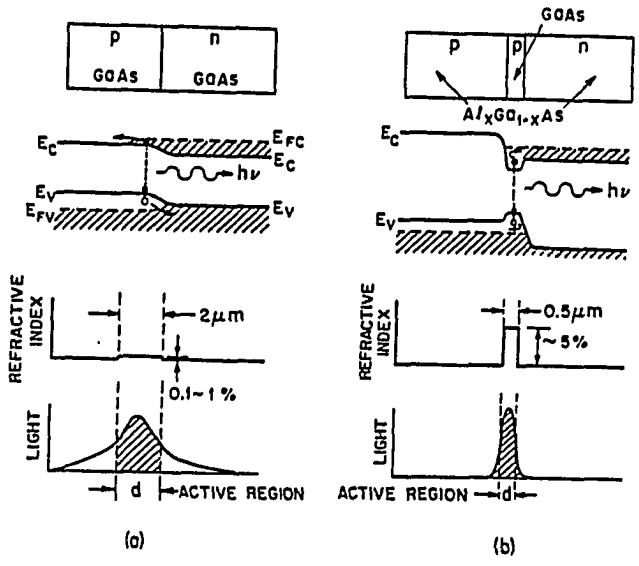

Figure 1.10: Comparison of some characteristics of (a) homojunction and (b) DH laser. The figure shows the structure, the energy band diagram under forward bias, the refractive index change, and the confinement of light [2, page 271].

the high injection condition, one can get a high rate of spontaneous emission which is capable of overcoming the losses. This is what is known as population inversion. Mathematically the population inversion condition can be expressed as

$$E_{fc} - E_{fv} > E_g$$

1.2.2 Carrier and optical confinement

When high injection is achieved, one needs to confine injected carriers and the resultant light output. Figure 1.10 shows how this is done in a homojunction and a DH laser. The fact that a homojunction laser requires more current than a DH laser is apparent from Figure 1.10. This is due to the confinement properties of DH lasers. Successful operation of a semiconductor laser requires that the generated

optical emissions remain in the vicinity of the active region. In a DH laser the active region is really a layer with larger band gap (and higher refractive index) than the cladding layers. This makes the active layer behave like a dielectric waveguide and thereby limiting spread of the amplified light. This requires the following condition for the indices of refraction of the active and cladding layers (see Figure 1.11).

$$\bar{n_2} > \bar{n_1} \geq \bar{n_3}$$

Then, as indicated in Figure 1.11b, if θ_{12} and θ_{23} are greater than the critical angles for total internal reflection given by,

$$\theta_{12} > sin^{-1}(n_3/n_2)$$

$$\theta_{23} > sin^{-1}(n_1/n_3)$$

the propagation of electromagnetic radiation will be guided (confined) in a direction parallel to the layer interfaces. Since confinement is very important in keeping injected carriers together with laser radiation inside the active region, it is customary to define a confinement factor for a laser as the ratio of the light intensity within the active region to the total light intensity in the laser. The latter includes light both within the active region and outside the active region. It can be shown that the factor can be expressed as [2, page 272],

$$\Gamma = confinement factor = \Gamma \cong 1 - e^{-c\Delta\bar{n}d}$$

where c is a constant, $\Delta\bar{n}$ is the difference in the refractive indices, and d is the thickness of the active layer.

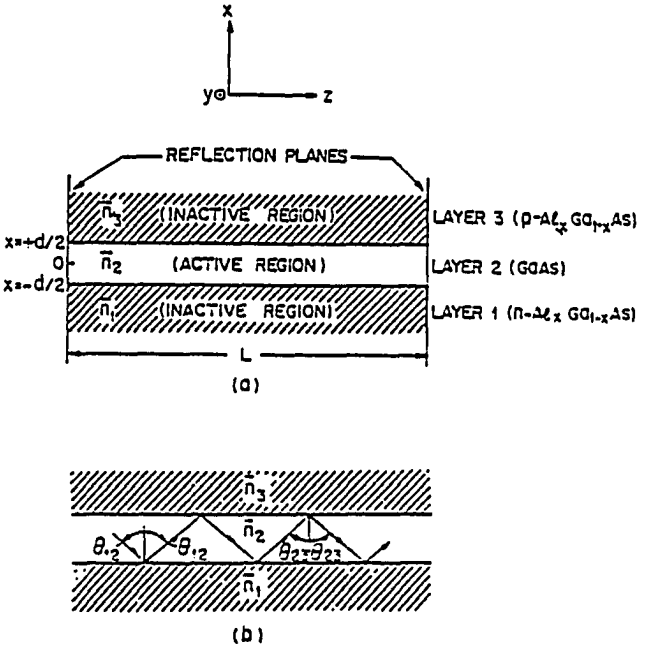

Figure 1.11: Diagram for structure and trajectory of a DH laser (a) Three layer waveguide (b) Ray trajectory of a guided wave [7, page 711]

1.2.3 Threshold parameters

When the injection level under the forward bias in a semiconductor laser reaches a point such that the radiation intensity overcomes the losses, threshold is reached. In other words, the threshold condition is the condition at which the laser begins to lase. At that point and above, we have laser action. The parameters of the laser at threshold and above are very important in the characterization of the laser and prediction of its behavior.

One of the important parameters is the threshold current density J_{th}, defined as the minimum current density required for lasing. Another important parameter is the light output power P_L. As we will discuss later, these two parameters, as well as many other parameters in a semiconductor laser, depend on the temperature of the structure. However, one generally sees a relationship between output power and injected current as shown in Figure 1.12. Before threshold all the output is by spontaneous emission. At threshold stimulated emission begins to take over.

In an actual laboratory measurement, one observes a behavior for light output versus injected current at different heat sink temperatures as shown in Figure 1.13. As the laser begins to lase, increasing the injected current will result in higher output, but after a certain point current increase will result in losses which will gradually overcome the light output power, and eventually the device will stop lasing.

The threshold current of a semiconductor laser is an exponential function of temperature. Empirically this behavior is formulated as

$$I_{th} \sim e^{(T/T_0)}$$

where T is the temperature of the active region and T_0 is called the characteristic

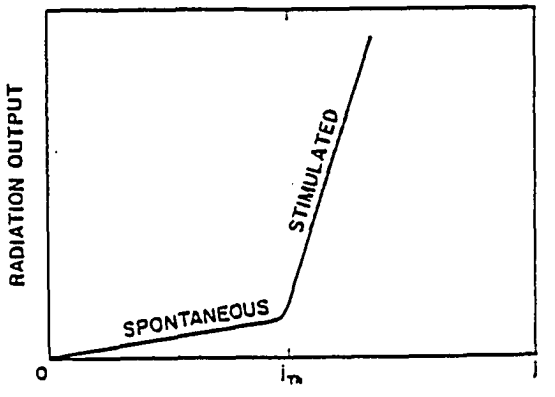

Figure 1.12: Radiant output versus excitation rate in a semiconductor laser [11. page 219]

temperature. There is temperature dependence for almost all parameters of a semiconductor laser as we will discuss later. It is important to remember that the laser operates at its best when the injection current and the operating temperature are as low as possible. Hence, the most efficient use of a semiconductor is when the input current and laser temperature are controlled to give the most efficient output power.

1.3 Problem Statement

The fact that all laser parameters are temperature dependent can be empirically verified. For instance threshold current density of a semiconductor laser depends on the temperature of the active region T and is given by

$$J_{th} = J_0 e^{(T/T_0)}$$

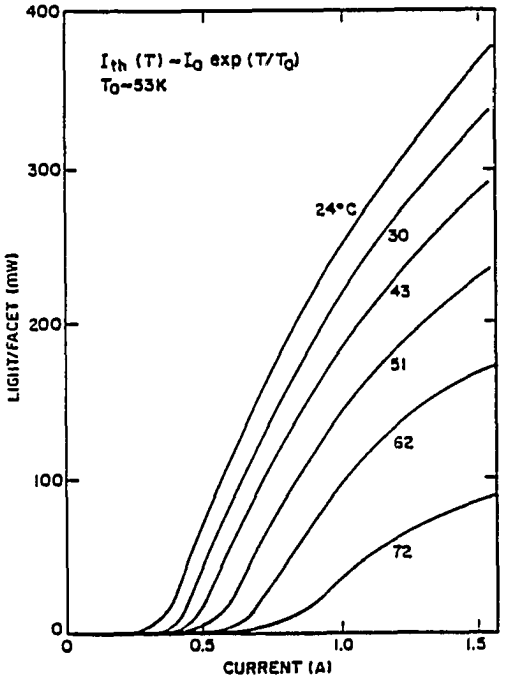

Figure 1.13: L-I characterization at several temperatures for gain guided 1.3 μm InGaAsP laser [3, page 213]

where T_0 is called the laser characteristic temperature (which is itself a temperature dependent quantity), and J_0 is a reference current density.

Recently, due to their stable output at 1.3 and 1.55 μm, InGaAsP/InP lasers have become very important for the purpose of optical communication. At present researchers are working on systems which will put 40 to 50 cable channels on a single optical line using CW (continuous wave) operation of InGaAsP lasers. This calls for better understanding of CW operation of these lasers. However, the performance of these lasers is not very well understood. At room temperature the typical value of T_0 for InGaAsP, is low enough to cause excessive heating and a poor light output power versus current behavior. For a typical 1.3 μm DH laser, T_0 is about 100 K for $T < 255K$ and about 65 K for $T > 255K$. The low value of T_0 results in a high J_{th} for $T > 255K$, specially about room temperature. Under continuous operation, this behavior of current around room temperature will cause the structure to heat up. As the temperature of the laser gets higher, there will be a need to pump more current to keep lasing. However, increasing the current will result in more heating and more heating will raise the temperature of the structure. This process will continue until the current level reaches a point where losses become dominant and laser action will stop. From then on, the current injected will only heat up the laser and eventually the device will burn out.

The effect that was just explained is called the runaway problem. This is a serious problem in InGaAsP lasers. The temperature sensitivity of these lasers is still under investigation. Almost all investigators agree on the fact that the poor temperature behavior is due to losses inside the laser. These losses include, nonradiative recom-

bination processes like Auger recombination inside the active region, ohmic losses in the the structure due to current spreading, current leakage, contact resistance, and many other losses. While the exact reasons can differ from one laser to the other, and while it is probably due to various mechanisms (not just one), it is the author's feeling that in almost all InGaAsP lasers one of the most important loss mechanism is Auger recombination. This is probably one of the most important processes inside the active region which creates acute temperature sensitivity above 255 K and specially around room temperature.

It is very interesting to look at the light output of InGaAsP DH lasers in CW operation considering Auger recombination as the main loss mechanism. It is important to see how light output, threshold current, T_0, and other threshold parameters behave when we assume Auger recombination as the main loss. This study can be very helpful in predicting light output versus injected current, injected current versus temperature and thermal behavior of other laser parameters. There is a need for a better theoretical understanding of these lasers, and this is one of the goals of this study.

The purpose of this study is to investigate the behavior of InGaAsP/InP DH lasers, and the effect of internal heating on their output. We will use a model proposed by Albert Haug (1985) to calculate the number of injected carriers inside the active layer at different temperatures. Then, using Haug's model, laser threshold current density is calculated [18, 19, 20]. The results obtained by this model can then be utilized to obtain other laser parameters such as quantum efficiency and light output power. In order to obtain a more exact prediction, one needs to know the average

temperature of the active region. To obtain better values of temperature inside the active region we will use a two dimensional model of the temperature distribution. This way, we will get a better idea of the temperature values inside the active region, and will use them to predict the behavior of these lasers under CW operation. It will be very interesting to predict light output power (P_L) versus injected current. With the help of the model developed here, one can investigate threshold parameters as well as the output behavior for these lasers. Doing so, we can get a better understanding of how to control injection current in these lasers in order to get a more stable and efficient behavior.

We assume only two kinds of losses, a simple internal optical loss and Auger recombination as the most dominant carrier loss mechanism in the laser. This will be the first time that this type of modelling is applied to predict the light output behavior of InGaAsP lasers under CW operation. Although, it may be simplistic to assume only one carrier loss mechanism, it is a starting step for developing a model that predicts the behavior of InGaAsP/InP DH lasers. If the model is successful other losses can be added in future studies. It should be pointed out that there are some investigators who question the importance of Auger recombination effects in the behavior of such lasers. Despite this the author believes that this study will point out (even though very heuristically like many other phenomenological models) the importance of Auger process in both pulsed and CW operation of InGaAsP lasers.

2. LASER PARAMETERS

There are many microscopic phenomena taking place inside a semiconductor laser which are not very well understood. In fact, in most cases our understanding of the laser threshold is only based on a set of assumptions and speculations. One of the purposes of this study is to make specific assumptions about some of these microscopic phenomena and see their effects on the macroscopic behavior of the injection laser. Our ultimate goal is to make a model to describe and predict the behavior of macroscopic parameters of InGaAsP lasers (i.e., I_{th} and P_L).

Our understanding of these lasers is based on the macroscopic entities that we can directly measure such as injected current, power output and so on. That is why, before going any further, we need to perform a step by step analysis and derivation of the general laser formulation. In doing so, it is essential to introduce the nomenclature for the study, as well as to clarify definitions and reexamine the threshold conditions.

2.1 Threshold Condition

As mentioned before, the threshold condition is reached when the current injection level into the laser is just enough to achieve lasing. This process starts once population inversion is achieved. As illustrated in Figure 2.1, under high current injection the upper states (in the conduction band) of a direct band gap semiconductor

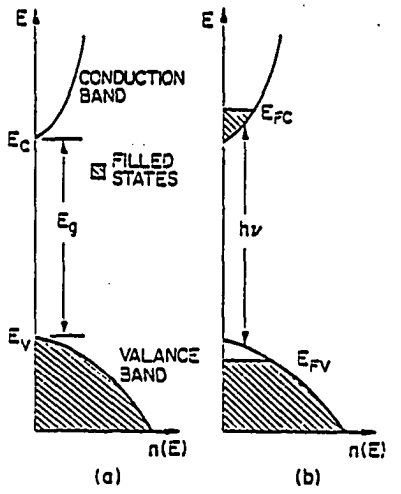

Figure 2.1: Energy versus density of states in a direct band semiconductor for two cases (a) Equilibrium. T=0 K (b) Inverted. T=0 K [7. page 720]

are filled up to the energy level ξ_n with electrons (measured from the bottom of the conduction band, $\xi_n = E_{fc} - E_c$). At the same time the lower states (in the valence band) are filled up to the energy level ξ_p with holes (measured from the top of the valence band, $\xi_p = E_{fv} - E_v$).

In the case of population inversion, the states that are involved in the process are occupied and will not be available for absorption (see Figure 2.2). So in the ideal case, the states within the ξ_n and ξ_p ranges in the conduction and valence bands respectively are already occupied. At such a point, an incident photon can only stimulate emission. Once the emission takes place the next photon can be absorbed and generate an electron-hole pair to fill the two empty states. For a system under

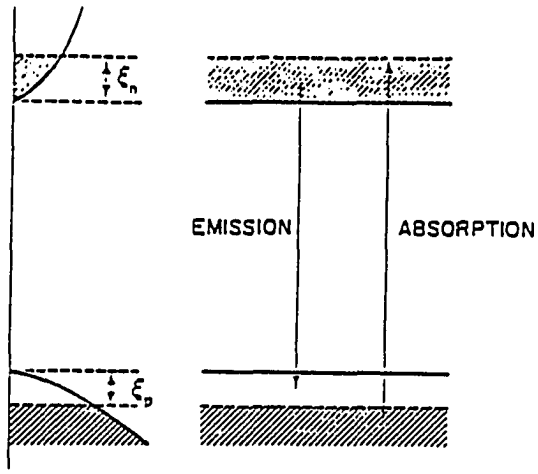

Figure 2.2: Degenerate band occupation at population inversion [11, page 216]

population inversion the necessary condition for laser action will be

$$\xi_n + \xi_p \geq 2k_B T$$

where k_B is the Boltzman constant and T is the absolute temperature, according to the quantum mechanical calculation done by Bernard and Duraffourg in 1961 [21]. This is the condition necessary to make the recombination rate greater than the absorption rate.

When spontaneous emission takes place, it will enhance stimulated emission. We have a photon flux which is not yet useful for laser operation. To utilize this photon flux and get laser action, two conditions need to be satisfied:

- The radiation needs to be coherent
- The gain must be at least equal to the losses.

Effective utilization of laser geometry can favor the growth of only one frequency and phase. This selective amplification is due to positive feedback of the electromagnetic waves that form a standing wave pattern inside the cavity. As of today, many structures and methods of achieving the desired coherence and gain have been suggested. However, probably the most popular and basic one is the Fabry-Perot-Cavity structure which was previously mentioned.

It is important to know that almost all structures use the Fabry-Perot-Cavity structure with two cleaved sides for enhancing the desired gain, together with other frequency selective devices. For good examples one can refer to two very popular lasers C^3 (Cleaved Coupled Cavity) and DFB (Distributed Feedback) [2, 4, 7]. Due to the popularity and the simplicity of Fabry-Perot-Cavity, in this study we will base all arguments on such a structure.

2.1.1 Simple model

To achieve lasing, gain must be at least equal to losses. This can be done in two steps. First by increasing the current injected into the laser, one can achieve a higher rate of spontaneous emission. Consequently, we will also get a higher rate of stimulated emission in all directions. Then, as we increase the injection level the laser cavity helps pick coherent output in one preferred direction. Eventually there will be an injection level at which the gain (related to the rate of increase of directional stimulated emission) will be high enough to overcome the losses. Such an instant is called the threshold point. To see this, consider Figure 2.3 representing a one dimensional Fabry-Perot-Cavity. Let us assume this cavity has two partially

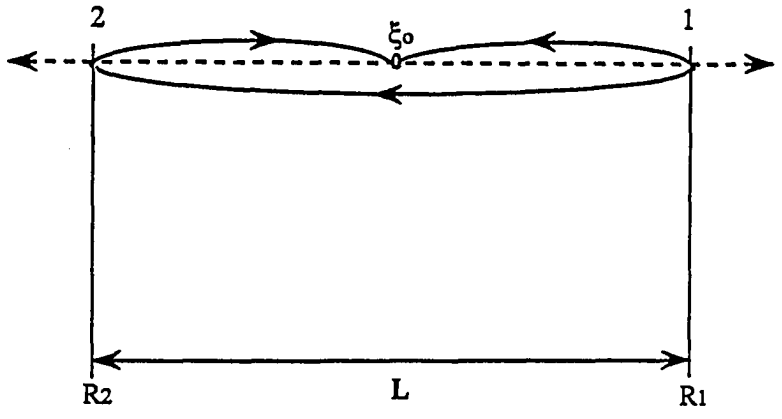

Figure 2.3: A simplified picture of Fabry-Perot-Cavity

reflecting sides 1 and 2 with reflection coefficients R_1 and R_2. The cavity has length of L as shown in the Figure.

Consider a point at the center of the cavity. Let us say there is light emission of intensity ξ_0 at that point. If the intensity is a high enough the radiation will be reflected off of surface 1 with the reflected intensity of $R_1\xi_0$. This fraction will go toward side 2 and on its way it will stimulate more radiation. After reflection from side 2 the intensity will become $R_2R_1\xi_0$. This in turn will begin to return to the starting point. As the radiation travels inside the cavity it also stimulates more and more coherent emission part of which will be absorbed. If g represents incremental energy flux created per unit length as radiation travels inside the cavity, then after traveling x units of length, ξ_0 (initial radiation) gains energy and becomes $\xi_0 e^{gx}$. On the other hand, there will be losses which can be represented for the same distance as $\xi_0 e^{-\alpha x}$, where α represents energy loss per unit length inside the laser [11, page 217].

One can write the light intensity at the center of the cavity after reflection from the two sides, adjusted for gain and absorption as

$$\xi = \xi_0 R_1 R_2 e^{2(gL-\alpha L)}$$

Laser action is achieved when the traveling beam with coherent photons has the same intensity (ξ_0) after the round trip journey. This means that the initial flux has gained enough to balance the losses. So, one can write

$$\xi_0 = \xi_0 R_1 R_2 e^{2(gL-\alpha L)}$$

which can be rearranged as

$$gL - \alpha L = 0.5 \ln(\frac{1}{R_1 R_2})$$

This is the threshold condition for a laser that has all the radiation, gain, and losses confined inside the active region (100% confinement). This development contains assumptions of uniform current injection, coherent gain, and coherent losses inside the active region for developing the above equation.

In reality there is no laser with 100% confinement. If the optical confinement is not completely within the active region (i.e., in a DH laser with Γ as the confinement factor), then some changes will be required. First of all the gain at threshold will be Γg_{th}, since we will be only interested in the gain inside the active region. On the other hand, the total losses (α_T) can be due to losses both inside and outside the active region. Theoretically they both can contribute and can compete with the gain. So, one can say

$$\alpha_T = \Gamma \alpha_a + (1 - \Gamma)\alpha_c$$

where α_T is the total losses in the laser, α_a and α_c are the losses of the active and cladding layers respectively. Letting $R = \sqrt{R_1 R_2}$, the threshold gain can be represented as

$$\Gamma g_{th} = \alpha_T + (\frac{1}{L}) \ln(\frac{1}{R}) \tag{2.1}$$

which expresses the threshold condition quantitatively.

2.2 Carrier and Optical Losses

When the current flow (injection level) into a semiconductor laser is increased, charge carriers (electrons and holes) are injected into a thin region called the active region, where they can recombine and emit radiation. At the threshold the number of injected carriers is high enough to provide a sufficient emission rate for laser action. However, in reality, there are many unfavorable mechanisms which prevent lasing. These mechanisms can be any of the number of losses inside the laser structure. The amount of input current required to achieve lasing is directly proportional to the losses that appear in the laser. More injection means an increase in the power input which results in heating of the laser. Unfortunately an increase in the laser temperature results in even more losses. One can easily see that such a cycle can result in the destruction of the laser chip.

Major loss mechanisms inside a laser (which compete with the gain) will either absorb radiated photons, or cause a reduction of injected carriers. In the latter case the mechanism is called carrier loss, and in the former it is called optical loss. Carrier loss can occur according to two major categories. In general, any phenomenon which reduces the number of carriers inside the active region without resulting in

radiative processes is called carrier loss. The two major classes of carrier loss are nonradiative recombination and current leakage. In the former type, electrons and holes will recombine without resulting in radiation, while in the latter type they escape from the active region without contributing to the radiation. In both cases, however, the result will be a need for a higher gain to overcome the losses, which in turn means a higher injection level. It is important for the purpose of this study to have a good understanding of these losses. Thus, we must briefly review the two major loss mechanisms inside the semiconductor lasers.

2.2.1 Optical loss

The most trivial way of losing photons in a semiconductor is through its interaction with an atom's bound electrons. In this way the photon can be absorbed and an electron-hole pair generated. This happens when the valance band electron absorbs the photon and obtains sufficient energy to jump into the conduction band. It will eventually recombine and return to the lower state, but it will not necessarily occur radiatively or by stimulated emission.

Another kind of optical absorption occurs when a photon is absorbed by the lattice structure and results in lattice vibrations (also known as a phonon) and lattice heating. Such an effect by itself can increase the chance of even more of the same type of absorption, which will cause more heating.

Free carrier absorption is another kind of optical absorption. It occurs when an electron in the conduction band absorbs a photon and moves to a higher state (in the conduction band). Figure 2.4 shows this mechanism. The electron at the higher

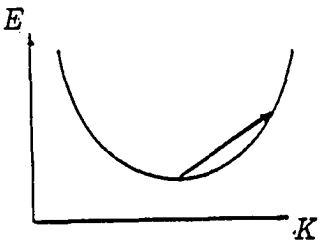

Figure 2.4: Transition of a free electron in the conduction band valley under a free carrier absorption process [11, page 74]

state is really not useful for the purpose of laser radiation and can also cause lattice heating and carrier loss as it drops back to a lesser energy state.

There is also a possibility of absorption by impurities and defects. It is possible for some impurities like metal oxides, hydrogen, and similar atoms and molecules to absorb photons and get excited to a higher state. They can even release their electrons to the conduction band and remain as deep inter-valence ions. In this way they are capable of absorbing even more photons as well as acting as traps for recombining electrons. Figure 2.5 summarizes these processes.

2.2.2 Carrier loss

Under population inversion and high injection, carrier loss occurs whenever any mechanism decreases carrier concentration without resulting in a radiative transition and further stimulation. A homojunction laser is a good example of such an effect. In such a laser, carriers can flow out of the active region very easily since the structure uses no confinement mechanism. Hence, due to the carrier loss in its active region, homojunction lasers require higher current injection levels compared to DH lasers.

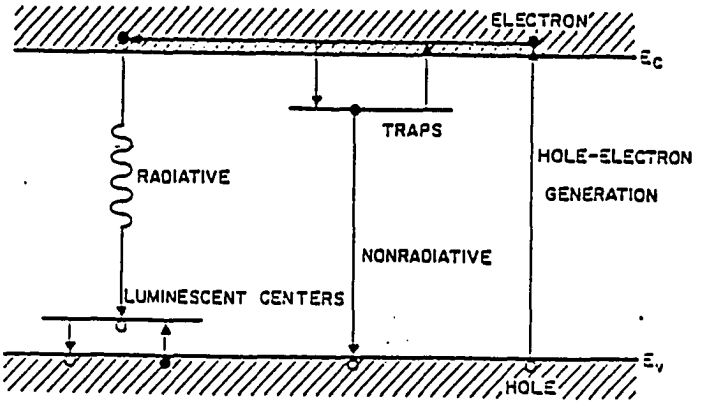

Figure 2.5: How traps can cause nonradiative recombination [7, page 687]

Carrier loss can take place as a result of many different mechanisms. There can be processes called nonradiative recombination during which electrons and holes recombine without resulting in the appropriate radiation. Whereas a radiative process is a definite and explicit process during which a photon is emitted. A nonradiative process is a very indefinite action. The term vaguely indicates any mechanism that does not result in a radiative photon. It is left to one's imagination and creativity to construct an acceptable model. That is why it is very complicated to think of models based on such processes. A degree of uncertainty is an inherent characteristic of models which are based on nonradiative recombination losses.

It is worth mentioning that an experimental study of nonradiative recombination is generally very difficult. The process manifests itself only by the absence of an expected by-product. On the other hand, we can only measure entities like emission efficiency, carrier lifetime, and the kinetics of the recombination process in response to some variables such as temperature or injection level [18, 20, 22, 23, 24]. Con-

sequently, the final judgment is guided inductively as opposed to deductively [11, page 160]. Through the years of active research on this subject, many mechanisms like surface recombination (carriers get absorbed by dangling bonds at the surface of the semiconductor), lattice defects (ionized deep intervalence band recombination centers), and many similar processes (which are temperature dependent) have been suggested. There is some strong evidence indicating the processes of carrier leakage and band-to-band Auger recombination are the most significant carrier loss mechanisms for InGaAsP lasers [18, 20, 25. 26, 27].

In a DH laser with a nonperfect lattice match between the active layer and surrounding (cladding) layers, some carriers can escape from the active layer (or be absorbed by the ions at the boundaries) [28, 29, 30]. Such an action can take place under two major mechanisms. The first one occurs due to the diffusion process. Under high injection the active layer will be saturated with free carriers, while the cladding is virtually empty of such carriers. Consequently, carriers can leak out of the active layer by diffusion under the concentration gradient effect. This causes a current flow which is called the diffusion current. The second one occurs when the carriers have some kinetic energy when reaching the boundary of the active and cladding layers. If they leak out, it will be called the drift leakage current [30]. There is some experimental evidence which indicates the effect of leakage current losses is more important for ternary compound lasers such as AlGaAS and can be made less important in InGaAsP DH lasers [18, 28, 29, 30].

It is widely accepted that the Auger recombination process (AP) is one of the most important loss mechanisms in InGaAsP lasers. In AP the energy released by

a recombination process is immediately absorbed by another electron jumping into a higher state. This can also effectively create phonons to heat the lattice. AP is like a complicated free carrier absorption process. It involves three carriers (which can consist of two electrons and a hole or two holes and an electron) and deactivates them for the purpose of laser action. Many experimental results seem to point to the Auger Processes as the most important inherent loss mechanism for InGaAsP lasers. It seems there is no way to eliminate this effect for such lasers. However, there are ways to fabricate these lasers in order to reduce the other carrier loss mechanisms like leakage. It is worth mentioning that nowadays with the introduction of quantum well structures the AP effect can be reduced, but not abolished. For the purpose of our simple InGaAsP DH lasers AP needs to be considered as an inherent loss mechanism, since there is no fabrication process that can reduce Auger effect. That is why we will consider AP as the major nonradiative loss mechanism to see its effect on the output of InGaAsP DH lasers. In the next chapter, AP will be discussed in a more detail.

2.3 Generation, Recombination, and Lifetime

In general, radiation emission can be considered as the inverse of the absorption process. A carrier occupying a higher than equilibrium energy state, cannot stay there forever. It will eventually decay to the original state. The average time that the excited carrier spends in the higher energy state is called average lifetime τ. The transition to an empty lower energy state is called the recombination process. The rate for recombination is determined by the product of the density of the higher energy state (n_u, number of carriers in the upper state per unit volume), the density

of the lower state (n_l, number of carriers in the lower state per unit volume) and the probability for one carrier per unit volume in the upper state to make a transition to one vacancy per unit volume in the lower state (P_{ul}). Then the recombination rate can be defined as

$$R = n_u n_l P_{ul}$$

In a direct bandgap semiconductor, when excess carriers are introduced (by applying an external current) there will be a high probability for electron-hole recombination. This is due to the fact that the bottom of the conduction band and the top of the valence band occur at the same momentum and thus no additional crystal momentum is required for transition across the bandgap for radiative recombination [2, page 43]. For such a system the recombination rate is given by

$$R = B_{rad} np \tag{2.2}$$

where the proportionality constant B_{rad} is called the radiative recombination coefficient.

When excess carriers are introduced in a doped medium (i.e., p-doped) with doping of p_0, equation 2.2 becomes:

$$R = B_{rad} n_i (n_i + p_0) = B_{rad} n_i^2 + B_{rad} n_i p_0$$

where n_i is the number of carriers for an intrinsic medium and p_0 is number of holes due to doping. In a semiconductor the total recombination rate R(n) has three parts, which can be summarized as follows

$$\begin{aligned} \text{R(n)} = {} & \text{Radiative recombination} + \text{Internal optical loss} \\ & + \text{nonradiative recombination (NRR)} \end{aligned}$$

If we assume that the optical loss is proportional to the number of carriers with K as the proportionality constant, then for a p-type active region in a semiconductor laser one can write,

$$\begin{aligned} \mathrm{R(n)} &= B_{rad}\ \mathrm{n\ p} + \mathrm{K\ n} + \mathrm{NRR} \\ &= B_{rad}\ \mathrm{n\ (n} + p_0) + \mathrm{K\ n} + \mathrm{NRR} \\ &= B_{rad}n^2 + \mathrm{n}(B_{rad}\ p_0 + \mathrm{K}) + \mathrm{NRR} = B_{rad}n^2 + \mathrm{A\ n} + \mathrm{NRR} \end{aligned}$$

We can also relate lifetime to recombination rate using

$$R(n) = n/\tau \tag{2.3}$$

If we assume no nonradiative recombination exists (NRR = 0) and use the definition given in equation 2.3 we can say

$$1/\tau = B_{rad}n + A$$

This linear proportional relation of $1/\tau$ and n has been experimentally observed for GaAlAs lasers [24, 28, 29, 30, 31, 32]. However, the reports on almost all InGaAsP lasers show a distinct nonlinearity [28, 29]. That is why many investigators have suggested the following empirical power series for recombination rates and lifetimes of an undoped active layer [25, 28, 29, 33, 34, 35].

$$1/\tau = A + Bn + C'n^2 + Dn^3..... \tag{2.4}$$

$$R(n) = An + Bn^2 + C'n^3 + Dn^4..... \tag{2.5}$$

It is important to recognize that in equations 2.4 and 2.5 the the first terms on the right hand side represent the internal optical losses. The second terms which indicate

a two body process represent radiative recombination. The third terms, which are indicative of a three body interaction, represent nonradiative recombination. There is some experimental evidence that in InGaAsP lasers the n^3 term is always present. However, depending on the type of layering and method of fabrication, there can also be higher terms indicating leakage current effects [18, 28, 33].

Auger recombination (which is a three body process) manifests itself in the n^3 term. Since the leakage current of many lasers can be neglected compared to the Auger effect term[18, 23, 25, 28, 29, 34, 35, 36], we can write

$$1/\tau \cong A + Bn + Cn^3 \tag{2.6}$$

and

$$R(n) \cong An + Bn^2 + Cn^3 \tag{2.7}$$

It should be mentioned that for AlGaAs lasers the Auger effect is negligible. This result has been experimentally verified. Many investigators have studied the behavior of AlGaAs and it seems that the majority agree on the explanation. They agreed to be due to the fact that in that particular material (AlGaAS) Auger recombination effect is overcome by changes of the radiative coefficient [29, 34].

The values of A, B, and C, which are very important quantities for InGaAsP lasers, have been both experimentally and theoretically studied [18, 20, 28, 33]. Figure 2.3 shows a typical measurements of these coefficients. One can see that the real temperature dependences are in the B and C terms. The typical values for these numbers are given in many studies and indicate the following averages, for A = $10^8 s^{-1}$, B =10^-12 to $10^{-10} cm^3/s$, and C = $10^{30} cm^6/s$ [18, 33]. These coefficients

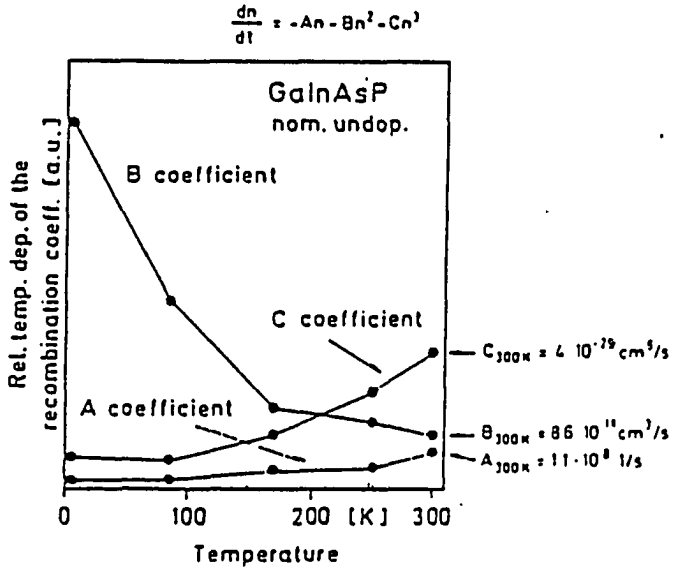

Figure 2.6: Temperature dependence of A, B, and C coefficients in a nominally undoped InGaAsP laser [33]

and their effects will be discussed in the next chapter.

2.4 Threshold Current

One of the most important parameters for semiconductor laser operation is the threshold current I_{th} (or the threshold current density J_{th}), which is defined as the minimum current (or current density) required for lasing to take place. It is very important to be able to predict the behavior of the laser threshold current, because it leads to the prediction of laser behavior. That is why the study of this parameter has occupied many investigators' time and effort, and research groups have devoted years of labor to obtain a better understanding of laser threshold current and its behavior.

2.4.1 Basic current density equation

In a semiconductor laser, the gain g (incremental optical energy flux per unit length) depends on the current density. Gain can be expressed as a function of nominal current density J_{nom}, where nominal current density is the current density required to uniformly excite a 1 μm thick active layer, for a laser with unity quantum efficiency (quantum efficiency η is defined as number of carriers generated per photon). Then the actual current density can be written as

$$J = J_{nom} d/\eta \ A/cm^2 \tag{2.8}$$

where d is active layer thickness in μm and η is the quantum efficiency. It can be seen from the above equation that for d = 1 and η = 1 we get the current density to be the same as J_{nom} as it was defined. The gain which increases linearly for most cases with J_{nom}, can be represented by [37].

$$g = (g_0/J_0)(J_{nom} - J_0) \tag{2.9}$$

where g_0 and J_0 are constant values for the given laser. Using equations 2.8 and 2.9 we can get a general equation for threshold current density as

$$J_{th} = J_0 d/\eta + \frac{J_0 d(\alpha + \ln(R)/L)}{g_0 \eta \Gamma} \tag{2.10}$$

Despite the fact that this equation is not very useful for calculation of J_{th}, unless one has the values of every term, it can be very helpful intuitively. It indicates the very important observation that J_{th} decreases when η, Γ, L, and R increase, and when d and α decrease. Probably the most important point in the equation, which may seem trivial, is the fact that, when losses increase, J_{th} of the laser will also increase.

2.4.2 Temperature dependence of J_{th}

J_{th} of InGaAsP lasers shows a very strong temperature dependence at room temperature and above. Empirically, J_{th} is shown to have exponential dependence on temperature. As suggested by Pankove this dependence has the form [38],

$$J_{th}(T) = J_0 exp(T/T_0)\ A/cm^2$$

where J_0 is the current density at $T = 0$ K, and T_0 is the characteristic temperature of the laser diode. The value of T_0 is suggested to depend on doping, loss mechanisms, and many other material characteristics. Ternary lasers like AlGaAs, have higher values of T_0, which indicates that they are less temperature sensitive (see Figure 2.7). However the quaternary compound lasers made of InGaAsP, show two different regions of operation. T_0 is about 90–100 K for temperatures below 255–266 K , and for the active layer temperatures above 260 K T_0 is about 50–60 K. Figure 2.8 shows a typical behavior of the current density of InGaAsP lasers.

The exact reason for this T_0 behavior is not well known. However, all data suggest that the excess losses which appear in the laser cause higher J_{th} and lower T_0. Looking at the behavior of InGaAsP lasers it seems that for active layer temperatures above 255–260 K some losses start to increase to much higher values than they have temperatures below 250 K. Consequently, we see low values of T_0 at the room temperature and above due to an increase in the loss mechanisms with a break point of about 250–260 K.

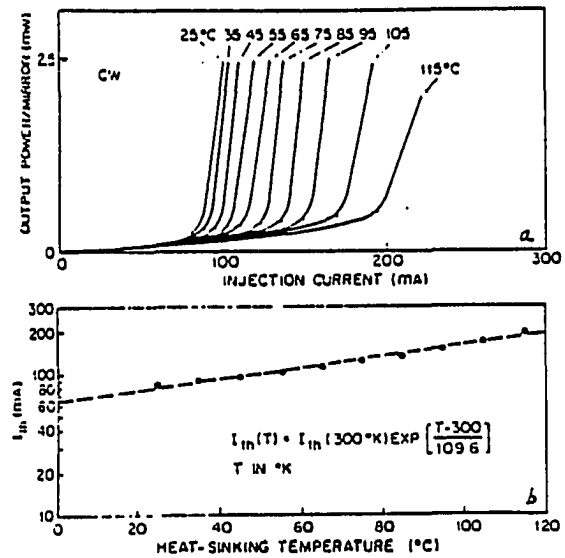

Figure 2.7: Light output versus diode current and temperature dependence of CW current threshold for a stripe-buried heterojunction AlGaAs/GaAs laser [39]

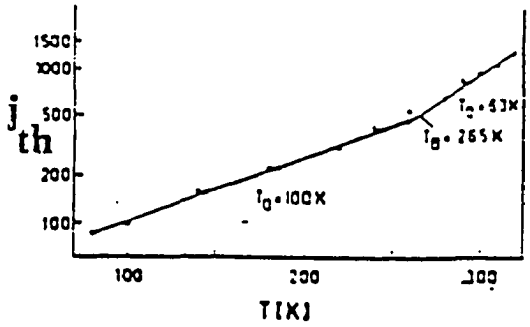

Figure 2.8: Pulsed J_{th} of InGaAsP/InP DH laser as a function of active layer temperature [40]

2.4.3 Empirical models for current

In a semiconductor one can write the continuity equation in the following form

$$\mathrm{dn/dt} = \text{Generation rate} - \text{Recombination rate}$$

where n is the injected carrier density. This injection is done by applying current I to the laser chip. An increase in laser injection current can increase the gain by increasing the generation rate inside the active region. So, we can say

$$Generation\ Rate = I/eV = G(n)$$

where V is the active layer volume and e is electronic charge. Conversely, by recognizing that the recombination rate is given by

$$R(n) = n/\tau$$

where τ is carrier lifetime, we can use the generation rate equation together with the continuity equation and write

$$dn/dt = I/eV - R(n)$$

In the steady state situation (dn/dt — 0) we can find the current using

$$I = eVR(n) = eVn/\tau \tag{2.11}$$

Looking at equation 2.11 it is easy to conclude that it represents the current level at which the generation and recombination rates are equal. Hence, equation 2.11 represents the threshold current by definition. Consequently we can write

$$I_{th} = eVR(n_{th})\ (amperes) \tag{2.12}$$

Assuming that the only losses inside the laser are due to internal optical losses and nonradiative Auger recombination, using equations 2.7 with 2.12 we can get the approximation formula for threshold current of an undoped active region,

$$I_{th} = eV(An_{th} + Bn_{th}^2 + Cn_{th}^3) \tag{2.13}$$

This is a very interesting equation. It shows that by knowing the values of A, B, C, and n_{th} of the laser the threshold current can be approximated.

It is important to remember that B, C, and n_{th} are all strongly temperature dependent quantities. Even though in using equation 2.13 one does not need to deal with T_0 values explicitly, there is an implicit temperature dependence in the parameters used in it. That is why it is probably better to write the threshold current in the following temperature explicit form

$$I_{th}(T) = eV\left(An_{th}(T) + B(T)n_{th}^2(T) + C(T)n_{th}^3(T)\right) \tag{2.14}$$

2.5 Quantum Efficiency

One of the more interesting parameters of a semiconductor laser is quantum efficiency. By definition it is a measure of the ratio of output light power to the input power. In a semiconductor laser there are two important types of quantum efficiencies and they are related to one another. For the sake of clarity it is better to consider the two types of quantum efficiency separately.

2.5.1 Internal quantum efficiency

Internal quantum efficiency, η_i, is defined as the ratio of the radiative recombination rate to the total (both radiative and nonradiative) recombination rate in the active region. Thus, one can say,

$$R_r = \text{Radiative Recombination Rate}$$

$$R_{nr} = \text{Nonradiative Recombination Rate}$$

$$R_t = \text{Total recombination rate}$$

$$\eta_i = R_r/R_t = \left(\frac{R_r}{R_r+R_{nr}}\right)$$

Using the fact that R(n) = n / τ one can rewrite the above equation as,

$$\eta_i = \frac{\tau_r^{-1}}{\tau_r^{-1}+\tau_{nr}^{-1}} = (1+\tau_r/\tau_{nr})^{-1} \tag{2.15}$$

Below threshold the internal quantum efficiency is for spontaneous radiation. It is related to the spontaneous parts of radiative and nonradiative carrier lifetimes. On the other hand, for above threshold (which is what we are interested in), our real concern is in regard to stimulated emission lifetimes and recombination rates. The values of the nonradiative lifetimes in equation 2.15 will change a great deal from below to above the threshold. For above the threshold we can write the stimulated quantum efficiency as,

$$\eta_{stim} = (1+\tau_r/\tau_{nr})^{-1} \tag{2.16}$$

For InGaAsP lasers above the threshold, the value of τ_r/τ_{nr} is very small, since experimental results show τ_r is about 4 orders smaller than τ_{nr} [22, 41]. Hence, we can consider $\eta_{stim} = 1$ for above the threshold considerations. It should be mentioned that in the event of leakage current in a particular laser diode, this number can be

affected, but in the case of a laser with small leakage current our approximation is valid [42, 43].

2.5.2 Differential quantum efficiency

Differential quantum efficiency is defined as the number of photons emitted per radiative electron-hole recombination. The external photon emission rate (or number of photons emitted) is the difference between the stimulated rate and the absorption rate. This can be summarized as

$$\eta_d/\eta_i = (g_{th} - \alpha)/g_{th}$$

Using the result of equation 2.1 for g_{th} we get,

$$\eta_d = \eta_i \left(\frac{\ln(1/R)L}{\xi\alpha_a + (1-\xi)\alpha_c + \ln(1/R)/L} \right) \tag{2.17}$$

where ξ is the confinement factor of DH laser.

There have been some models for explaining the behavior of differential quantum efficiency [22, 41]. However, the simplest way to explain the behavior is by using the empirical formula given as

$$\eta_d = \eta_0 exp(-T/T_E) \tag{2.18}$$

where η_0 is a reference efficiency and T_E is the characteristics temperature for quantum efficiency. In reality T_E is also temperature dependent, but for InGaAsP one can approximate it with two values. The first value, which is typically about 150 K, is for active layer temperatures below the room temperature, and the second value which is about 50 K is for temperatures greater than room temperature. The reader may recall that there is also a break point for the threshold current characteristic

temperature T_0. However, as tempting as it may sound to assume the same break points for both T_E and T_0, the experimental results do not justify this assumption. In general the break point of the differential quantum efficiency and the threshold current are different and they are not necessarily sensitive to the same type of losses for InGaAsP lasers.

2.6 Laser Power

A large portion of the power supplied to a laser is dissipated internally as heat. For a semiconductor laser the internal power dissipation consists of:

- Joule heating: It takes place due to Joule losses or I^2r type heating, where r is the laser series resistance. It is important to know that Joule heating is probably highest in the layers around the active region where current spreading takes place [44, 45].

- Nonradiative recombination inside the active region: This heating is due to the fraction of the power within the active region that never gets used in the radiative process.

- Optical losses: Optical losses cause heating due to the fraction of radiation power that never leaves the laser and is absorbed inside the structure. Optical loss can be from absorption of stimulated radiation inside the active region, or from absorption of spontaneous radiation both within the active region and in the adjacent layers. However, in most lasers the losses within the active region is the overwhelming part.

In power calculations, differential quantum efficiency will account for the last two types of losses. We can write the dissipated power as,

Power Dissipated = Input Power - Output Power

As we start to inject current into a laser, until we get to the threshold all the input power will be dissipated (since below threshold the lasing light output power will zero). Therefore, up to the threshold all the input power will go towards heating the laser. At threshold a cooling process takes place. This is due to the fact that from then on some of the supplied power will be emitted out. In a sense, the light output will carry a portion of the input power out of the laser structure. The laser will not heat up excessively while there is light output. If we keep pumping current into the laser, the losses will start to dominate and there will be a point at which the lasing stops. From then on, all the input power will be dissipated and the laser will start to heat up until it burns out.

Dissipated power is the power due to ohmic losses (I^2r), and the part of the power that is not used for lasing. If V_j and I represent the voltage across the active layer and the injected current respectively we can write,

$$P_d = (1 - \eta_d)IV + I^2r \tag{2.19}$$

where V is the voltage across the laser chip ($V = V_j + Ir$). On the other hand, power output can be given as,

$$P_L = \eta_d(I - I_{th})V \tag{2.20}$$

where I_{th} is the threshold current. One should note that this equation is only valid for $I \geq I_{th}$. If I is less than I_{th} it will result in negative power which is not physically

acceptable. This equation has an interesting behavior. As the injection current I starts from zero and increases, we see no light output until the threshold is reached. This is indicated as a negative P_L, although physically there can not be a negative power we use the negative results as the indicative that the lasing has stopped. Then, from the point that I and I_{th} are equal (P_L is zero), increasing the input current (I) will result in an increase in P_L. Under CW operation, as I increases, so will the active layer temperature, which will result in an increase of I_{th}, and the laser requires more current to keep lasing. This process continues and as the active layer temperature increases more losses appear in the active layer which in turn reduces the output power. After a maximum power is reached, an increase in the injected current will result in a decrease in the output power. That is the point that losses start to dominate. If we pump enough current into a laser it will eventually stop lasing.

In reality P_L, η_d, and I_{th} are all strongly temperature dependent quantities. Consequently, one can rewrite a more precise equation as

$$P_L(T) = \eta_d(T)\left(I - I_{th}(T)\right)(V_j + Ir) \tag{2.21}$$

where T is the average active layer temperature.

In order to find the light output power for a given temperature T and a given current I, one needs to find η_d and I_{th} at the given temperature, and use them together in the equation 2.21 to get the result. The purpose of this study is to use Haug's model [18] to get $I_{th}(T)$ and Asada and Suematsu's [22] model for $\eta_d(T)$ and look at the behavior of the light output power of InGaAsP DH lasers assuming Auger process as the main nonradiative loss inside the active region. In the following chapter, we will briefly discuss the detail of these models for I_{th} and η_d.

3. N_{TH}, J_{TH}, AND η_{th}

In order to formulate laser behavior at threshold, a good understanding of laser characteristics is required. In the previous chapter, definitions as well as basic operational characteristics were discussed. In this chapter, we will use the previously defined concepts to get a quantitative evaluation of laser parameters.

The three most important laser quantities to understand are threshold current density J_{th}, threshold carrier density n_{th}, and external quantum efficiency at threshold η_{th}. When these are known, laser behavior can be predicted as shown in Chapter 2. In our discussion, we have assumed two kinds of losses and these are indicated in the equation for threshold current density of a laser with an undoped active region:

$$J_{th}(T) = An_{th}(T) + Bn_{th}^2(T) + Cn_{th}^3(T) \tag{3.1}$$

The first term on the right hand side is the basic internal optical losses due to cavity structure, material losses (like dielectric absorption), and other linear losses. The second kind of loss, which is believed to be responsible for the acute temperature behavior of InGaAsP lasers, is the Auger recombination (AR). This is manifested by the third term. AP is a carrier loss mechanism which involves three interacting bodies. In our study, we assume that AP is the most important carrier loss mechanism inside the active region. That is why Auger phenomena need to be discussed before going

any further.

3.1 Auger Phenomena

Auger process was first suggested by Beatie and Landsberg in 1959 to explain losses in InSb [46]. Their results showed that Auger process (AP) could explain their problem successfully. Soon after that, the same idea was applied to other materials (Si, and GaAs) for the explanation of nonradiative losses [47].

Auger effect is a proposed mechanism for nonradiative electron-hole recombination in many semiconductors. AP requires a relatively large free carrier density to make a significant contribution and become an important factor. Since inside of the active region of a semiconductor laser high carrier injection is required for lasing to take place , it is a favorable environment for Auger process to take place [48, page 46]. Consequently, AP has been proposed as a major loss mechanism in some semiconductor lasers.

There have been some experimental reports indicating loss mechanisms involving three interacting bodies play important role in the determination of the threshold behavior of carrier lifetime and current density [24, 25, 29]. Since AP is a three body process, and there is experimental evidence of the importance of such phenomena in InGaAsP material [26, 27, 34], it has been proposed that AP is an important loss mechanism in InGaAsP lasers [8, 18, 19, 29, 31, 33, 35, 41, 42].

AP involves the interaction of three carriers. In the band-to-band AP (as shown in Figure 3.1) there can be two electrons and a hole. This way two electrons collide which causes one to decay and recombine with a hole in the valence band. Meanwhile,

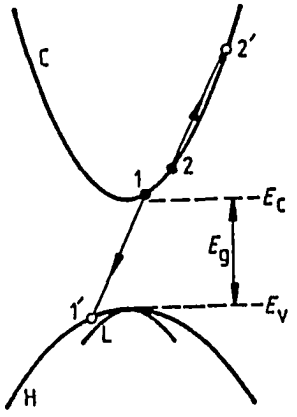

Figure 3.1: A basic conduction band Auger process [36, page 4160]

the energy released be the recombination will cause the other electron to move to a higher state in the conduction band. This new electron is called a hot electron. It eventually transfers its energy to the lattice and heats up the laser. Such a recombination process can take place with two holes and one electron which will result in an energetic hole as a by-product.

3.1.1 Auger calculation

Many investigators have studied Auger lifetime (τ_a), Auger recombination rate (R_a), and Auger coefficients of the injected carriers in 1.3 μm InGaAsP [25, 26, 34]. These studies involve extensive, laborious, and nontrivial modelings and calculations. We will not go into the details of calculation process in this study. We will merely look at the kinds of processes involved, and summarize the important ones.

There can be six different types of band-to-band Auger recombination processes

as shown in Figure 3.2. Let us assume C stands for conduction band, H for heavy hole band, and S for spin split-off band. The type of processes involved can be CCCH meaning one electron from the conduction band recombines with a hole in the valence band (which is the heavy hole) and the energy is used by an electron in the conduction band to go to a higher state. There are two electrons and one heavy hole involved in the recombination. On the other hand there are three electron and one heavy hole states in the process. Abbreviations such as CCCH stand for the types of states involved in the recombination process.

Whenever there are three bodies interacting inside a solid there are all combinations of energy and momentum exchanges that can take place. Consequently, certain processes may or may not involve a phonon. It is not hard to see that there can be two general categories of AP, phononless, and phonon assisted processes. In the first category the recombination does not involve a phonon. However, there can be a case that a phonon facilitates the process which will be called phonon assisted AP. Figure 3.2 shows the two types of Auger recombination. Phononless processes are the three figures in 3.2a, while the figures in 3.2b are phonon assisted types. When in the CCCH process a phonon is involved (which is called phonon assisted CCCH) we call it CCCHP, where P stands for phonon assisted. This particular method of abbreviation for such processes has been suggested by Takeshima and is commonly used [49].

It should be mentioned that in a semiconductor there can be other types of Auger processes besides the band-to-band ones, which includes AP via traps, via defects, and so on. However it has been shown that the processes in Figure 3.2 are the most

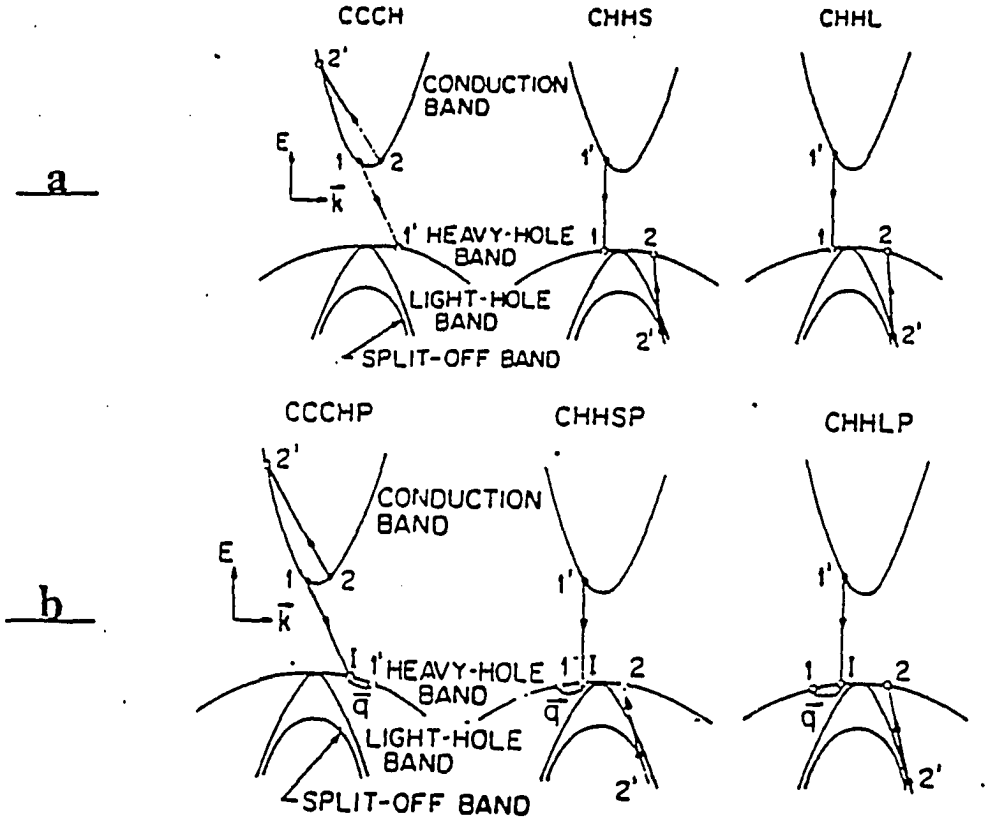

Figure 3.2: Band-to-band Auger process in InGaAsP, (a) Phononless processes, (b) phonon assisted processes [8, page 17]

important ones in InGaAsP based structures [25, 26, 49]. In an n-type InGaAsP sample the CCCH and CCCHP processes which involve two electrons and one hole will be dominant due to the high availability of states, whereas in a p-type case CHHS, CHHSP, CHHL, and CHHLP can be the most dominant ones.

Several authors have reported Auger calculations for InGaAsP. The first major calculations were reported by Sugimura in 1981 [27], and Dutta and Nelson reported in 1982 [26]. Dutta and Nelson used Fermi and Boltzman statistics for electrons and holes respectively, parabolic band structures, and Kane's model for GaAs. They assumed that GaAs band structure is basically the same as InGaAsP. Hence, they used the GaAs band structure modified by Kane, and utilized the Halperin-Lax band tail model with kp-perturbation theory to calculate Auger values [26]. In 1983, Albert Haug used different band curves. He used the curves given by Chelikowsky and Cohen which were for InP. Haug assumed that InP structure is closer to InGaAsP band structure since it has a better lattice match to InGaAsP. On the other hand Haug's structure used nonparabolic bands (which is a more realistic model) so he could get a more reliable set of values.

Haug's results indicated that the only processes important in InGaAsP are CCCH and CHHS. He also indicated that the phonon assisted processes are much more important in CCCH and they are so dominant that the phononless processes are negligible by comparison. Another important result reported by Haug was that CHHS (phononless) increases substantially above 250 K. As a matter of fact Haug's calculation showed the important fact that all Auger processes show a break points at 250 K. This is the same break point observed for InGaAsP laser currents. The almost

Table 3.1: Values for various Auger coefficients in $10^{-29} cm^6/s$ [25]

$T(K)$	100	200	300	400
C_n	5×10^{-17}	5×10^{-7}	5×10^{-4}	0.065
C_p	5×10^{-5}	0.065	0.7	1.985
C_n^{ph}	1.475	1.66	1.98	2.355
C_p^{ph}	0.255	0.235	0.23	0.335

exact break point of these coefficients and the threshold current of InGaAsP lasers is the reason for proposing it as the most important carrier loss mechanism in InGaAsP lasers.

Haug's results for 1.3μm InGaAsP are shown in Table 3.1. In Table 3.1 C_n and C_n^{ph} represent phononless and phonon assisted CCCH processes and C_p and C_p^{ph} represent corresponding CHHS process. The total Auger coefficient can be defined as C and will be related to the above mentioned coefficients as $C_{tp} + C_{tn} = C_n + C_p + C_n^{ph} + C_p^{ph}$. Figure 3.3 shows the total coefficient as a function of temperature in Kelvin (K) reported by Haug. Looking at the behavior of total C versus temperature, one can see the similar behavior as the behavior of threshold current versus temperature. In particular, the fact that there is a change of slope of C around 255 K, together with the fact that the slope gets to be much sharper after 255 K, reminds us of the behavior of threshold current of InGaAsP lasers.

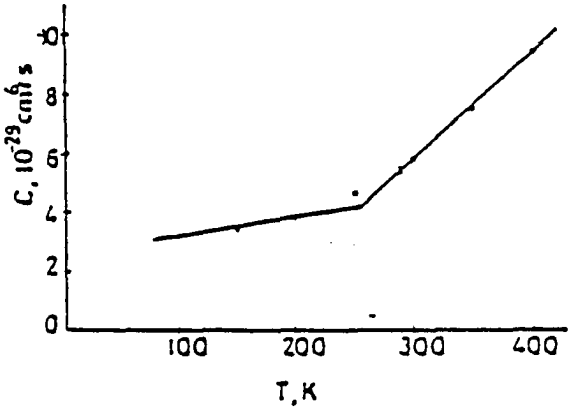

Figure 3.3: Temperature dependence of total Auger coefficient [25]

3.1.2 Experimental results

It is difficult to measure the Auger effect experimentally. However, many investigators have reported the results of some particular measurements. The results of all different reported measurements indicate that the total Auger coefficient varies from 2 to 6 (with units of $10^{-29} cm^6/sec$) around room temperature. Table 3.2 shows some typical reported results.

The more recent measurements are done by Mozer et al. [33], and the results were given in Chapter 2 in Figure 2.6. Their reported values show very close correlation to the Haug's calculation. There is no reported information about how Auger coefficients are effected by different dopings and injection levels (especially when the doping and injection levels get to be in the extreme, like what we may encounter in CW operation). However, due to the nature of the problem there is so much uncertainty in the available numbers that the changes due to other effects can be neglected. Both experimental and theoretical results of Auger coefficients and lifetimes are very

Table 3.2: Measured total Auger coefficient in $10^{-29}\ cm^6/s$ [8, page 25]

C_{total}	*Comment*	*Reference*
5	$\lambda = 1.3\mu m$	*Mozer*(1982)
4	$\lambda = 1.58\mu m$	*Asada*(1982)
2.3 ± 1	$\lambda = 1.3\mu m$	*Semage*(1983)
1	$\lambda = 1.3\mu m$	*Henry*(1981)
~ 3	$\lambda = 1.3\mu m$	*Su*(1982)
$3 - 8$	$\lambda = 1.3\mu m$	*Uji*(1983)

uncertain. The degree of uncertainty in some of the calculations due to approximations and lack of exact knowledge of InGaAsP structure can be up to 20 percent [8, 36, 30]. Consequently, it seems that the choice of Haug's results (see Table 3.1) for all doping can be considered to be a good quantitative description of the process with the correct order of magnitude (which is the best we can hope for). Hence in this study, all the calculations involving the use of Auger coefficients will utilize the values given in Table 3.1.

3.2 J_{th}

According to the equation

$$J_{th} = edn_{th}(A + Bn_{th} + Cn_{th}^2) \tag{3.2}$$

knowing A, B, C, d, and n_{th}, one can get J_{th} for a laser with an undoped active layer. In this equation B describes the radiative recombination, C the Auger recombination, and A additional contributions mainly due to internal optical losses. Sometimes a carrier leakage term with $Dn_{th}^{4.5}$ can be added inside the parentheses. There is some

strong experimental evidence that one can neglect this latter term for many lasers without any loss of generality [28].

For the case of doped active layer, there can be two categories. First, it can be an n-doped with n_0 doping density. Even though this type of doping is not very popular for InGaAsP lasers, it is interesting to look at the results of our model for it. In an n-doped case there are so many electrons in the conduction band ready to recombine, one can write the current density as,

$$J_{th} = ed\left(A(n - n_0) + B(n - n_0)p + C'_{tn}(n + n_0)^2 p + C'_{tp}(n + n_0)p^2\right) \qquad (3.3)$$

where p and n are the injected hole and electron densities, C'_{tn} and C'_{tp} are the total Auger coefficients (both phononless and phonon assisted, as given by Haug). In a laser at threshold the number of injected holes and electrons are equal. This means n_{th} and p_{th} are equal as the pairs are generated together. Hence, using the fact that $n_{th} = p_{th}$ and substituting C' for $C'_{tn} + C'_{tp}$ we can write

$$J_{th} = ed(n_{th} - n_0)\left(A + Bn_{th} + C'n_{th}^2 - C'_{tn}n_0 n_{th}\right) \qquad (3.4)$$

as the J_{th} for a laser with n-type active layer doping.

In a laser with p-type doping, there will be many holes in the valance band ready for recombination, so with a similar procedure one can derive threshold current density for such a laser as

$$J_{th} = ed(n_{th} - p_0)\left(A + Bn_{th} + C'n_{th}^2 + C'_{tp}p_0 n_{th}\right) \qquad (3.5)$$

where p_0 is the doping density of a p-type active layer. Knowing A, B, C', p_0 or n_0, d, C'_{tn} or C'_{tp}, and n_{th} will allow us to find injected current density. The question

Table 3.3: A, B, C values observed experimentally by Mozer et al. [33]

$T(K)$	$A(10^7 1/sec)$	$B(10^{-10} cm^3/sec$	$C(10^{-29} cm^6/sec)$
0	5.5	4.58	1.33
~ 90	5.5	2.48	1.33
~ 180	7.33	1.18	1.94
~ 250	8.27	1.014	3.01
~ 300	11.0	0.86	4.0

at this point is how to get or choose these values. For the purpose of this study we use the values of A, B, and C reported by Haug in his calculations which in turn are verified by Mozer [18, 20, 25, 33]. Table 3.3 shows a summary of values reported by Mozer.

3.3 η_{th}

The differential quantum efficiency may be written as

$$\eta_d = \eta_{stim} \left(\frac{\ln(1/R)}{\alpha l + \ln(1/R)} \right) \tag{3.6}$$

where R is the reflectivity of the end mirrors, α is the effective absorption coefficient along the laser, L is the cavity length of the laser, η_{stim} is the internal quantum efficiency above threshold.

To model differential quantum efficiency we will use a model proposed by Adams, Asada, and Suematsu in 1980 [50]. It has also been mentioned that the internal quantum efficiency can be written as

$$\eta_i = (1 + \tau_r/\tau_{nr})^{-1} \tag{3.7}$$

where τ_r and τ_{nr} are the radiative and nonradiative lifetimes respectively for that portion of the injected current above threshold. τ_r is the stimulated lifetime which is limited by the carrier interband relaxation time that has been measured to be approximately 10^{-13} s [50]. It has been also shown that the lower limit for the nonradiative recombination lifetime τ_{nr} is the total recombination lifetime below threshold and is 10^{-9} s. That is why we may conclude that the ratio $\tau_r/\tau_{nr} \leq 10^{-4}$. We can then use $\eta_i = 1$ which means internal quantum efficiency above threshold is almost 1 ($\eta_{stim} = 1$). It is clear from the equation 3.7 that in order to find a physical explanation for changes in η_d we must examine the absorption coefficient α.

The actual absorption in a laser is due to the effects of absorption inside and outside the active region, and can be shown as

$$\alpha = \Gamma\alpha_a + (1 - \Gamma)\alpha_c$$

where α_a and α_c are the absorption loss coefficients for inside the active region and the cladding respectively, and Γ is the confinement factor.

It is possible to use the definitions of α and η_d together with the measured variation of differential quantum efficiency, and to get the temperature variation of α_a. This result is shown in Figure 3.3. It can be seen that α_a must rise swiftly at higher temperature if the experimental values of η_d are to be explained. Figure 3.4 shows schematically the fact that α_1 appears as a result of electronic transition from the split-off band into holes which have either been injected into the heavy hole band by forward bias, or arise from thermally excited acceptors. In the figure, transitions to the partially empty acceptor level (α_2) is also shown.

Since α_1 will be directly dependent on the hole density available at energy E_1,

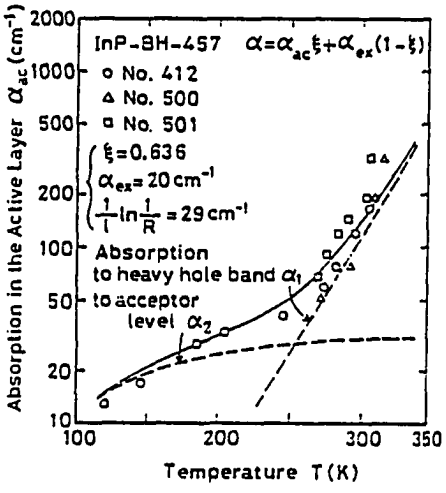

Figure 3.4: Temperature dependence of absorption coefficient, both experimental and theoretical values of α_a which is the sum of α_1 and α_2 (ξ is the confinement factor) [50]

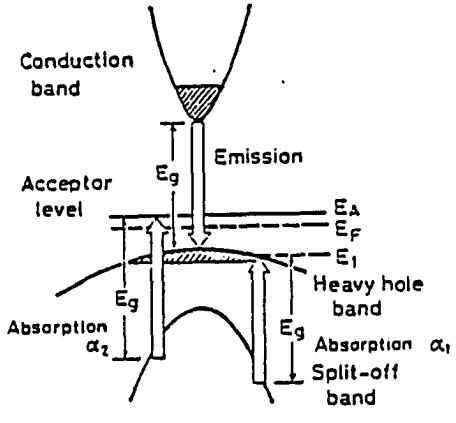

Figure 3.5: Schematic diagram of the band structure of the quaternary material indicating photon emission across the band gap and its reabsorption by transition from the split-off band into the heavy hole band at energy E_1 and into the acceptor level at energy E_A. These are designated α_1 and α_2 respectively [50]

we can write

$$\alpha_1 = B1/\left(1 + exp(E_1 - E_F/kT)\right) \tag{3.8}$$

where B_1 is a constant. Such an absorption mechanism will tend to decrease with increasing photon energy. The temperature dependenc of α_2 may be written in a similar way as

$$\alpha_2 = B2/\left(1 + \frac{1}{2}exp(E_A - E_F)/kT\right) \tag{3.9}$$

where E_A is the energy of acceptor level and B_2 is a constant. In order to find the results using the model shown in Figure 3.4 (which uses an intervalance band absorption) it is necessary to find E_1, E_A, and E_F. Studies have shown that E_1 is approximately 0.15 eV below the valence band maximum. This value is subject to large possible errors due to the sensitivity of the band structure to exact values of effective mass, and degrees of nonparabolicity of the band. E_A can be taken to be about 30 meV above the top of valence band from a comparison with GaAs [50].

Since $E_A - E_F$ is generally small, α_2 does not show a strong temperature dependence. On the other hand since $E_1 - E_F$ is always as big as many factors of kT, α_1 is an increasing function of temperature.

In the model α_1 is given as [22, 41],

$$\alpha_1 = K_0 n \tag{3.10}$$

where

$$K_0 = B_1 \left(\frac{2\pi\hbar^2}{m_v^* KT}\right)^{3/2} exp(-E_a/kt)$$

where k is the Boltzman constant, T is temperature in Kelvin, and m_v^* is the effective hole mass. The values of the constants and the energy levels are obtained experimen-

tally, so knowing the temperature, the doping material, and the number of carriers injected (n) into the laser we can find η_d. Then, to η_{th} which is differential quantum efficiency at threshold can be obtained by using n_{th} in equation 3.11.

In order to find the results we can take $\alpha_a = \alpha_1 + \alpha_2$. The magnitudes of B_1 and B_2 should be adjusted to give the best fit to experimental measurements ($B_1 = 3.7 \times 10^5\ cm^{-1}$ and $B_2 = 63\ cm^{-1}$). This way, knowing the temperature of the active layer (T), injected carrier density (n_{th}), and constants B_1, B_2, E_A, and E_1 one can find the differential quantum efficiency η_d.

3.4 n_{th}

Up to this point we have been looking at methods of finding J_{th}, and η_d knowing active layer temperature and the injected carrier density at threshold. It is important to have a method to find the injected carrier density at threshold (n_{th}) at a given active layer temperature. There have been many models presented for this calculation. For instance Dutta and Nelson in 1981–1982 used Kane's model for extrapolation, Halperin-Lax band tail approximation, and Stern's matrix elements to find the number of carriers [8, 26]. These calculations are not trivial and are very tedious. However in 1985, A. Haug presented a model which has a quick way of doing the same type of approximation but in a very simple and intuitive process. The method which will be discussed in this section is one for DH lasers made of InGaAsP as well as any other III-V compounds. It is a quick, and very intuitive way of obtaining n_{th} without going through a long and tedious process involved in models like the one proposed by Dutta and Nelson [26].

The significant point about this model is the fact that in utilizing it one is able to get n_{th} without the knowledge of the exact absorption, gains, band tail information, and so on. To develop the model one needs to go through a series of intuitive steps. First, for an ideal lossless laser the lasing condition can be written (as discussed previously) as

$$E_{fc} - E_{fv} \leq h\nu$$

where hν is the photon energy, and E_{fc} and E_{fv} are the Fermi levels of electrons and holes with respect to a common base energy. If we assume that ξ_n and ξ_p are the quasi-Fermi levels for electrons and holes measured from the respective band edges, they will be given as,

$$\xi_n = E_{fc} - E_c \tag{3.11}$$

$$\xi_p = E_v - E_{fv} \tag{3.12}$$

Using the above equations in the lasing condition, and substituting E_g for E_c - E_v one can get,

$$\xi_n + \xi_p \geq h\nu - E_g \tag{3.13}$$

This is the lasing condition for of any semiconductor laser. However, in the case of an ideal laser the photon emitted will be exactly the same energy as the band gap energy since there is no band tail effect nor any losses. This leads to the lasing condition for an ideal laser as,

$$\xi_n + \xi_p = 0 \tag{3.14}$$

Solving this equation will lead to the threshold injected carrier density of an ideal laser (here presented as n_i). However solving this equation involves dealing with de-

generacies and Fermi level calculations which are also nontrivial. As suggested and used by Haug, the quickest way to solve this equation is by using an approximation formulation developed by Nilsson in 1978 [18, 51]. In his formulation, Nilsson introduced an approximation for the calculation of the Fermi level in a degenerate as well as nondegenerate semiconductors when carrier concentration is known [51]. The details of his work will not be presented here. It has been done in his original paper in 1978 [51], and the particular steps for calculation of the case of InGaAsP have been generated by the author in 1987 [52]. At this point we just indicate that by using Nilsson's method to solve equation 3.14, one can solve for the threshold injected carrier density of an ideal laser (n_i).

The ideal carrier density n_i, however, underestimates the actual values for the threshold carrier density in the active region. This is due to the fact that in a real laser there are losses, and as discussed before, when we have losses in a laser we need to pump in more current to overcome the losses. The losses consist of internal optical loss presented by An_{th} factor, and the nonradiative recombination due to Auger effect presented by Cn_{th}^3 in equations 3.1, 3.4, and 3.5. As a result, the actual value of the threshold carrier density needs to be enhanced to compensate for the losses.

To enhance n_i one needs to look at the ratio of the nonradiative recombination rate (in the form of $A + Cn_i$) to the radiative recombination rate (Bn_i) inside an ideal laser in which losses are to be introduced. Hence, intuitively we can come up with approximated value of n_{th} as,

$$n_{th} = n_i \left(1 + \frac{A + Cn_i}{Bn_i}\right) \tag{3.15}$$

The above equation represents the threshold injected carrier density of a laser

with an intrinsic active layer. This usually calculated in a much more complex way using other models. Our model can be extended for the case of an n or p type doped active layer with n_0 or p_0 dopings respectively. As a result we can add an appropriate term for additional losses due to electrons in the conduction or holes in the valence band, and the new equations can be written as,

$$n_{th} = n_i \left(1 + \frac{A + C n_i + C_n n_0 n_i}{B n_i}\right) \tag{3.16}$$

$$n_{th} = n_i \left(1 + \frac{A + C n_i + C_p p_0 n_i}{B n_i}\right) \tag{3.17}$$

Using these equations one can find n_{th} at any given temperature by knowing the values for A, B, and Cs. Thus, using n_{th} we can approximate J_{th} and η_{th} for a given temperature and doping of active layer. As a result, we can find all threshold parameters knowing the type of doping and the average active layer temperature.

4. CW OPERATION

A semiconductor laser is always mounted on a heat sink as shown in Figure 4.1. The purpose of the heat sink is to help cool the laser diode chip to avoid excessive heating of the laser. In many systems the heat sink is kept at a constant temperature by a cooling mechanism like liquid nitrogen. This was the case for the first semiconductor lasers ever invented. They were cooled by liquid nitrogen while they were operating.

An injection laser can be operated in two ways. It can be operated in a pulsed mode, where the laser is injected with current during short intervals. This will avoid heating of the active region while lasing takes place. On the other hand, the laser can be operated continuously. This is known as CW operation. In CW operation the active layer as well as other layers keep heating up and the temperature of the active layer will be different from the heat sink. This is in contrast with the pulsed operation during which the active layer is not allowed to heat up, and as a result the temperature of the active layer is more or less the same as the heat sink. In order to understand this point let us do a thought experiment.

Let us assume the laser is sitting at the heat sink temperature T_A without any injection current. To make this laser lase we need to supply a current just above the threshold current at a temperature of T_A ($I_{th}(T_A)$). If we send the current into the

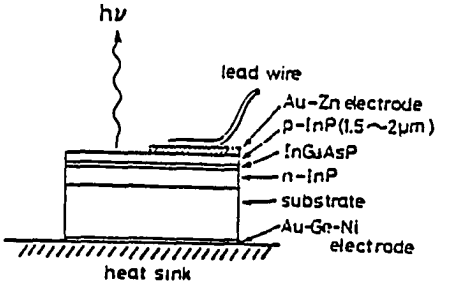

Figure 4.1: A typical set up of a semiconductor injection DH laser [23]

laser, the loss mechanisms discussed earlier like ohmic losses, junction losses, active laser loses, and optical losses will start to act and as the result the laser will start to heat up. This means that the active layer will be at a different temperature than the heat sink. To avoid heating the active layer one can make the duration of the injected current sufficiently short [32]. In this mode heating can be limited and the active layer will be at more or less same temperature as the heat sink. This is the idea behind the pulsed operation of laser diodes. On the other hand there are merits in letting the laser run over longer time periods. For instance if we use continuous operation we can eventually use different modulation schemes and thereby make a light wave system with greater capability. However, fast modulation can create some interesting problems of its own which are beyond the scope of this study. In this study we look at the temperature distribution in InGaAsP DH laser at steady state CW operation. Under CW operation all the heating mechanisms which occur throughout the structure will be present. Consequently, the active layer will be at a different temperature than the heat sink. This can cause the infamous runaway problem, and

there is an urgent need to understand the temperature behavior of these lasers.

The purpose of this study is to look at the CW operation of InGaAsP DH lasers. In order to do this we need to develop a model to find the average temperature of the active layer for different input levels. This is a nontrivial multi-variable problem. The problem is manyfold as we will see. However, to begin our understanding of the depth of the problem let us first look at a two dimensional model for temperature distribution inside a multi-layer structure with planar sources.

4.1 Temperature Distribution

Two dimensional temperature distribution models for semiconductor heterostructure laser diodes have been introduced by various investigators [44, 45, 53, 54]. The idea is that in an actual laser structure under CW operation, due to the thickness of layers and their thermal resistance, the average temperature in the active layer is different from that of the heat sink and can only be determined by mathematical models. We therefore introduce a two dimensional model for temperature distribution inside the layers of a heterostructure diode. Utilizing the following basic model, temperature at any point in any layer of a semiconductor laser can be found. Our ultimate goal is to come up with a model for the temperature distribution for all the points inside the laser structure.

4.2 The Model

For our basic model consider Figure 4.2. We assume that heat is generated uniformly and steadily by a planar stripe source which is embedded at the boundary

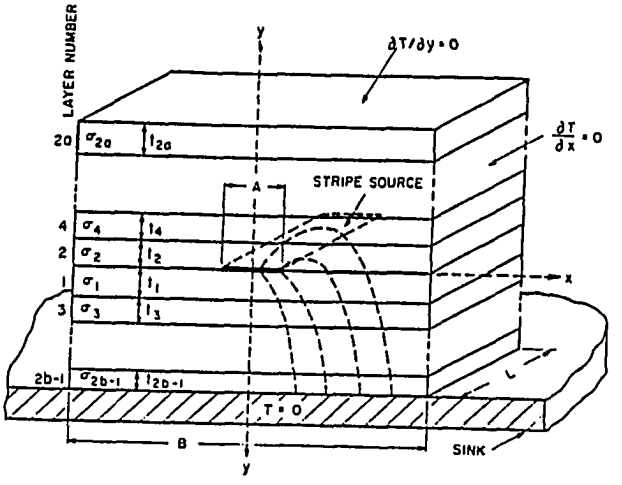

Figure 4.2: Two-dimensional heat flow from a uniform stripe heat source in a rectangular parallelopiped consisting of b layers below the source and a layers above. σ_i and t_i are the conductivity and thickness of the ith layer. T is the temperature [45]

of two layers in a rectangular layered laser. No heat escapes through the sides, ends, or top of the laser. We also consider heat flow is two dimensional into a highly conductive sink which we approximate as a reservoir at zero temperature. Letting the thickness of the $i-th$ layer be t_i, and its thermal conductivity be σ_i (which we take as a constant), we can proceed to develop our formulation.

As shown in Figure 4.2 we assume there are b layers (1, 3, 5, ...) below the source and a layers (2, 4, 6, ...) above the source (the planar stripe source is at the boundary of the two layers 1 and 2). A separation-of-variables solution of Laplace's equation under steady state condition for temperature ($\nabla^2 T_i(x,y) = 0$) results in T_i which can be presented as.

$$T_i(x,y) = \beta_{i,0}(1 - r_{i,0}y) + \sum_{n=1}^{\infty} \beta_{i,n} \left(cosh(k_n y) - r_{i,n} sinh(k_n y)\right) cos(k_n x) \quad (4.1)$$

where $T_i(x,y)$ is the temperature in the $i-th$ layer at position (x,y), $\beta_{i,n}$ is an undetermined coefficient of $cosh(k_n y)cos(k_n x)$ and $-r_{i,n}$ is the ratio of the coefficients of $sinh$ and $cosh$ terms.

One should notice that $sin(k_n x)$ does not appear because of symmetry. In order to satisfy the requirement of no heat escaping from the lateral faces. we should match the following boundary condition

$$\partial T(|x| = \pm B/2)/\partial x = 0$$

which will result in the separation constant $k_n = 2n\pi/B$. In our formulation it is important to remember that in each layer positive y is in a direction away from the source with the origin of y at the face nearest to the source. This way all the points (x,y) for the layer i are well defined. At this point we should be very careful in numbering the layers. There are a layers on the top of the source which are layers 2, 4, 6, and so on. That means that the very top layer is layer $2a$. Similarly, the layer at the bottom next to the heat sink is $2b-1$ layer.

4.2.1 Unique solution

In order to get a unique solution we need to solve for the constants $\beta_{i,n}$ and $r_{i,n}$ for a given set of boundary conditions. The first boundary condition was imposed on the sides of the laser structure. Assuming there was no heat escaping from the sides resulted in obtaining values for our separation constant k_n. If we assume no heat

escapes from the top of the laser structure we impose

$$\partial T_{2a}(y = t_{2a})/\partial y = 0$$

and this implies that for the top layer we can write,

$$r_{2a,n} = tanh(k_n t_{2a}) \tag{4.2}$$

Similarly for the assumption that the heat sink is at zero temperature ($T_{2b-1} = 0$ for all (x, y) in the $(2b-1)-th$ layer), we get

$$r_{2b-1} = coth(k_n t_{2b-1}) \tag{4.3}$$

The interfaces between adjacent layers are either source free or there is a stripe source at the interface. Boundary conditions for each interface can be done in the following manner. For the source free interface between any two layers, the continuity of temperature and normal heat flow ($\sigma \partial T_i(x, y)/\partial y$) relates the coefficient ratio $-r_{i,n}$ in the neighboring layers as

$$r_{i,n} = \frac{tanh(k_n t_i) - (\sigma_{i+2}/\sigma_i) r_{i+2,n}}{1 + (\sigma_{i+2}/\sigma_i) tanh(k_n t_i) r_{i+2,n}} \tag{4.4}$$

For the boundary between two layers with the stripe heat source at the interface, we know that the heat flow can be a complicated function of x. However, the combined flow per unit area into each layer (top and bottom of the heat source) is equal to the source power per unit area at the boundary. Letting J be the source power per unit area (W/m^2), we can say

$$-\sigma_2 \partial T_2(x, y)/\partial y - \sigma_1 \partial T_1(x, 0)/\partial y|_{y=0} = \begin{cases} J & 0 \leq |x| < A/2 \\ 0 & A/2 < |x| \leq B/2 \end{cases}$$

where one can use a Fourier expansion of the right hand side and obtain

$$-\sigma_2 \partial T_2(x,y)/\partial y - \sigma_1 \partial T_1(x,0)/\partial y|_{y=0}$$

$$= JA/B + 4J/B \left(\sum_{n=1}^{\infty} k_n^{-1} sin(k_n A/2) cos(k_n x) \right) \quad 0 \leq |x| < A/2$$

From the continuity of temperature T through the source plane, one can get $\beta_{1,n} = \beta_{2,n}$ and using above equations we can get

$$\beta_{1,n} = \frac{4sin(k_n A/2)}{bk_n^2(\sigma_1 r_{1,n} + \sigma_2 r_{2,n})} \tag{4.5}$$

Finally by comparison of the $n = 0$ terms we find

$$\beta_{1,0} = \frac{JA}{B(\sigma_1 r_{1,0} + \sigma_2 r_{2,0})} \tag{4.6}$$

The above discussion represents a method for obtaining the temperature distribution at all points in all layers knowing the structural dimensions, the material of each layer, and the position and strength of the source. Once these are all known we start from the evaluation of k_n. We then use equations 4.2 and 4.3 to find the $r_{2a,n}$ and $r_{2b-1,n}$ terms. Then using the recursive equation 3.4 for the top layers and bottom layers we find all the $R_{i,n}$'s. Finally we will use the equations 3.5 and 3.6 to calculate all of the values of $\beta_{i,n}$. It is important to note that by knowing J, k_n, $r_{i,n}$, and $\beta_{i,n}$ we will have a unique solution, and we can find the temperature at any point (x,y) in any layer using equation 3.1.

4.3 Typical laser

In a typical laser we may have heat generation by the active layer, ohmic losses and other heat sources. However, no matter how many heat sources we want to

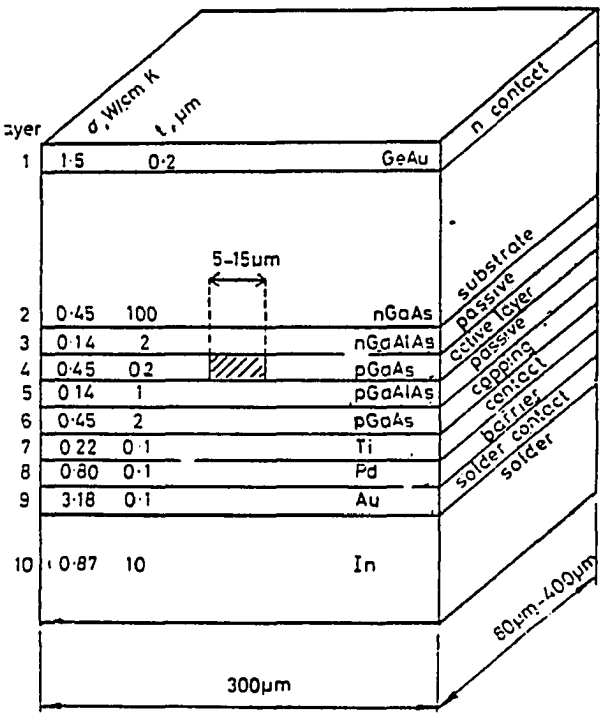

Figure 4.3: Dimensions and thermal conductivities of a typical device structure [54]

include. using this model we can calculate temperature distribution of more than one heat source by superposition.

Another important point to consider is that in a typical semiconductor DH laser the active layer has a finite thickness. This is also true for other heat sources that we would want to include. In our model. however. we consider sources with zero thickness at the interface of layers 1 and 2. To deal with a laser structure such as the one shown in Figure 4.3 we replace the active layer by two layers of half thickness each with the active source at the interface of the two (see Figure 4.4).

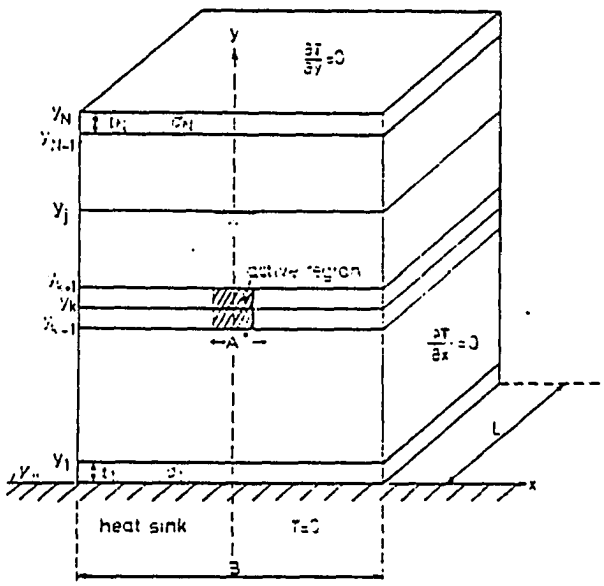

Figure 4.4: Model used for calculation of temperature distribution [54]

To get the average temperature of the active layer due to a source with the width of A (e.g., for the case of the heat source due to losses inside the active layer) we can do the following. When the temperature distribution is known we can get T for all points in layers 1 and 2, which are the layers on the top and bottom of the heat source. We can do a two dimensional integration to find the average temperature

$$T_{average} = \left(\frac{1}{A(t_1 + t_2)}\right) \int_{t_1}^{t_2} \int_{-A/2}^{A/2} T(x, y) dx dy \tag{4.7}$$

It should be mentioned that such a temperature calculation can, in general, be applied to any heat source (or sources) at any position by just changing 1 and 2 with i's and replacing A with A^* (which is the desired width of the given heat source) [54].

4.4 Heat Sources

There are definitely more than one type of heat sources in a semiconductor DH laser. We can generally have three major types of heat sources. The major source of the most heat is losses inside the active region from nonradiative recombination and internal optical losses. Another source is current spreading and ohmic losses in the layer adjacent to the active region. The latter is called the ohmic losses (or passive layer heating). In the presence of carrier leakage the effect of ohmic losses will increase. The third type of the heat source is radiation that never leaves the laser although it leaves the active region as spontaneous radiation. This part of the radiation, which did not get absorbed inside the active layer, gets absorbed in the layers adjacent to the active layer, thus sometimes called the capping layer heating. In reality there may also be some heating due to poor contacts between the laser and

the connecting conductors. This is called contact heating. These losses have been considered by several investigators [44, 45, 53, 54, 55].

It is important to note that in CW operation all these losses can contribute to the heating. Using the previously described formulation, one can approximate the effect fairly easily. The only difficulty is in the positioning of the equivalent heat source. As far as our model is concerned we can put as many sources as we desire and use superposition to get the net result. The way we include a source is by putting an equivalent power source at an appropriate boundary. For instance, for the case where heat is generated in the active layer, the heat source is assumed to be situated along a line at the center of the active layer. This way the active layer is considered to be two layers with a heat source in between. Despite the fact that this model seems to give a satisfactory approximation, one should realize that the actual position of any of these heat sources is really not exactly known. There is a great deal of uncertainty in the positioning of the heat sources using our model. In this study, however, due to the fact that we are isolating the active layer heating (in order to focus on the effect of only one kind of nonradiative loss at a time) we locate the active heat source in the middle of the active layer. This is a common practice, and seems to provide reasonable approximation of an actual system [45, 53, 54].

It needs to be mentioned that the effective temperature rise of the laser structure has a strong dependence on the position of the heat sources. However, it should be noted that the heat sources are really distributed (as a microscopic phenomena) all over the corresponding layers.

4.5 Thermal Conductivity

Using our model one needs to know thermal conductivity of each layer. Thermal conductivity is itself a temperature dependent entity. Hence, as the temperature of each layer changes, so does the thermal conductivity of the layer. However, thermal conductivity of InGaAsP material is still under investigation and all the questions about its thermal behavior are not answered.

There have been different models describing thermal conductivity of InGaAsP [56, 57]. Thermal conductivity of InGaAsP is also very sensitive to the doping type and concentration [37]. Once thermal conductivity of a typical composition of InGaAsP is calculated, the approximation involved is uncertain enough that the temperature dependence of thermal conductivity can be neglected. It is observed that within the temperature range that we are interested (250–420 K) thermal conductivity of InGaAsP is not greatly temperature dependent [58, 59, 60]. Consequently, for the purpose of this study we try to assume a reasonable value for thermal conductivity and neglect the temperature variations as a secondary effect.

4.6 Calculation method

After picking a laser structure for which we know the dimensions, the material types, and their constants such as conductivity, we can start our study of CW operation. The idea is to study light output power versus injected current, and the behavior of the laser as we pump current continuously. Let us assume the laser is on a heat sink with a constant heat sink temperature of T_{sink}. In order to start laser action we need to supply an injection current at least equal to (or greater than) the

threshold current $I_{th}(T_{sink})$. This current will be the smallest current possible to start the laser action. From then on, as we increase the injected current, the active layer will heat up, resulting in the need to calculate a new threshold current. One must remember that the governing equation is

$$P_L(T) = V\eta(T)\left(I - I_{th}\right) \tag{4.8}$$

where

$$V = V_0 + rI$$

in which V_0 is the voltage across the active region and r is the series resistance of the laser. In the above equation the most important factor is T, the average temperature of the active region. In order to find that we use the two dimensional model discussed in this chapter in the following manner.

First of all, when starting to increase injected current from $I_{th}(T_{sink})$, we use the new current and the corresponding V to get the input power. This input power will be used in the boundary conditions. The input power will be divided by the surface area of the stripe source to get the equivalent active layer heat source assumed in our model to be situated in the middle of the active layer. Using this information, we can solve the two dimensional equation and find the average temperature of the active layer. Once we find the average temperature, we need to increase the injected current and find the new threshold current for the active layer temperature. This process needs to continue until P_L becomes a negative number which means the laser action is stopped. Once again one should note that a negative power is not a physical entity. In our formula we get negative P_L when equation 2.20 is no more valid. This

means negative power indicates that lasing has stopped and nonlasing dissipation is taking place. The algorithm is as following.

- STEP 1: Find $I_{th}(T_{sink}), \eta(Tsink)$.
- STEP 2: Start with $I = I_{th}(T_{sink})$.
- STEP 3: Find V and use $\frac{IV}{(active-layer-area)}$ as the boundary condition and solve the 2-dimensional model to get ΔT.
- STEP 4: Active layer average temperature is $T_{ave} = T_{sink} + \Delta T$.
- STEP 5: Use T_{ave} to find $\eta(T_{ave}), I_{th}(T_{ave})$, and P_L.
- STEP 6: If $P_L > 0$, increase I with steps of$H.I_{th}(T_{ave})$ where H is a constant (1, 2, 3, and so one for different steps) and goto step 3.
- STEP 7: If $P_L \leq 0$ stop.

In the above algorithm it is interesting to notice the following points. First of all, there are some heat sink temperatures for which lasing action is not possible since T_{sink} is so high that P_L is always less than zero (which means the light out put is zero in reality). Second, I_{th} and η at different temperatures have the Auger recombination effect in them, therefore as the average temperature of the active region increases there will be more Auger losses and the need for a higher injection current. This is the way that the effect of AP is incorporated into this study. Finally, using this method we can get P_L versus I, the maximum possible output power, and maximum operating temperature together with other pieces of information about a given DH laser structure.

It should be mentioned that one of the strong points about this method is the fact that there is no need to use values of T_0 and T_E. T_0 and T_E are the characteristic temperatures for threshold current and quantum efficiency respectively. In an InGaAsP laser, these factors have intrinsic temperature dependences. However, in many investigations, they have been approximated as constant factors with a change after a break point [11, 18]. Using our I_{th} and η model we can calculate effective T_0 and T_E values, even though there is no need for them in our calculation processes. In our CW study we get Jth and η directly from our models. This is a very important characteristic of our model. The two characteristic temperatures are empirical factors and are used to help understand the experimental result of the behavior of InGaAsP lasers. In our theoretical model however, there is no need to use these two factors, and we can calculate them as a by-product of our results. In the following chapter we will use the models for $n_{th}, I_{th}, \eta, T_{ave}$, and P_L to make some calculations and compare them with some experimental observations to show the validity of our theoretical model.

5. RESULTS AND DISCUSSIONS

To check the usefulness and success of our model, we need to look at its application in some practical systems. The results should really be viewed from two different angles. The first and more general one is to see if they make qualitative and intuitive sense. This means that the results should not contradict our general physical intuitions, since intuition is what led us to the proposed model. The second point of view is quantitative analysis, which means our results for n_{th}, J_{th}, η, and P_L must be in the same order of magnitude and behave similarly to experimental results that have been reported. Even though the true test of the validity of a model is its close correlation with experimental results, for the case of our model we should be limited to general agreements of our results with the experimental values. This is a cosequence of the lack of experimental data on the exact behaviors that we are interested in. Since we are only looking at the Auger recombination effect, our results will not be general enough to give a close correlation with experimental values.

In this chapter we will look at the results provided by our model. We will start with the basic Haug model for ideal carrier density n_i, threshold carrier density n_{th}, and threshold current density J_{th}. Once these calculations are introduced and discussed we will look at the results of the two dimensional temperature distribution and use that to calculate $J_{th}(T)$, and P_L of lasers with typical structures. At the

Table 5.1: Measured wavelengths and energy gaps related to different values of x and y in InGaAsP [8, 61]

x	y	$\lambda(\mu m)$	$E_g\ eV$
0.0	0.0	0.920	1.350
0.155	0.083	1.005	1.234
0.516	0.247	1.217	1.019
0.610	0.280	1.301	1.019
0.787	0.346	1.470	0.843
0.906	0.395	1.546	0.802
1.000	0.466	1.656	0.749

end an overview of the model and final discussion will be presented.

5.1 N_i Evaluation

In order to get the values of injected carrier density for an ideal laser (n_i) we will use Nilsson's method [51]. We will not look in details of this process but simply present the results. It is important to realize that in the case of $In_{1-x}Ga_xAs_yP_{1-y}$ different values of x and y (indicating the ratio of each material in the compound) will create material with different band structures, different band gaps, and different n_i values. This study will focus on 1.3 μm semiconductor injection lasers, since more experimental data are available for these lasers. For a 1.3 μm laser typical x and y values are $y = 0.6055$ and $x = 0.2794$. Tables 5.1 and 5.2 show how energy gap, wavelength, and n_i are effected by x and y. The relation between wavelength λ and the energy gap E_g is given by equation 1.1.

Table 5.2: Calculated values of n_i for small variations of x and y at 300 K

x	y	$n_i(\times 10^{17} cm^{-3})$
0.599	0.27	10.02
0.599	0.28	10.04
0.600	0.27	10.01
0.600	0.28	10.03
0.608	0.27	9.94
0.610	0.27	9.92
0.610	0.28	9.95
0.606	0.28	9.98

Table 5.2 shows how the values of n_i are related to changes in the x and y. It is interesting to see that the values of n_i are very sensitive to changes in both x and y. This is due to the fact that by changing x or y, we really are changing the shapes of the energy bands and the values of band gaps as well as the effective mass and the density of state.

The values of n_i are temperature dependent. One expects to see more carrier injection at a higher temperature, because due to more excitation there will be more carrier injection required. This characteristic is observed in Table 5.3.

When we have doping inside the active layer, the values of the threshold carrier density for the ideal laser will change. Table 5.4 gives the results of calculations for the case of an n-doped active region at three different temperatures for different active layer dopings. Similar calculations for a p-doped active region are shown in Table 5.5. Figure 5.1 shows this information graphically.

In Tables 5.4 and 5.5 (as well as Figure 5.1) some very interesting phenomena

Table 5.3: Threshold injected carrier density (n_i) for an ideal laser with intrinsic active layer ($\lambda = 1.3\mu m$)

T (K)	n_i ($10^{17} cm^{-3}$)
50	0.679
100	1.92
150	3.53
200	5.43
250	7.59
260	8.06
270	8.52
280	9.00
290	9.49
300	9.98
350	12.58
400	15.37
450	18.34

Table 5.4: N_i values for different n-type doping levels (n_0 is the number of acceptors in the active region) at different temperatures ($\lambda = 1.3\ \mu m$)

n_0 cm^{-3}	$n_i(T = 150K)$ $(10^{17} cm^{-3})$	$n_i(T = 298K)$ $(10^{17} cm^{-3})$	$n_i(T = 400K)$ $(10^{17} cm^{-3})$
0.0	3.53	9.88	15.37
10^{16}	3.46	9.82	15.30
5×10^{16}	3.21	9.56	15.04
10^{17}	2.90	9.24	14.72
5×10^{17}	1.07	6.87	12.26
10^{18}	0.22	4.44	9.498
5×10^{18}	0.00	0.06	0.602

Table 5.5: N_i values for different p-type doping levels (p_0 is the number of acceptors in the active region) at different temperatures ($\lambda = 1.3\ \mu m$)

p_0 cm^{-3}	$n_i(T = 150K)$ $(10^{17} cm^{-3})$	$n_i(T = 298K)$ $(10^{17} cm^{-3})$	$n_i(T = 400K)$ $(10^{17} cm^{-3})$
0.0	3.53	9.88	15.37
10^{16}	3.50	9.85	15.34
5×10^{16}	3.36	9.71	15.20
10^{17}	3.21	9.55	15.03
5×10^{17}	2.30	8.37	13.78
10^{18}	1.65	7.20	12.45
5×10^{18}	0.36	3.06	6.593
10^{19}	1.10	1.53	5.30

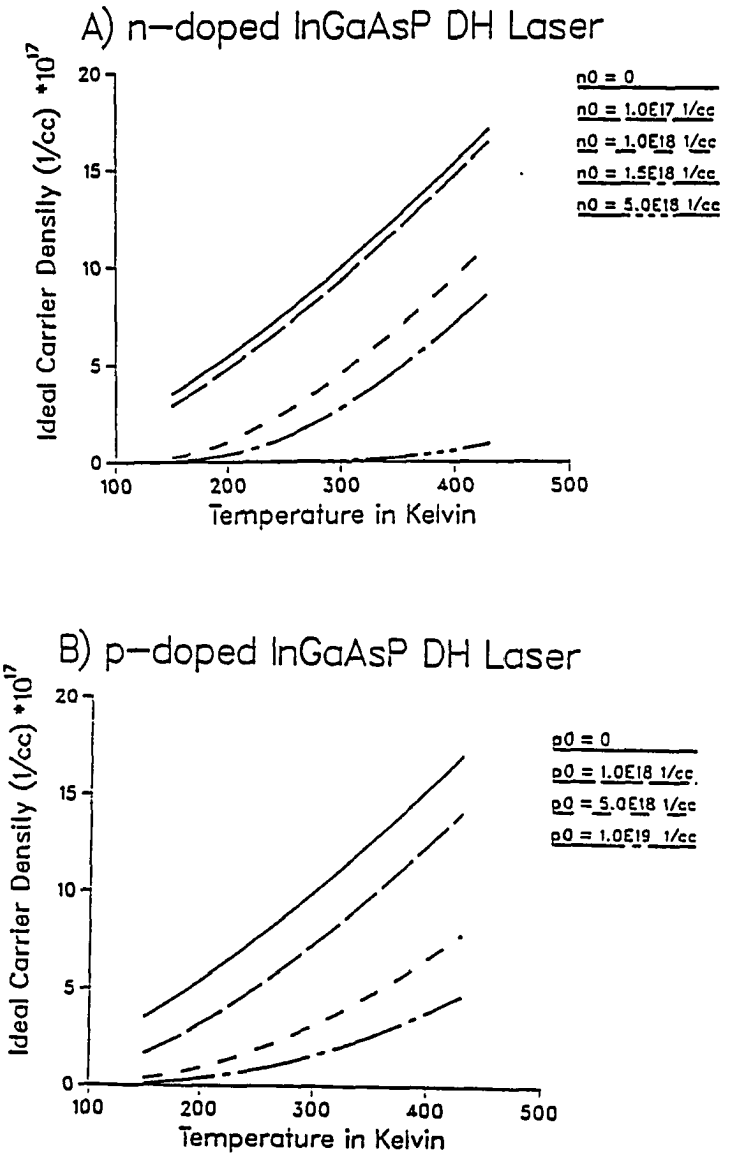

Figure 5.1: Ideal injected carrier density n_i as a function of active layer temperature for different active layer dopings a) n-type, and b) p-type (cc = cm^3)

are involved. First of all, for a given doping, an increase in the temperature (which is the active layer temperature) will result in an increase the ideal threshold carrier densities. On the other hand, for a given temperature, as the doping of the active layer increases, the ideal threshold carrier density decreases. This behavior can be explained intuitively. As the doping of the active layer increases there are more carriers available for recombination. Therefore, there will be less need to inject external carriers in order to reach the threshold. Consequently, for a laser with a higher active layer doping we need less ideal carrier density to achieve ideal lasing.

Another interesting point from Tables 5.4 and 5.5 is the fact the lasers with n-doped active layer require less ideal threshold carrier density than the p-doped laser. It is also true that for equal doping levels, an n-doped laser need less injection current than a p-type laser. It is the author's feeling that this effect is the manifestation of the fact that electrons have much smaller effective mass than holes. With a smaller effective mass they can be moved much easier and their effect of injection will be seen much sooner. This picture very qualitatively describes the effect and provides an intuitive way of understand the results.

One should note that up this point in the discussion calculations no losses have been introduced. Although n_i values have temperature dependent, the temperature dependence of the ideal threshold carrier density n_i is not a major contributor to the temperature sensitivity of the threshold current density. This point is especially apparent when one notices no sharp changes in the values of n_i in 250–300 K range.

5.2 A, B, and C Values for Calculation

Knowing values of n_i one can use equations 3.1 , 3.16, and 4.8 to get n_{th}, J_{th}, and the light output power P_L. However, before going any further one needs to know the values of A, B, and C's for different situations. We know these values both theoretically and experimentally. Therefore, let us review what these values are.

According to experimental results and theoretical calculations it is reasonable to choose the value of 10^8 for A. There have been some experimental reports that indicate values up to 10^{10} s^{-1} for A in heavily doped InGaAsP materials [29, 33] but it is more commonly assumed to be around 10^8. For the purpose of this study we will use the value 0.5×10^8 s^{-1} suggested by Haug and Burkhard [20].

The other coefficient is the bimolecular recombination coefficient or $B(T)$, that obeys approximately a $T^{-3/2}$ law indicated by theoretical and experimental investigations [20, 33, 62, 63, 64, 65]. As a consequence the product $Bn_i = n_i(300) \times 10^{-10}$ is independent of temperature. That is why for the different values of $B(T)$ we use the following equation also suggested by Haug and Burkhard[20],

$$B(T) = \left(\frac{T}{300}\right)^{\frac{-3}{2}} \times 10^{-10}\ cm^3/s$$

For the Auger coefficients we will use the values reported by Haug in Table 3.1. These values were originally presented in Figure 3.3. However, Haug made a correction in his results in 1987 and the values given in Table 3.1 are the corrected values [20, 25]. The original values are almost twice the corrected values. During this study we will use the corrected values given in Table 3.1.

Table 5.6: N_i, n_{th}, and J_{th} for an InGaAsP laser with an undoped active layer (d = 1 μm)

T (K)	n_i (10^{17})	n_{th} (10^{18})	J_{th} $(\frac{kA}{cm^2})$
100	1.92	0.290	0.935
150	3.53	0.538	1.784
200	5.43	0.847	2.977
250	7.59	1.232	4.805
300	9.98	1.793	9.313
350	12.58	2.656	22.62
400	15.37	4.031	69.78

5.3 N_{th} and J_{th} Results

Using the equations 2.1, 2.4, 2.5, 2.15, and 2.16 together with the values of A, B, C, and d (active layer thickness), we can approximate the values of n_{th} (equations 2.15 and 2.16) and J_{th} (equations 2.1, 2.4, and 2.5) at different active layer temperatures and for various dopings. For example Table 5.6 shows the result for an InGaAsP laser with an undoped active layer.

Figure 5.2 shows the our calculated result of n_{th} for different dopings and temperatures for both p and n doped lasers. Due to the considerations of losses (specially of Auger losses) one can see the enhanced temperature sensitivity of n_{th} around room temperature. We can see that the effect of increased losses results in a sharper increase of n_{th} values compared to n_i values. A very interesting effect in these results is the fact that the threshold carrier density of lasers with doped active layers is smaller than those with an undoped active layer. As the doping increases (similar to the case

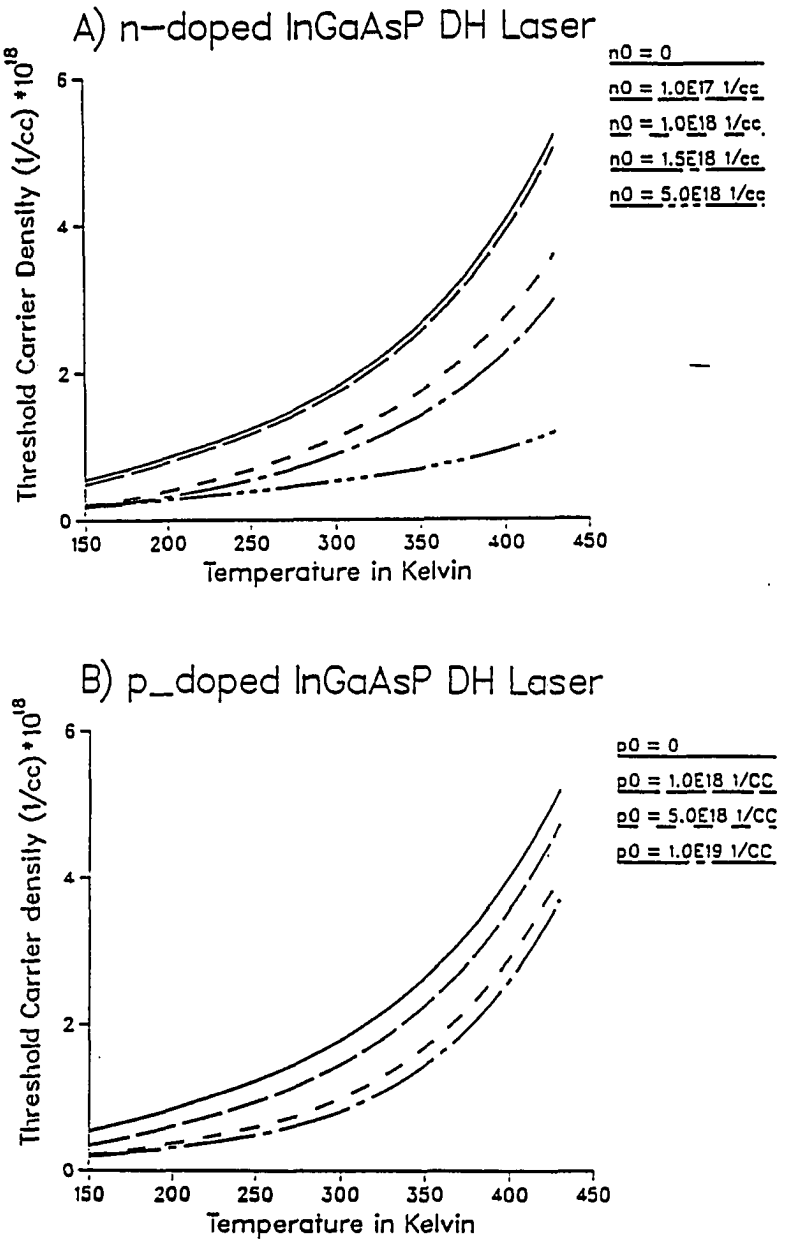

Figure 5.2: Threshold injected carrier density (n_{th}) as a function of temperature for different active layer dopings: a) n-type, and b) p-type (cc = cm^3)

Table 5.7: Doping dependence of n_i, n_{th}, and J_{th} in n-doped active layer InGaAsP lasers at 300 K

n_0 (10^{18})	n_i (10^{17})	n_{th} (10^{18})	J_{th} (kA/cm^2)
0.0	9.98	1.79	9.313
0.1	9.34	1.71	9.010
1.0	4.53	1.11	7.347
1.5	2.76	0.88	7.127
2.0	1.601	0.73	7.337
3.0	0.52	0.58	8.771
10.0	7.6×10^{-4}	0.5	34.692

for n_i) the threshold carrier density will decrease. On the other hand, due to losses, threshold current density will increase as the doping increases. This effect can be seen in Figure 5.3.

Figure 5.3 shows another important result. The fact that the threshold current density is sharply increasing around the room temperature is something that has been experimentally verified. One can see in Figure 5.3 the behavior of the threshold current density is as expected. To give a better feeling about some of the relative values for n_i, n_{th}, and J_{th} for different dopings Tables 5.7 and 5.8 give the results of some calculations. For the case of light to medium doping the n-type laser shows an initial decrease of J_{th} (see Table 5.7). This is an effect from variation in the effective mass of the electrons and has not been experimentally verified. This is a very interesting fact theoretically, although no confirming experimental reports have been found so far.

For the case of a p-doped active layer, all the values of injected carrier densities as

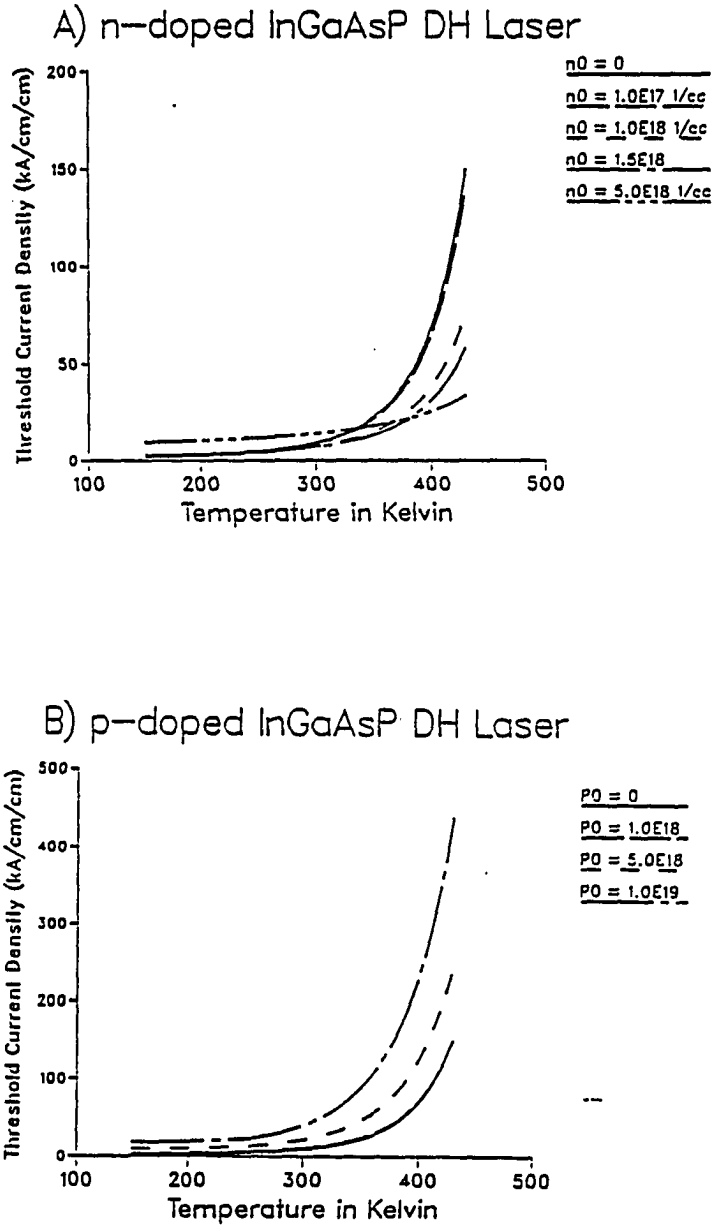

Figure 5.3: Threshold injected current density (J_{th}) as a function of temperature for InGaAsP lasers with different dopings: a) n-type, and b)p-type

Table 5.8: Doping dependence of n_i, n_{th}, and J_{th} in p-doped active layer InGaAsP lasers at 300 K

p_0 (10^{18})	n_i (10^{17})	n_{th} (10^{18})	J_{th} (kA/cm^2)
0.0	9.98	1.79	9.313
0.1	9.65	1.75	9.39
1.0	7.29	1.46	10.736
1.5	6.36	1.35	11.80
2.0	5.62	1.27	13.00
3.0	4.50	1.14	15.68
10.0	1.57	0.82	40.145

Table 5.9: Comparison of calculated and experimental values of n_{th} (in $10^{19}cm^{-3}$)of a laser with undoped active layer (experimental results taken from Haug) [34]

$T(K)$	100	150	200	250	300
$n_{th}(theory)$	0.29	0.538	0.847	1.232	1.793
$n_{th}(exp.)$	0.251	0.510	0.895	1.307	1.818

well as the injected currents are larger than the corresponding n-doped ones. Tables 5.7 and 5.8 illustrate this effect.

The general behavior of values for n_i, n_{th}, and J_{th} are very intuitively sound and provides a good qualitative check for the results. Quantitatively these results also show close correlation with experimental values. To indicate the close correspondence to the experimental values one can look at Table 5.9 which compares the theoretical approximations with the reported experimental values of threshold injected carrier densities at different temperatures.

Table 5.10: Experimental results for n_{th}, J_{th}, and T_0 at 300 K [24, 30]

Laser	$192-3$	$159-4$
Doping	*Zn*	*Zn*
$p_0(cm^{-3})$	8×10^{17}	16×10^{17}
$n_{th}(10^{18}\,cm^{-3})$	1.7	1.5
$J_{th}(KA/cm^2)$	23.85	27.69
$T_0(K)$	65	50

If we look at the values of J_{th} as a function of temperature given for an undoped laser as in Table 5.5, and if those values are compared to the values reported by Jung et al. (see Figure 2.8) [40], a close correlation and similar quantitative values for injected current densities can be observed.

The reported data cited above and the results reported in the next section show the strength and validity of our method both qualitatively and quantitative or intuitively. That is why we adapt the same model in approximating the light output power under CW operation

5.4 J_{th}, η_{th}, and T_0 Calculation

In this section further evidence for quantitative support of our method for the calculations of differential quantum efficiency at threshold η_{th}, characteristic temperature T_0, and J_{th} values are reported. First of all let us look at some experimental values in Table 5.10 as reported by Su et al. [29, 30] on some actual experimental lasers.

Using the model introduced earlier, a similar type of lasers can be studied easily.

Table 5.11: N_{th}, J_{th}, and T_0 at 300 K for p-type active layer InGaAsP DH lasers

$p_0(cm^{-3})$	8×10^{17}	16×10^{17}
$N_{th}(10^{18}\ cm^{-3})$	2.0	1.831
$J_{th}(KA/cm^2)$	19.618	22.571
$T_0(K)$	63.79	67.08

The results from our approximation are given in Table 5.11. Looking at the results in Table 5.11 one should remember that, considering the approximations and the limits of our model, these are very good quantitative results and they support the the usefulness and accuracy of our model.

In Table 5.11 we see a good approximation of the values for T_0 given by our model. In reality, the characteristic temperature is a temperature dependent entity [44, 55]. However, one of the most important characteristics of our model, as described in the previous chapter, is the fact that although it predicts very reasonable values for T_0 and T_E, there is no need for such calculations. Table 5.12 shows some typical values for η_{th} (threshold differential quantum efficiency), T_E, and T_0 as a function of temperature.

One should notice the following about the results of Table 5.11: First, the values of η (differential quantum efficiency), T_E, and T_0 are reasonable. Second, the values of η_{th}, which are calculated using Asada and Suematsu's model, are estimated with threshold injected carrier density as the number of carriers injected in the active layer. Even though this is an under estimated value for quantum efficiency, the results are not only reasonable but are very similar to the experimental results reported

Table 5.12: η_{th}, T_E, and T_0 for different temperatures around the room temperature for an undoped active layer (reference T for T_0 is 200 K and for T_E is 255 K)

$T(K)$	η_{th}	$T_E(K)$	T_0
250	0.475	151.31	104.43
280	0.376	124.0	93.74
300	0.307	111.41	87.70
320	0.243	102.14	81.8
350	0.165	92.81	73.97

by Tamari, Asada and Suematsu, and Pankove. That is why we use this in our calculations (with confinement factor $\xi = 0.5$).

5.5 Light Output Power

In order to use our model to study the CW operation of an InGaAsP DH laser, we need to specify particular structures. These structures must have some reasonable dimensions and characteristics to make the results more physically realistic. Consequently, we choose two basic structures with similar geometries to the ones studied by Steventon et al. [44]. Figures 5.4 and Figure 5.5 show our two structures which we will refer to as Lasers 1 and 2 respectively. Laser 1 and Laser 2 are very similar except for two specific layers. Laser 2 has a thicker passive layer ($d_p = 4\mu m$) and a thinner substrate ($d_s = 50\mu m$) compared to Laser one (which has $d_p = 2\mu m$ and $d_s = 100\mu m$). All calculations will be made on both of these lasers to give the reader an idea of how different layer dimensions will effect the output. The width of the active layer (w_a) shown as A in the figures will also be changed. However, active

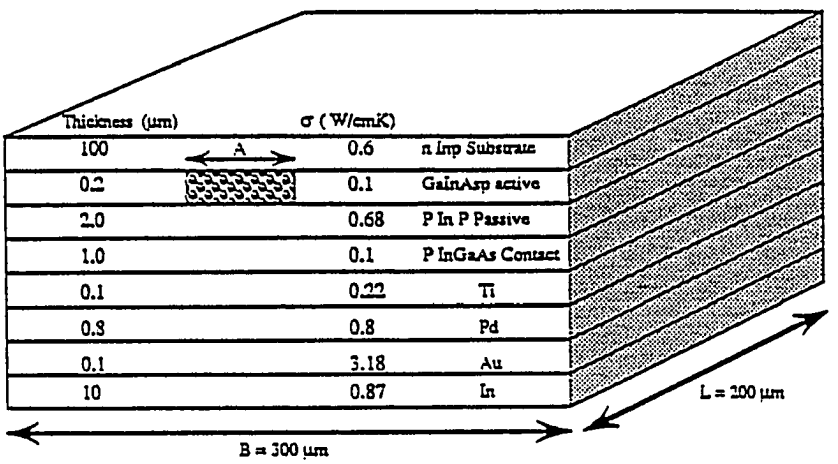

Figure 5.4: Prototype laser for calculation of CW operation of InGaAsP DH lasers. This structure has a thin passive layer and a normal size substrate (Laser 1)

layer thickness (d_a = 0.2 μm) will be kept the same for both of the lasers. Unfortunately, there are no experimental results measuring the type of light power output that we are interested in. Therefore, we have to examine our final result with respect to general behavior and magnitude of the quantities rather than with verification by experimental data.

For the purpose of our study we will look at three different active layer widths. These will be called narrow-stripe (w_a=10 μm), medium-stripe (w_a=150 μm), and broad area laser (w_a=300 μm). The operation of these lasers will be studied assuming different heat sink temperatures as well as different active layer dopings. We will study the results by considering the characteristic quantities P_{Lm} (the maximum value of light output power P_L), I_m (the value of the injection current at which P_L takes its

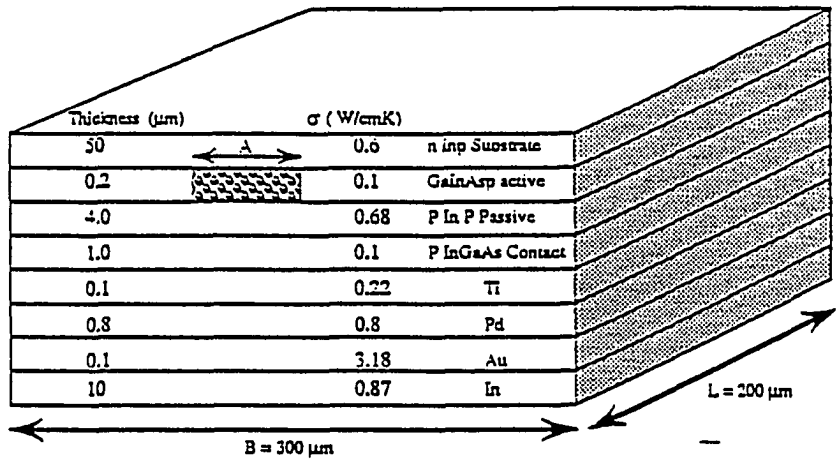

Figure 5.5: Prototype laser calculation of CW operation of InGaAsP DH lasers. This structure has a thick passive layer and a relatively thin substrate substrate (Laser 2)

maximum value), and ΔI (the range of injection current over which CW operation is possible) for different heat sink temperatures (T_H). We will also consider ΔT_H which represents the range of heat sink temperatures over which CW operation is possible. However, ΔT_H is only considered qualitatively, since theoretically we are not interested in the lower value of T_H. We are really interested in the behavior of these lasers for T_H values around room temperature. Thus, in this study we will consider the concept of ΔT_H very generally and use it for the purpose of comparison between different lasers.

Figure 5.6 shows the results for narrow-stripe Lasers 1 and 2 with undoped active layers. The approximate results for the characteristic quantities (P_{Lm}, I_m, and ΔI) of the lasers is given in Tables 5.13 and 5.14.

Table 5.13: Approximate characteristic values of Laser 1 ($d_p = 2\ \mu m$, $d_s = 100\ \mu m$) with narrow-stripe ($w_a = 10\ \mu m$, $d_a = 0.2\ \mu m$) and undoped active layer (see Figure 5.6a)

$T_H(K)$	$P_{Lm}(W)$	$Im(A)$	$\Delta I(A)$
280	0.43	1.10	1.95
290	0.37	1.08	1.87
300	0.32	1.06	1.80
310	0.27	1.02	1.72
320	0.22	0.99	1.65

Due to the fact that Laser 2 has a thinner substrate than Laser 1, its active layer will be at a relatively lower average temperatures compared to Laser 1. Consequently, in all of the results reported in this study we will see that Laser 2 is capable of CW operation over a broader range of heat sink temperatures than Laser 1. This means that ΔT_H of Laser 2 is larger than that of Laser 1. This fact can be verified for the case of narrow-stripe type of lasers by the results reported in Tables 5.13 and 5.14. One can see that at the same heat sink temperature Laser 2 has a higher P_{Lm}, I_m, and ΔI values than Laser 1. These values illustrate that Laser 2 has a better dynamic range for CW operation at the given heat sink temperature.

There are some other general observations to be made regarding Figure 5.6. As the heat sink temperature increases the light output power will decrease. In P_L versus I figures one can see the lower output levels corresponding to higher heat sink temperatures. This is an important behavior since it shows how the losses are temperature dependent. This type of behavior can be seen in all of the P_L versus I figures reported in this study.

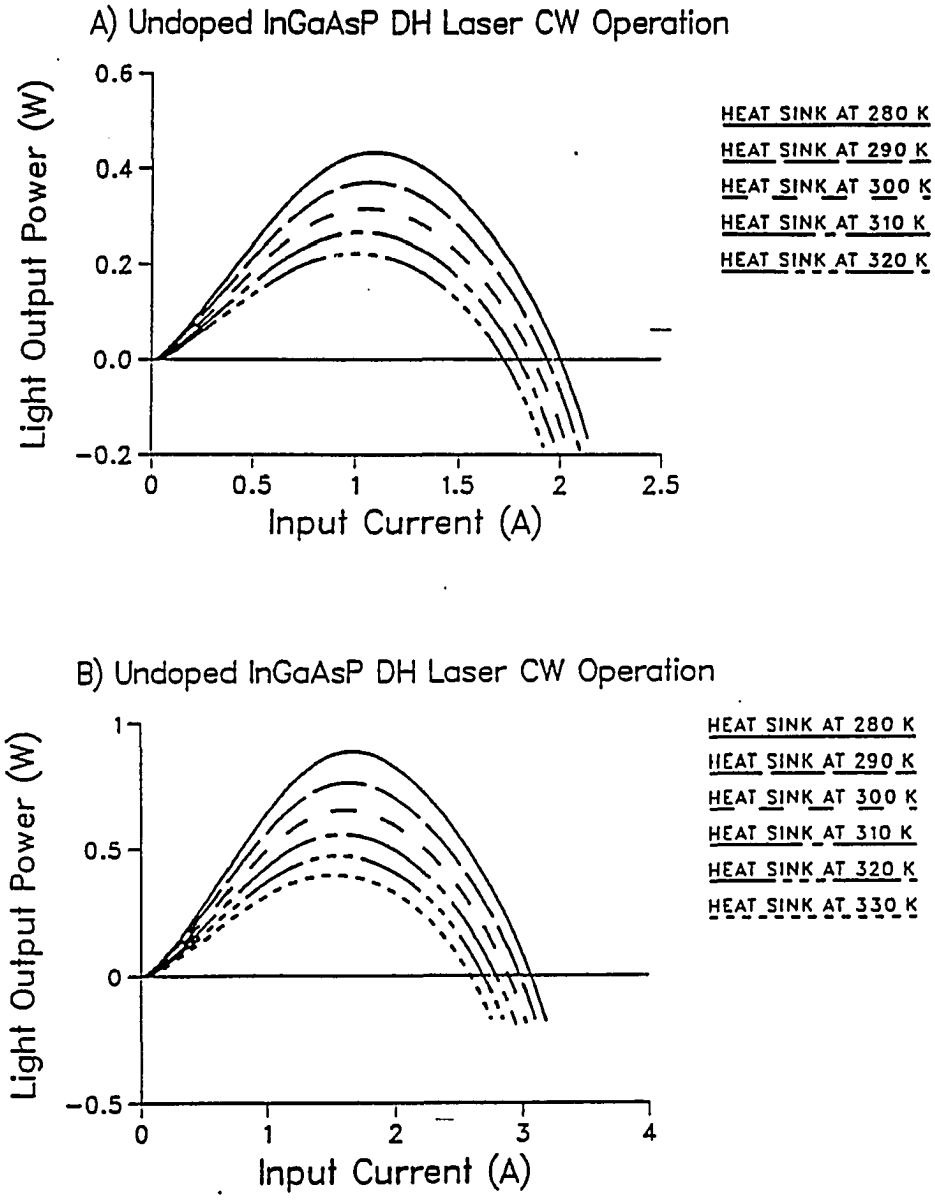

Figure 5.6: Light output power versus input current for InGaAsP DH lasers with narrow-stripe ($w_a = 10\ \mu m$, $d_a = 0.2\ \mu m$) undoped active layers: (a) Laser 1 ($d_p = 2\ \mu m$, $d_s = 100\ \mu m$), (b) Laser 2 ($d_p = 4\ \mu m$, $d_s = 50\ \mu m$) (see Tables 5.14 and 5.15)

Table 5.14: Approximate characteristic values of Laser 2 ($d_p = 4\ \mu m$, $d_s = 50\ \mu m$) with narrow-stripe ($w_a = 10\ \mu m$, $d_a = 0.2\ \mu m$) and undoped active layer (see Figure 5.6b)

$T_H(K)$	$P_{Lm}(W)$	$I_m(A)$	$\Delta I(A)$
280	0.89	1.65	3.01
290	0.76	1.63	2.91
300	0.66	1.61	2.81
310	0.56	1.58	2.72
320	0.47	1.56	2.61
330	0.40	1.53	2.50

According to our formulation a negative calculated light output power indicates the condition of nonlasing. In the case of a heat sink temperature high enough to make the losses dominant, lasing can never take place. Figure 5.7 demonstrates how the behavior of light output power as a function of injected current is different in the case of two heat sink temperatures. The lower temperature allows lasing action to take place while the higher does not. The fact that the laser with the higher heat sink temperature has negative calculated light output power through the whole current range indicates that it never gets to lase. This point should be contrasted against the laser with its heat sink at the lower temperature value. Such a laser goes through a range for output power that indicates lasing action is taking place. This behavior of our model is physically what is expected.

Figure 5.8 shows the calculated light output power versus injected current for medium-stripe ($w_a = 150\ \mu m$) lasers with undoped active layers and the characteristic quantities are given in Tables 5.15 and 5.16. In this type of laser, there is more current

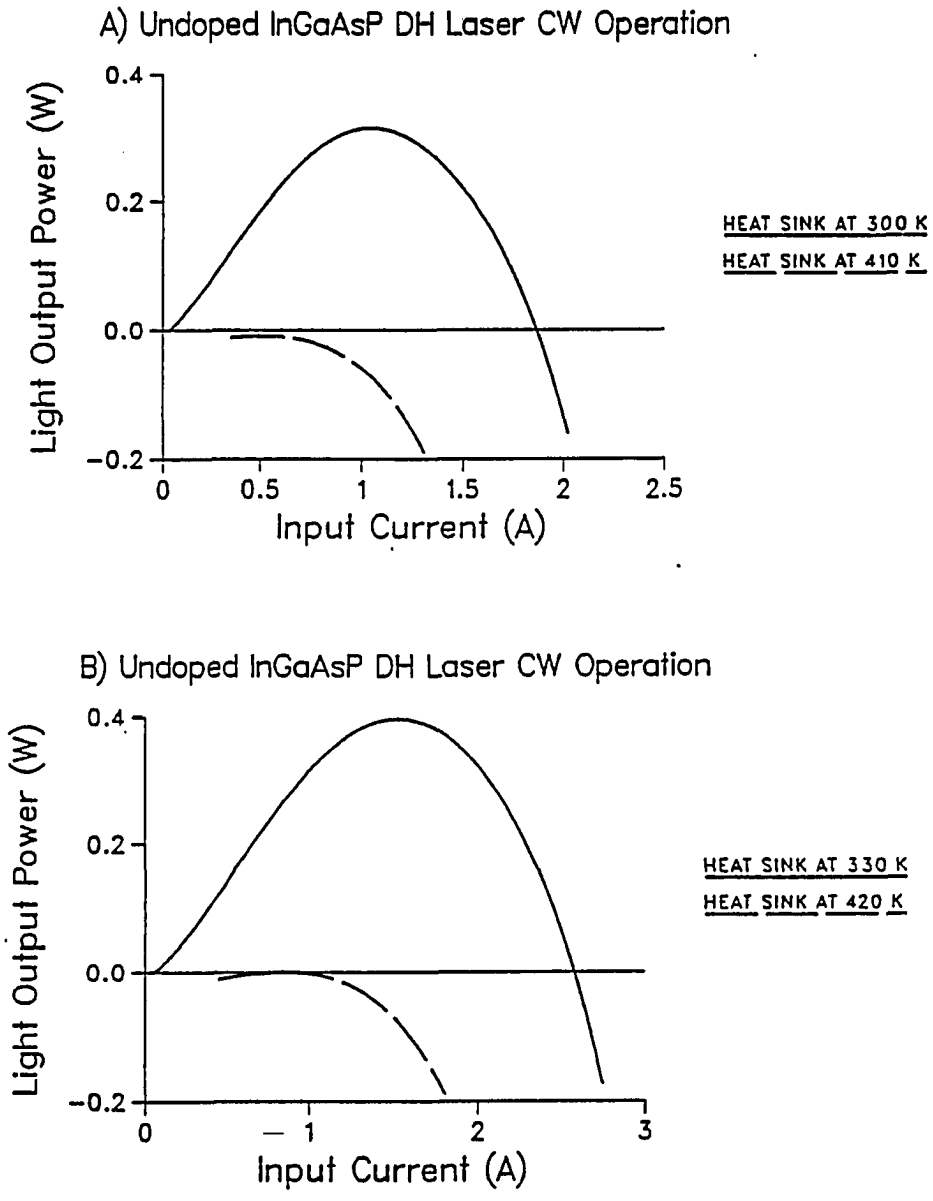

Figure 5.7: Light output power versus input current for InGaAsP DH lasers with narrow-stripe ($w_a = 10\ \mu m$, $d_a = 0.2\ \mu m$) undoped active layers, demonstrating lasing versus nonlasing results: (a) Laser 1 ($d_p = 2\ \mu m$, $d_s = 100\ \mu m$), (b) Laser 2 ($d_p = 4\ \mu m$), $d_s = 50\ \mu m$)

Table 5.15: Approximate characteristic values of Laser 1 ($d_p = 2\ \mu m$, $d_s = 100\ \mu m$) with medium-stripe ($w_a = 150\ \mu m$, $d_a = 0.2\ \mu m$) and undoped active layer (see Figure 5.8a)

$T_H(K)$	$P_{Lm}(W)$	$I_m(A)$	$\Delta I(A)$
260	0.15	0.87	0.84
270	0.07	0.82	0.60
280	0.001	0.75	0.1

injected into the active region. The average temperature of the active region will be rising faster than it would in narrow-stripe lasers. Consequently, there will be more losses in the active region and the laser light output power will be limited. Comparing Tables 5.13 and 5.14 with 5.15 and 5.16, one can see some interesting results. First, for a given heat sink temperature the values of the characteristic quantities P_{Lm}, I_m, and ΔI of the medium-stripe lasers are lower than they are for narrow-stripe lasers. This is a direct indication that the CW operation of medium-stripe laser is more restricted than for lasers with narrower stripes. In medium-stripe lasers the higher current levels in the active region and corresponding increase in the injection level will result in higher average temperatures of the active layer. This in turn will result in still higher losses. Second, the results of Figure 5.8 and Tables 5.13 to 5.16, together with the above discussion indicate lower values of ΔT_H for medium-stripe lasers. This means a narrower allowed range of heat sink temperatures for CW operation.

In general, as the active layer of a laser gets wider, the current levels will be larger and the laser will only lase at relatively low heat sink temperatures. In the case of broad area laser the current levels are the largest. That is why the broad area

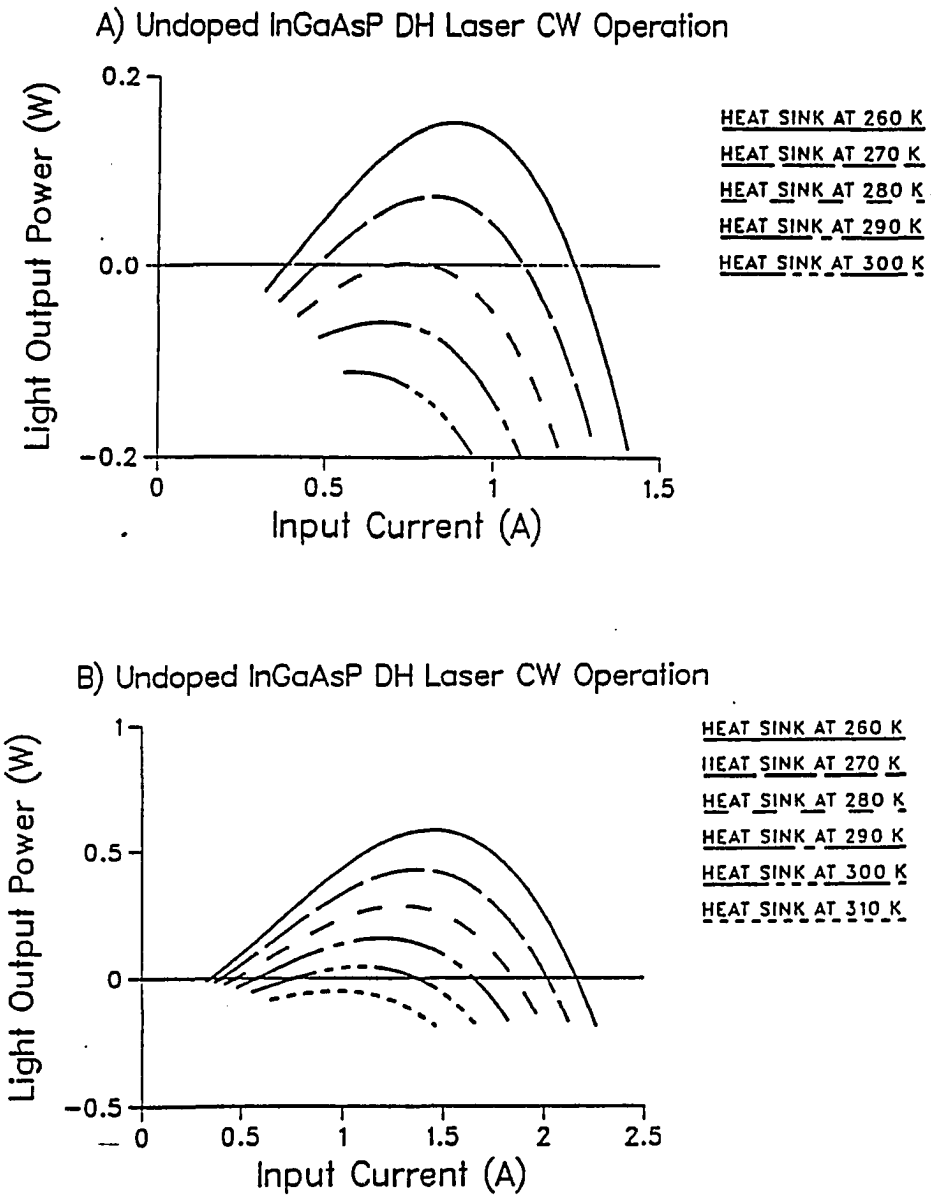

Figure 5.8: Light output power versus input current for InGaAsP DH lasers with medium-stripe ($w_a = 150\ \mu m$, $d_a = 0.2\ \mu m$) undoped active layers: (a) Laser 1 ($d_p = 2\ \mu m$, $d_s = 100\ \mu m$), (b) Laser 2 ($d_p = 4\ \mu m$, $d_s = 50\ \mu m$) (see Tables 5.15 and 5.16)

Table 5.16: Approximate characteristic values of Laser 2 ($d_p = 4\ \mu m$, $d_s = 50\ \mu m$) with medium-stripe ($w_a = 150\ \mu m$, $d_a = 0.2\ \mu m$) and undoped active layer (see Figure 5.8b)

$T_H(K)$	$P_{Lm}(W)$	$I_m(A)$	$\Delta I(A)$
260	0.58	1.45	1.80
270	0.43	1.35	1.61
280	0.28	1.29	1.38
290	0.16	1.19	1.06
300	0.05	1.08	0.62

Table 5.17: Approximate characteristic values of Laser 1 ($d_p = 2\ \mu m$, $d_s = 100\ \mu m$) with broad area ($w_a = 300\ \mu m$, $d_a = 0.2\ \mu m$) and undoped active layer (see Figure 5.9a)

$T_H(K)$	$P_{Lm}(W)$	$I_m(A)$	$\Delta I(A)$
210	0.27	1.00	0.93
220	0.15	0.94	0.72
230	0.05	0.88	0.43

lasers show lasing at heat sink temperatures much lower than the narrower stripe laser. This effect is demonstrated in Figure 5.9 and Tables 5.17 and 5.18.

Tables 5.17 and 5.18 together with Figure 5.9 show that due to the high of injection currents in the active regions of the broad area lasers, CW operation of these lasers is only possible at very low heat sink temperatures compared with the narrow or medium stripe structures. Thus, due to the fact that losses inside the active regions of these lasers are dominant, ΔT_H for broad area lasers is the narrowest. At

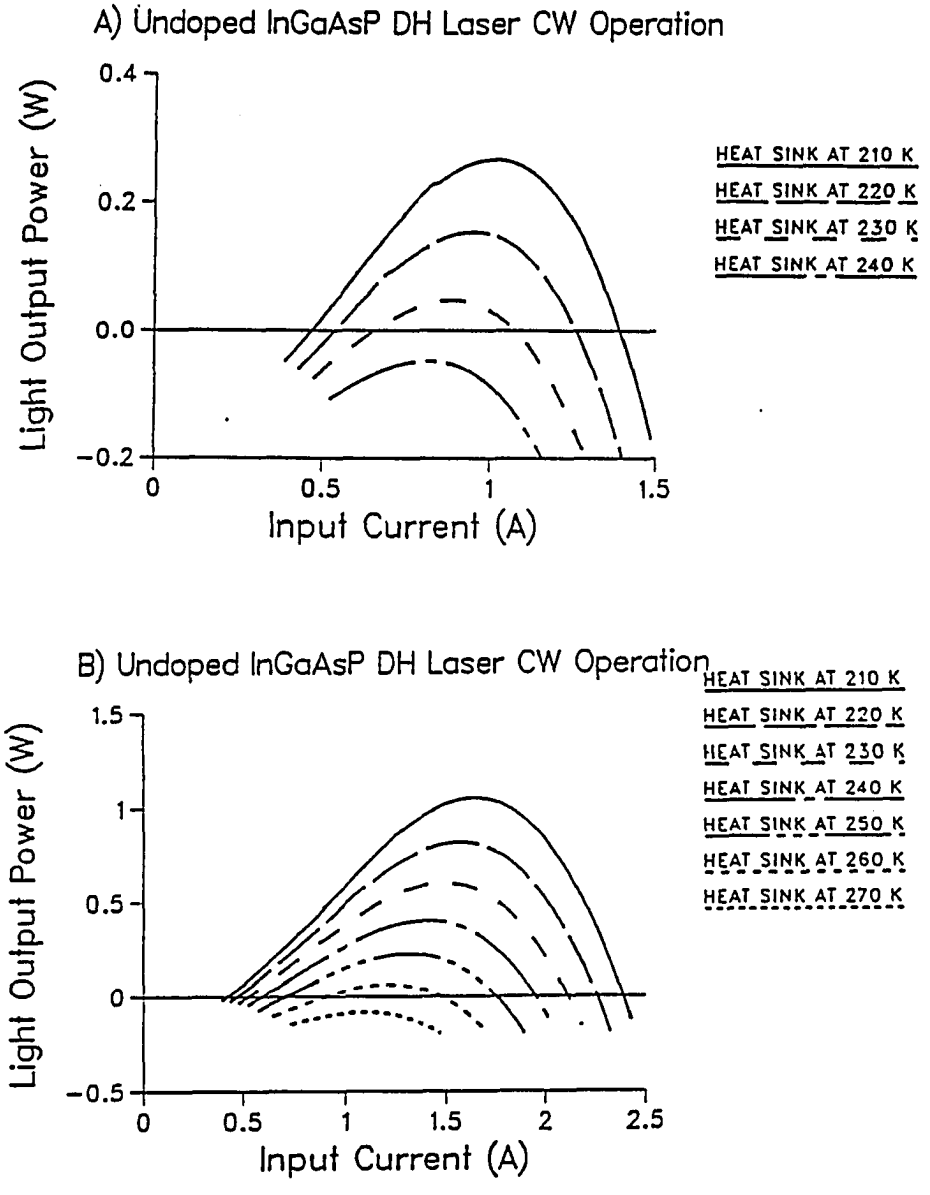

Figure 5.9: Light output power versus input current for InGaAsP DH lasers with broad area ($w_a = 300\ \mu m$, $d_a = 0.2\ \mu m$) undoped active layers: (a) Laser 1 ($d_p = 2\ \mu m$, $d_s = 100\ \mu m$), (b) Laser 2 ($d_p = 4\ \mu m$, $d_s = 50\ \mu m$) (see Tables 5.17 and 5.18)

Table 5.18: Approximate characteristic values of Laser 2 ($d_p = 4\ \mu m$, $d_s = 50\ \mu m$) with broad area ($w_a = 300\ \mu m$, $d_a = 0.2\ \mu m$) and undoped active layer (see Figure 5.9b)

$T_H(K)$	$P_{Lm}(W)$	$I_m(A)$	$\Delta I(A)$
210	1.05	1.65	1.95
220	0.82	1.55	1.80
230	0.60	1.49	1.59
240	0.41	1.41	1.34
250	0.23	1.32	1.03
260	0.06	1.20	0.57

the same time the values of P_{Lm}, I_m, and ΔI for the same heat sink temperatures will be much lower for these lasers than the lasers with smaller active layer widths. Historically, the investigators in this area were forced to abandon broad area lasers to avoid excessive heating and instead concentrate on lasers with lower current levels. Our model clearly justifies and explains the need for this action.

One would expect that under the condition of active layer doping and the resultant need for more injection to make the lasing action possible, the laser behavior would be more restricted than for the undoped cases. Figure 5.10 and Tables 5.19 and 5.20 show the results for medium-stripe ($w_a = 150\ \mu m$) lasers with p-doped active layers. The values in Table 5.19 should be compared with the values given in Table 5.15 (the undoped case) and the values of Tables 5.20 and 5.16 should be considered together.

In the case of p-doped active regions one can see that both Lasers 1 and 2 show that the doping increases I_m and decreases the values of P_{Lm} and ΔI. This indicates

Table 5.19: Approximate characteristic values of Laser 1 ($d_p = 2\ \mu m$, $d_s = 100\ \mu m$) with medium-stripe ($w_a = 150\ \mu m$, $d_a = 0.2\ \mu m$) and p-doped active layer (see Figure 5.10a)

$T_H(K)$	$P_{Lm}(W)$	$I_m(A)$	$\Delta I(A)$
260	0.11	0.88	0.68
270	0.02	0.82	0.32

Table 5.20: Approximate characteristic values of Laser 2 ($d_p = 4\ \mu m$, $d_s = 50\ \mu m$) with medium-stripe ($w_a = 150\ \mu m$, $d_a = 0.2\ \mu m$) and p-doped active layer (see Figure 5.10b)

$T_H(K)$	$P_{Lm}(W)$	$I_m(A)$	$\Delta I(A)$
260	0.52	1.44	1.57
270	0.35	1.34	1.33
280	0.20	1.27	1.05
290	0.06	1.17	0.60

a more restricted CW operation and narrower ΔT_H range for p-doped active layer lasers as opposed to undoped ones. In general our results show that lasers with heavier p-doped active regions require higher injection currents for lasing. This has a substantial effect on the dynamic range of CW operation of such lasers. This is an unfavorable effect, and that is why in actual systems utilizing InGaAsP semiconductor lasers we generally use undoped active layer lasers.

Figure 5.11 and Tables 5.21 and 5.22 show the results for medium-stripe lasers with n-doped active layers. According to our model (comparing these results with the case of undpoed lasers in Figure 5.8 and Tables 5.15 and 5.16) some levels of

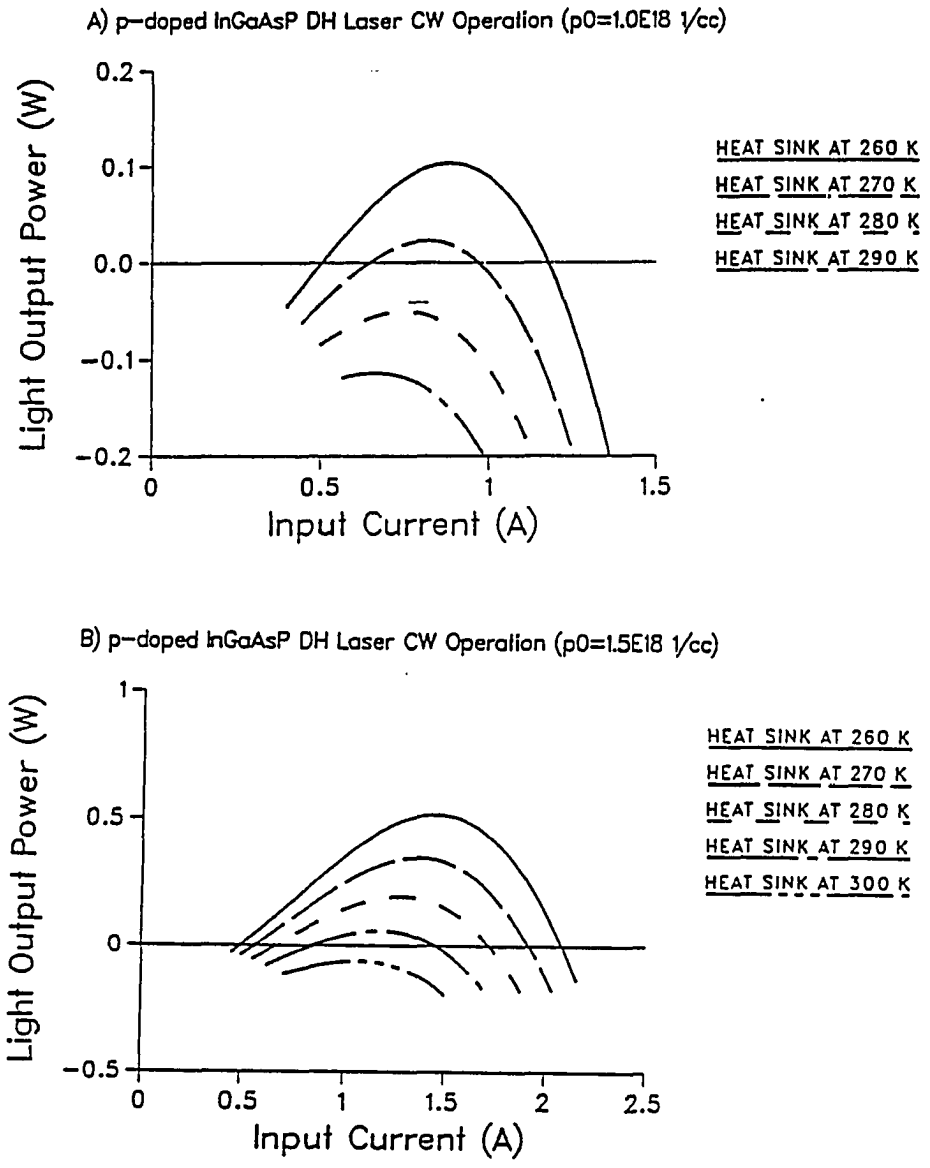

Figure 5.10: Light output power versus input current for InGaAsP DH lasers with medium-stripe ($w_a = 150\ \mu m$, $d_a = 0.2\ \mu m$) p-doped active layers: (a) Laser 1 ($d_p = 2\ \mu m$, $d_s = 100\ \mu m$), (b) Laser 2 ($d_p = 4\ \mu m$, $d_s = 50\ \mu m$) (see Tables 5.19 and 5.20)

Table 5.21: Approximate characteristic values of Laser 1 ($d_p = 2\ \mu m$, $d_s = 100\ \mu m$) with medium-stripe ($w_a = 150\ \mu m$, $d_a = 0.2\ \mu m$) and lightly n-doped active layer (see Figure 5.11a)

$T_H(K)$	$P_{Lm}(W)$	$I_m(A)$	$\Delta I(A)$
260	0.78	0.91	0.93
270	0.10	0.85	0.70
280	0.03	0.78	0.38

Table 5.22: Approximate characteristic values of Laser 2 ($d_p = 4\ \mu m$, $d_s = 50\ \mu m$) with medium-stripe ($w_a = 150\ \mu m$, $d_a = 0.2\ \mu m$) and lightly n-doped active layer (see Figure 5.11b)

$T_H(K)$	$P_{Lm}(W)$	$I_m(A)$	$\Delta I(A)$
260	0.64	1.47	1.87
270	0.48	1.41	1.69
280	0.33	1.32	1.46
290	0.20	1.24	1.19
300	0.08	1.14	0.80

n-type doping of the active layer can results in higher P_{Lm}, I_m, and ΔI values compared to the undoped case. It should be noted that this prediction has not been experimentally verified todate. The results suggest that with a moderate level of n-type doping, the optical output power can be enhanced. It would be very desirable to see this prediction verified.

Figures 5.12 and Tables 5.23 and 5.24 show the predicted results for medium-stripe lasers with n-doped active layers that are doped to higher levels than the ones

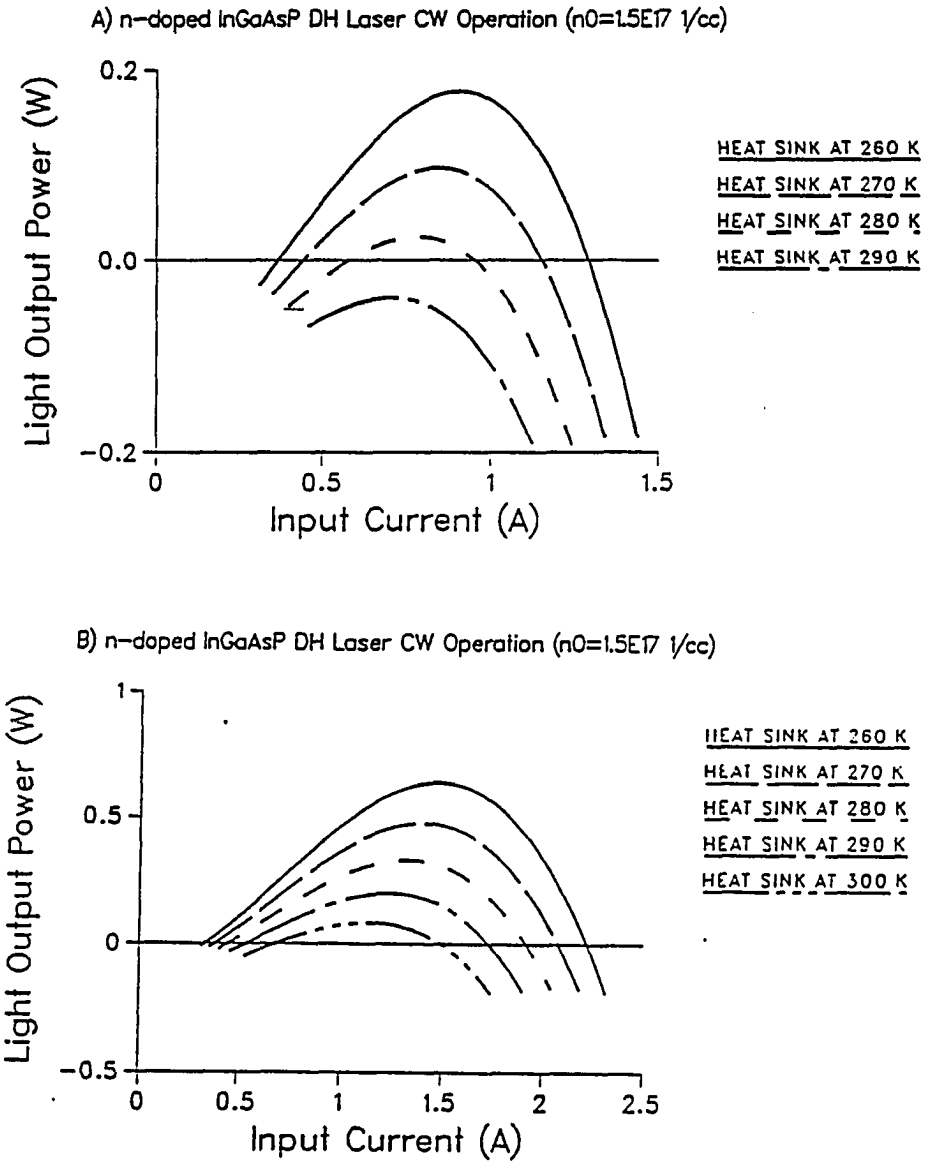

Figure 5.11: Light output power versus input current for InGaAsP DH lasers with medium-stripe ($w_a = 150\ \mu m$, $d_a = 0.2\ \mu m$) and lightly n-doped active layers: (a) Laser 1 ($d_p = 2\ \mu m$, $d_s = 100\ \mu m$), (b) Laser 2 ($d_p = 4\ \mu m$, $d_s = 50\ \mu m$) (see Tables 5.21 and 5.22)

Table 5.23: Approximate characteristic values of Laser 1 ($d_p = 2\ \mu m$, $d_s = 100\ \mu m$) with medium-stripe ($w_a = 150\ \mu m$, $d_a = 0.2\ \mu m$) and n-doped active layer (see Figure 5.12a)

$T_H(K)$	$P_{Lm}(W)$	$I_m(A)$	$\Delta I(A)$
240	0.14	1.49	0.71
250	0.06	1.45	0.46

Table 5.24: Approximate characteristic values of Laser 2 ($d_p = 4\ \mu m$, $d_s = 50\ \mu m$) with medium-stripe ($w_a = 150\ \mu m$, $d_a = 0.2\ \mu m$) and n-doped active layer (see Figure 5.12b)

$T_H(K)$	$P_{Lm}(W)$	$I_m(A)$	$\Delta I(A)$
240	0.84	2.32	1.97
250	0.67	2.23	1.75
260	0.51	2.20	1.56
270	0.36	2.15	1.34
280	0.22	2.10	1.06

in Figure 5.11 and Tables 5.21 and 5.22. They indicate that at various higher levels of doping, CW operation of these lasers can be restricted (similar to the p-type doping results) and lasing can take place over a narrower range of ΔT_H values.

5.6 Conclusion

As demonstrated by the calculations discussed earlier, our model successfully predicts the CW operation of InGaAsP DH lasers. These results show what we expected from physical intuitive reasoning as well as giving quantitative values that are

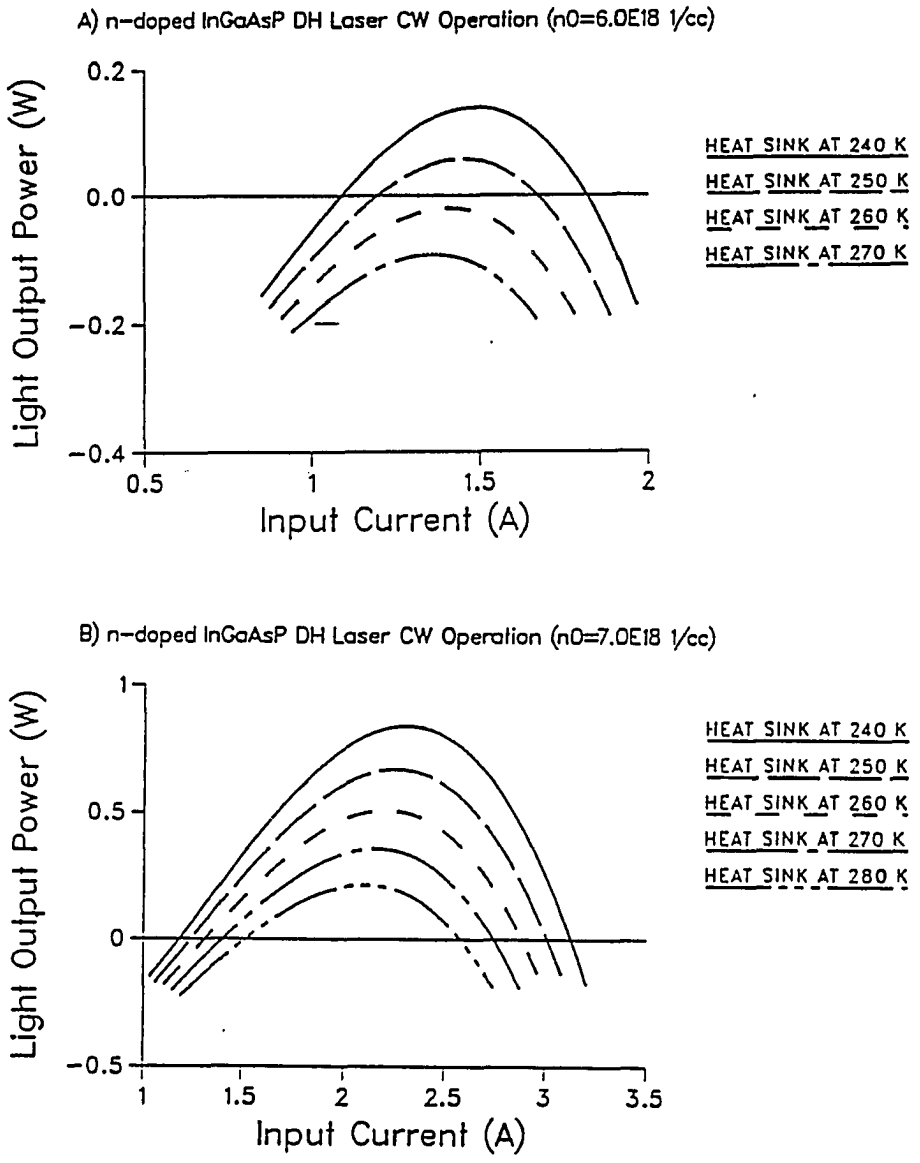

Figure 5.12: Light output power versus input current for InGaAsP DH lasers with medium-stripe (w_a = 150 μm, d_a = 0.2 μm) n-doped active layers: (a) Laser 1 (d_p = 2 μm, d_s = 100 μm), (b) Laser 2 (d_p = 4 μm), d_s = 6 μm) (see Tables 5.23 and 5.24)

reasonable. Unfortunately the type of measurements we need for detail comparison are not available. However, our results show the general behavior of the laser can be predicted by our model and that the quantitative values of the laser parameters are in agreement with those of a working semiconductor laser. For example as shown in Figure 5.13, we can look at the results reported for a typical laser. Figure 5.13 shows the general behavior (under different conditions however than the one we are concerned with) of an InGaAsP Mesa-laser used in actual fiber optics systems [66]. Although our results are for DH lasers, one can see that our calculations provide similar light output versus injection curent behavior (see Figures 5.8 to 5.12).

The important point in our study has been the fact that we could come up with a model for CW operation of InGaAsP DH lasers that assumes the Auger process to be the major nonradiative recombination type of losses. This type of modeling has not been previously applied to CW operation. In our work we incorporated a method proposed by Albert Haug in 1985 for such lasers. Extending his method and utilizing a model for quantum efficiency of InGaASP lasers we successfully predicted the behavior of InGaAsP DH lasers under CW operation. This was done by utilization of a two dimensional temperature analysis of the active layer to get better temperature values for our calculations. Important results are the fact that the model has very intuitive physical characteristics and shows reasonable predictions for light output power as a function of injected current. The model provides a straightforward and rapid way of getting practical answers which are usually obtained through a laborious and confusingly tedious processes. The model predicts reasonable values of all laser parameters, and shows a correct temperature dependence of the quantities. It is the

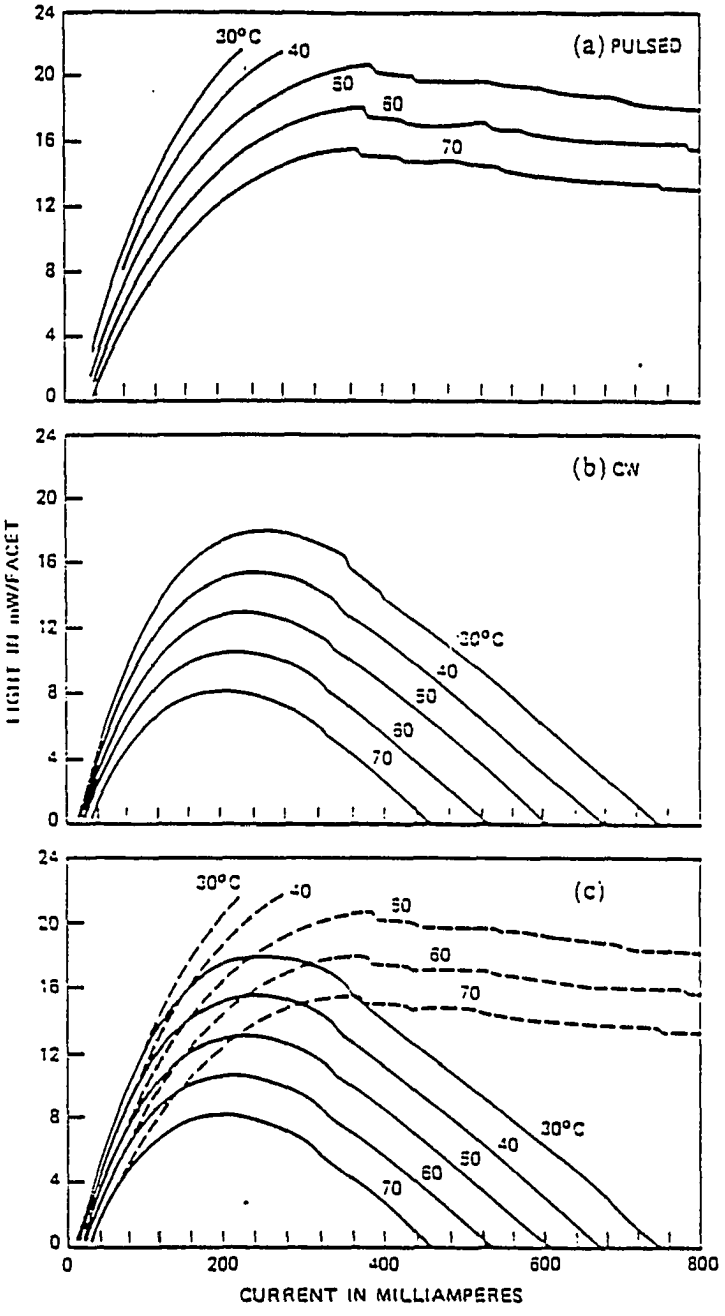

Figure 5.13: Light output power as a function of injected current for InGaAsP for different heat sink temperatures (a) pulsed (b) CW. and (C) composite [66]

author's feeling that this model can serve as a prefabrication tool for InGaAsP/InP lasers.

Another important point about the model developed here is that it is relatively simple to add other losses to it. For instance one can add the leakage current effect by a $Dn_{th}^{4.5}$ term to equation 3.1. On the other hand, one can include ohmic losses and other types of losses by including appropriate boundary conditions for the two dimensional temperature calculations. These are some of the possibilities of this model to be addressed in the future studies.

Finally, since we could successfully isolate and study the effects of Auger recombination on the light output power of InGaAsP DH lasers, we can say that this effect proves to be one of the most important inherent loss mechanism in InGaAsP lasers. It is probably the most important reason for the acute temperature characteristics of InGaAsP lasers.

6. BIBLIOGRAPHY

[1] Maiman, T. H. "Stimulated Optical Radiation in Ruby." *Nature*, 187, No. 4736 (1960), 493–449.

[2] Sze, S. M. *Semiconductor Devices Physics and Technology*, New York: John Wiley and Sons, 1985.

[3] Agrawal, G. P. ; Dutta, N. K. *Long Wavelength Semiconductor Lasers.* New York: Van Nostrand, 1986.

[4] Tsang, W. T. *Semiconductors and Semimetals.* 22A. Orlando: Academic Press, 1985.

[5] Li, T. "Lightwave Telecommunication" *Phys. Today*, 38, No. 5 (1985), 24–31.

[6] Newnam, N. H.; Ritchie S. "Sources and detectors for optical fibre communications applications: the first 20 years." *IEE proc.*, 133, No. 3 (1986), 213–229.

[7] Sze, S. M. *Physics of Semiconductor Devices.* New York: John Wiley and Sons, 1981.

[8] Dutta, N. K.; Nelson, R. J. "Review of InGaAsP InP Laser Structures and comparison of Their Performance ." In *Semiconductors and Semimetals.* 22c ; Tsang, W. T. , ed.; Orlando: Academic Press, (1985), 1–57.

[9] Yamamoto, Y.; Kimura, T. "Coherent Optical fiber transmission systems." *IEEE J. Quantum Electron.*, QE–17, No. 6 (1981), 919–934.

[10] Suematsue, Y. "Long-Wavelength Optical Fiber Communication." *Proc. IEEE*, 71, No. 6 (1983), 692-721.

[11] Pankove, J. I. *Optical Process in Semiconductors.* New York: Dover Publication, 1971.

[12] Javan. A. ; Bennett, W. R. Jr. ; Harriot, D, R. " Population Inversion and Continuous Optical Maser Oscillation in a Gas Discharge Containing a He–Ne Mixture ." *Phys. Rev. Lett.* , 6, No. 3 (1961), 106–110.

[13] Li, T. "Advances in Optical Fiber Communications: An Historical Perspective." *J. Selt. Areas Comm.*, SAC-1,No. 3 (1983), 356–372.

[14] Bartolini, R. A. ; Bell, A. E. ; Spong, F. W. "Diode Laser Optical Recording Using Trilayer Structure." *IEEE J. Quantum Electron*, QE-17,No. 1 (1981), 69–77.

[15] Asbeck, P. M. ; Cammak D. A. ; Danieles, J. ; Low, D. ; Heemskerk, J. P. J. ; klenters, W. J. ; Ophey, W. H. "High Density Optical Recording with (Ga,Al)As DH Lasers." *Appl. Phys. Lett.*, 34, No. 12 (1979), 835–837.

[16] Will, K. W. ; Blum, F. A. ; Calawa, A. R. ; Harman, T. C."PbSSe Tunable Lasers for High Resolution Infrared Spectroscopy." *J. Nonmetals*, 1, No. 3 (1973), 211–216.

[17] Kroemer, H."A Proposed Class of Hetrojunction Injection Laser." *Proc. IEEE*, 51, No. 12 (1963), 2–3.

[18] Haug, A. "Theory of the Temperature Dependence of the Threshold Current of InGaAsP Laser." *IEEE J. Quantum Electron*, QE-21, No. 6 (1985), 716–718

[19] Haug, A. "Influence of Doping on the J_{th} of InGaAsP Semiconductor Lasers." *Elect. Lett.*, 18, No. 21 (1985), 792–794.

[20] Haug, A.; Burkhard, H. "Temperature Dependence of Threshold Current of $In_{1-x}Ga_xAs_yP_{1-y}$ Lasers with Different Compositions." *IEE Proc*, 134, No. 2 (1987), 117–121.

[21] Bernard, M. G. A. ; Duraffourg, G. "Laser Condition in Semiconductors ." *Phys. Status Solidi*, 1, No. 7 (1961), 699–703.

[22] Asada, M.; Suematsu, Y. "Measurement of Spontaneous Emission Efficiency and Nonradiative Recombination in 1.58 μm Wavelength GaInAsP/InP Crystals." *Appl. Phys. Lett.*, 41, No. 4 (1982), 353–355.

[23] Horikoshi, Y.; Furukawa, Y. "Temperature Sensitive Threshold Current of InGaAsP-Inp DH Lasers." *Jpn. J. Appl. Phys.*, 18, No. 4 (1979), 809–815.

[24] Su, C. B.; Olshansky, R. " Carrier Lifetime Measurements for Determination of Recombination Rates and Doping Levels of III-V Semiconductor Light Sources." *Appl. Phys. Lett.*, 41, No. 9 (1982), 833-835.

[25] Haug, A."Evidence of Importance of Auger Recombination for InGaAsP Lasers." *Elect. Lett.*, 20, No. 3 (1984), 85-86.

[26] Dutta, N. K.; Nelson, R. J. " The Case of Auger Recombination in $In_{1-x}Ga_xAs_yP_{1-y}$." *J. Appl. Phys.*, 53, No. 1 (1982), 79-92.

[27] Sugimura, H. "Band-to-Band Auger Recombination Effect on InGaAsP Laser Threshold." *IEEE J. Quantum Electron.*, 17, No. 5 (1981), 627-635.

[28] Su, C. B.;Schlafer, J.; Manning, J.; Olshansky, R. " Measurements of Radiative Recombination Coefficient and Carrier Leakage in 1.3 μm InGaAsP Lasers with Lightly Doped Active Layers." *Electron. Lett.*, 18, No. 25 (1982), 1108-1110.

[29] Su, C. B.;Olshansky, R.; Manning, J.; Powazinik, W."Carrier Dependence of the Radiative Coefficient in III-V Semiconductor Light Sources." *Appl. Phys. Lett.*, 44, No. 8 (1984), 732-734.

[30] Su, C. B.; Olshansky, R. " Measurements of Threshold Carrier Density of III-V Semiconductor Laser Diode." *Appl. Phys. Lett.*, 43, No. 9 (1983), 856-858.

[31] Su, C. B.; Olshansky, R.; Manning, J.; Powazinik, W. "Temperature Dependence of Threshold Current in III-V Semiconductor Lasers." *A Phys. Lett.*, 44, No. 11 (1984), 1030-1032.

[32] Olshansky, R.; Su, C. B.; Manning, J.; Powazinik, W. "Measurement of Radiative and Nonradiative Recombination Rates of InGaAsP Lasers." *IEEE J. Quantum Electron.*, QE-20, No. 8 (1984), 838-853.

[33] Mozer, A. P.; Hausser, S.; Pilkuhn, M. H. "Quantitative Evaluation of Gain and Losses in Quaternary Layers." *IEEE J. Quantum Electron.*, 21, No. 6 (1985), 719-725.

[34] Haug, A. " Carrier Density Dependence of Auger recombination." *Solid-State Electron.*, 21, No. 11 (1978), 1281-1284.

[35] Haug, A. "Auger Recombination In InGaAsP." *Appl. Phys. Lett.*, 42, No. 6 (1983), 512-514.

[36] Haug, A. " Auger Recombination in Direct-gap Semicondutor: Band Structure Effects." *J. Phys. C.*, 16, No. 21 (1983), 4159-4172.

[37] Stern, F."Calculated Spectral Dependence of Gain In Excited GaAs." *J. Appl. Phys.* 47, No. 12 (1976), 5382–5386.

[38] Pankove, J. I."Temperature Dependence of Emission Efficiency and Lasing Threshold in Laser Diodes." *IEEE J. Quantum Elect.*, QE–4, No. 4 (1968), 119–122

[39] Tsang, W. T. ; Logan, R. A. ; Vander Ziel, J. P. "Low–Current–Threshold Stripe–Buried–Heterostructure Laser with Self–Alighed Current Injection Stripe." *A Phys. Lett.*, 34, No. 10 (1979), 644–647.

[40] Jung, H. ; Gabel, E. ; Romanel, K. ; Pilkuhn, M. "Temperature Dependenceof Optical Gain Spectra in InGaAsP/InP DH Lasers." *Appl. Phys. Lett.*, 39, No. 6 (1981), 468–470.

[41] Asada, M. ; Adams, A. R. ; Stubkjaer, K. E. ; Suematsu, Y. ; Itaya, Y. " The Temperature Dependence of Threshold Current Of GaInAsP/InP DH Lasers." *IEEE J. Quantum Elect.*, QE–17, No. 5 (1981), 611-618.

[42] Asada, M. ; Suemtsu, Y."The Effects of Loss and Nonradiative Recombination on the Temperature Dependence of Threshold Current in 1.5–1.6 μm GaInAsP/InP Lasers." *IEEE J. Quantum Electron.*, QE–19, No. 6 (1983), 917–923.

[43] Asada, M. ; Suemeatsu, Y. "1.11-1.67 μm (100) GaInAsP/InP injection Lasers Prepared by LPE." *IEEE J. Quantum Eectron.*, QE–16, (1980), 117–205.

[44] Steventon, A. G. ; Spillet, R. E. , Hobbs, R. E. ; Burt, M. G. ; Fiddyment, P. J. ; Callins, J. V."CW Operation of GaAsInP Stripe Lasers." *IEEE J. Quantum Electron.*, QE–17, No. 5 (1987), 602–610.

[45] Joyce, W. B.; Dixon, R. W. "Thermal Resistance of Heterostructure Lasers." *J. Appl. Phys.*, 46, No. 2 (1975), 855–862.

[46] Beatie, A. R.; Landsberg, P. T. "Auger effect in Semiconductors." *Proc. Roy. Soc. A.*, 249, No. 1256 (1959), 16–29.

[47] Beatie, A. R.; Landsberg, P. T. "One-dim Overlap Functions and Their Application to Auger Recombination in Semiconductors." *Proc. Roy. Soc. A.*, 258, No. 1295 (1960), 486–495.

[48] Kressel, H.; Butler, J. K. *Semiconductor Lasers and Heterojuction LEDs.*, New York: Academic Press, 1977.

[49] Takeshima, M. "Disorder-enhanced Auger Recombination in III-V Alloys." *J. Appl. Phys.*, 49, No. 12 (1978), 6118–6124.

[50] Adams, A. R.; Asada, M.; Suematsu, Y.; Arai, S. "The Temperature Dependence of Efficiency and Threshold Current of $In_{1-x}Ga_xAs_yP_{1-y}$ Lasers Related to Intervalence Band Absorption." *Jpn. J. Appl. Phys.*, 19, No. 10 (1980), L621–L624.

[51] Nilsson, N. G. "Empirical Approximation for the Fermi Energy in Semiconductor with Parabolic Band." *Appl. Phys. Lett.*, 33, No. 7 (1978), 653–654.

[52] Mina, M. *Temperature Sensitivity at Threshold in InGaAsP DH Lasers.* , Unpublished M.S.thesis, Iowa State University 1987.

[53] Ito, M.; Kimura, T. "Stationary and Transient Thermal Properties of Semiconductor Laser Diodes." *IEEE J. Quantum Electron.*, QE-17, No. 5 (1981), 787–795.

[54] Newman, D. H.; Bond, D. J.; Stefani, J. "Thermal- Resistance Model for Proton-Isolated Double-Heterostructure Lasers." *Solid-State and Electron Devices*, 2, No. 2 (1978), 41–46.

[55] Ritchie, S. "Thermal Properties of Semiconductor Lasers, and Interpretation of Thermal–resistance Measurements." *Solid-State and Electron Devices*, 3, No. 6 (1979), 201–205.

[56] Adachi, S. "Lattice Thermal Resistivity of III–V Compound Alloys." *J. Appl. Phys.*, 54, No. 4 (1983), 1844–1848.

[57] Nakwaski, W. "Thermal Conductivity of Binary, Ternary, and Quaternary III–V compounds." *J. Appl. Phys.*, 64, No. 1 (1988), 159–166.

[58] Abrahams, M. S.; Braunstein, R.; Rosi, F. D. "Thermal, Electrical, and Optical Properties of (In,Ga)As Alloys." *J. Phys. Chem. Solids*, 10(1959), 204–210.

[59] Both, W.; Herrmann, F. P. "Thermal Resistivity of Quaternary Solid Solution $Ga_xIn_{1-x}As_yP_{1-y}$ Lattice–matched to InP and GaAs." *Cryst. Res. Technol.*, 17, No. 11 (1982), K117–K122.

[60] Both, W.; Gottschalch, V.; Wagner, G. "Thermal Resistivity of GaInAsP Alloys. Experimental Results." *Cryst. Res. Technol.*, 21, No. 5 (1986), K85–K87.

[61] Agrawal, G. P.; Dutta, N. K. "Effect of Auger Recombination on the Threshold Characteristics of Gain-guided InGaAsP Lasers." *Electron. Lett.*, 19, No. 23 (1983), 974-975.

[62] Dehuang, W. "Threshold Current of High-temperature CW semiconductor Lasers." *Chinese Phys.-Lasers*, 15, No. 12(1988), 871-874.

[63] Dolginov, L. M.; Drakin, A. E.;Eliseev, P. G.; Sverdlov, B. N.; Shevchenko, E. G. "CW InGaAsP/InP Injection Lasers with Very Low Threshold Current Density at Room Temperature." *IEEE J. Quantum Electron.*, QE-21, No. 6 (1985), 646-649.

[64] Zielinski, E.; Schweizer, H.; Streubel, K.; Eisele, H.; Weimann, G. "Excitonic Transition and Exiton Damping Processes in InGaAsP/InP." *J. Appl. Phys.*, 59, No. 10 (1986), 2196-2204.

[65] Bardyszewski, W.; Yevick, D. "Composition Dependence of the Auger Coefficient for InGaAsP Lattice Matched to InP." *J. Appl. Phys.*, 58, No. 11 (1985), 2713-2723.

[66] Nash, F. R.; Sundburg, W. J.; Hartman, R. L.;Pawlik, J. R.; Ackerman, D. A.; Dutta, N. K.; Dixon, R. W."Implementation of the Proposed Reliability Assurance Strategy for an InGaAsP/InP, Planar Mesa, Buried Heterostructure Laser Operating at 1.3 μm for Use in a Submarine Cable." *AT& T Tech. J.*, 64, No. 3 (1985), 809-860.